WHITE NOISE ANALYSIS OF VISUAL SELECTIVITY IN AREA MT

DURING FIXATION AND EYE MOVEMENTS

by

TILL SEBASTIAN HARTMANN

A Dissertation submitted to the

Graduate School Newark

Rutgers, The State University of New Jersey

in partial fulfillment of the requirements

for the degree of

Doctor of Philosophy

Graduate Program in Behavioral and Neural Sciences

written under the direction of

Professor Bart Krekelberg

and approved by

_____

_____

_____

_____

_____

Newark, New Jersey

January, 2012

ABSTRACT OF THE DISSERTATION

WHITE NOISE ANALYSIS OF VISUAL SELECTIVITY IN AREA MT

DURING FIXATION AND EYE MOVEMENTS

By TILL SEBASTIAN HARTMANN

Dissertation Director:
Professor Bart Krekelberg

It is crucial for survival to rapidly and accurately determine the location of objects. As humans, we constantly estimate positions of stationary and moving targets around us, and do so successfully, despite eye movements that induce motion on the retina. One vital brain area has been identified for localization and motion processing: the middle temporal area (MT). We set forth to investigate the responses of single cells and local field potentials (LFP) in area MT of the rhesus macaque in order to study its tuning properties during eye movements. We presented randomly positioned, flickering bars to map neurons' visual responses. Meanwhile, we superimposed a fixation point to keep the eyes still or a moving random dot pattern, which induced Optokinetic Nystagmus, a specific type of eye movement. During fixation, we found the responses of area MT to be—contrary to the current beliefs in literature—polarity sensitive (project 1). Our findings indicate that the receptive field (RF) position in area MT is yoked to the eye, independent of eye position and eye movement. That is, the cells are coding in an eye-centered reference frame and the cells' RFs do not shift (project 2). We found that in area MT, eye position modulated not only neurons' firing rates; the power in the gamma

spectrum exhibited gain modulation as well—gain fields (project 3). Finally, we show dramatic changes during fast eye movements of both neuronal firing rates and LFP. The LFP modulation depended highly on the frequency band, i.e. theta power was strongly enhanced while the stimulus frequencies in the gamma range were decreased. We speculate that the LFP modulations allow us to identify layer specific differences. Furthermore, these modulations lead us to suggest a new mechanism for saccadic suppression: de-synchronization (project 4). In conclusion, we advanced the knowledge on motion processing and perceptual stability and proposed a novel role for de-synchronization in the phenomenon of saccadic suppression.

Acknowledgement

First, I want to thank Bart. My advisor and mentor for over seven years is more a friend than a professor to me. He patiently helped me through ups and downs, always having his door open so that I could tell him the newest results or biggest disappointments. I will miss our discussions most, were we try to make sense of our analysis results and to understand the brain. Bart taught me programming to create my stimuli, electrophysiological recording to conduct the experiments, analyzing the data, and English to survive in America. Thank you, Bart!

My committee members had to read my complete thesis, I give them my greatest gratitude. I always enjoy meeting and chatting with Jim, Denis, and Tibor, thanks for your continuing advice. Jim, your neurophysiology class was one of the best classes I ever took. Mickey, thanks for agreeing to be on my committee, it is a pleasure and an honor for me.

Kai, Adam, Jacob, Alex, Tamara, Jess, Jeroen, Jon, Mar, Kohitij, Freddie, you made the KLab my second home. I will miss our interactions, our interesting discussions, during the lab meeting as well as during lunch. Jonas, we had a great run in the time you were here. I hope we can repeat such collaboration soon again.

Josh, Dave, Sona, Frank, Alon, Katie, Amber, Kate, Stephan, Sean, Anushree, Arielle, Liz, Andres, Harry, and all other current and former grad student, it was a great time. Thanks for your help when I needed it, whether it was research or to relax at a nearby place.

Thanks to the entire CMBN faculty, for making the center such a unique research institution. Connie, Ann, and Wayne, thank you for your help with all that beloved paper work, registration etc. Thanks to RAF for taking care of the monkeys, especially Larry, Juan, Bob, Jason, Rob, Manuel, and Kay.

I recorded some of the data presented in this thesis in the Vision Center Laboratory at the Salk institute. I sincerely thank Tom for providing me lab space and a possibility to work in his lab. I want to thank Gene and John for the interesting discussions we had while I was there. Anja, Greg, and Jude helped me whenever I needed help. Special thanks to Micah.

And thanks to my mother, my father, my sister, and my brother. I am proud to have such a family, which gave me valuable advice and support when I needed it most.

Anna, your support was amazing, especially in the last months before handing in this document. Thank you!

Thank you all!

TABLE OF CONTENTS

Table of Figures

Chapter 1 General Introduction

For humans, vision is arguably the most important sense. We use it to orient ourselves in the environment, read, recognize each other, locate danger or look for food at the nearest restaurant.

Motivation

All the above mentioned activities involve both passive and active sensing. Light hits the retina and induces action potentials that travel to the brain. These action potentials relay information to the brain about contrasts and colors of the visual scenery in front of the eye. This process is an example of passive sensing. The retina has an area called the fovea, which has the highest density of photoreceptors and is therefore the area with highest visual acuity. We move our eyes and turn our head and body to center the fovea on the most salient areas in the visual scene. This is active sensing (Schroeder et al., 2010).

Passive sensing is studied while the visual scenery remains stable; the subject's eyes fixate on the same location throughout the experiment. "Polarity Sensitivity of MT Neurons (Project 1)" is an example of such an investigation. In this study, we analyzed the firing of neurons in the middle temporal area (MT) in the extra striate cortex of macaques (*Macaca mulatta*) during fixation. From this research we learn how these neurons convey information about the stimulus, in particular how they detect motion.

But prolonged fixation for seconds is not our usual state, we perform active sensing. We reposition our fovea approximately three times a second. Despite the eyes' frequent movements we perceive a stable visual world. For example, most of us can catch a ball that is thrown towards us rather easily. Neural substrates of this spatial stability are explored in projects two, three, and four. "RF Positions during Slow Eye Movements (Project 2)" investigates the spatial reference frame of neurons in area MT. "Gain Fields in Spikes and LFPs (Project 3)" explores the representation of eye position in area MT, and "Modulations during Fast Eye Movements (Project 4)" investigates changes in the neural response around fast eye movements.

We chose to record from area MT because the properties of neurons in area MT are relatively well understood and are deemed important in the localization of objects (Maunsell and Van Essen, 1983c, b, Albright, 1984, Born and Bradley, 2005). This general introduction will describe the general properties of area MT. Subsequently, we will describe our current understanding and models of motion perception, important for project one. Projects two, three, and four investigate the properties of neurons in area MT at different eye positions and during different eye movements, respectively. Therefore, we will discuss eye movements and effects they have on both perception and single neurons in the section "Spatial Stability" in detail.

Area MT

We start with a brief introduction to the visual system.

From the retina to MT

Most of our eye functions as a physical apparatus to project an image of the world onto our retina. There, photoreceptors detect the light and transform the information into voltage changes. Retinal ganglion cells (RGC) send this information via the optic nerve to the rest of the nervous system. Eighty percent of
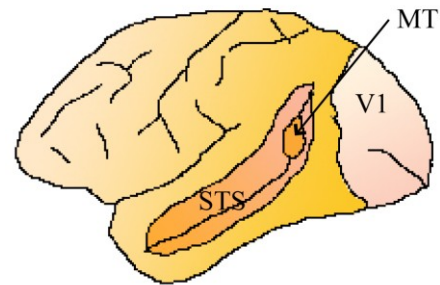
Figure 1: A Macaque Brain. Area MT is positioned on the posterior bank of the superior temporal sulcus.

the axons in the optic nerves terminate in the lateral geniculate nucleus (LGN). Neurons in the LGN relay then send the retinal information, via the optic radiation, to the primary visual cortex (V1).

Neurons in V1 represent the properties of visual stimuli. Some neurons receive information from photoreceptors of only one eye, while others integrate the visual information from both eyes. Neurons in the blobs—cell assemblies stained darkly by cytochrome oxidase—are selective for color, but not for the orientation of stimuli. The remainder of area V1 (or interblobs) is typically insensitive to the color of stimuli. Instead, these latter neurons are highly selective to orientation and also motion of stimuli.

Two streams of information originate from V1, the ventral "what" stream and the dorsal "where" stream (Mishkin and Ungerleider, 1982, Maunsell and Newsome, 1987) . The ventral stream, associated with object recognition and form representation, delivers

information to the temporal lobe. The dorsal stream is associated with location and motion and conveys information to the parietal lobe. The two streams are heavily interconnected and rather than two distinct physical entities, they serve as concepts to illustrate the different progressions of information. Nevertheless, area MT is the beginning of the dorsal stream; it is considered the motion area of the brain.

Tuning properties of area MT neurons

Area MT was simultaneously discovered by two research groups. Allman and Kaas (1971) recorded from a heavily myelinated structure located in the middle temporal lobe in the owl monkey (*Aotus trivirgatus*), a new world monkey. The majority of neurons in this area are direction selective. Dubner and Zeki (1971) studied a heavily myelinated structure in the rhesus monkey (*Macaca mulatta*) brain, situated on the posterior bank of the superior temporal sulcus, which they called visual area 5 (V5) (for position in the brain, see Figure 1).

The best known property of MT neurons is motion tuning. Albright (1984) presented random dot patterns moving in different directions and showed that the preferred direction enhances the neuron's activity dramatically. In contrast, the opposite or null direction often suppresses the activity (see Figure 2 for the responses of a direction selective MT neuron). Neurons are also tuned for the speed of motion, stimulus size, binocular disparity, and eye position. Eye position is coded indirectly by so-called gain
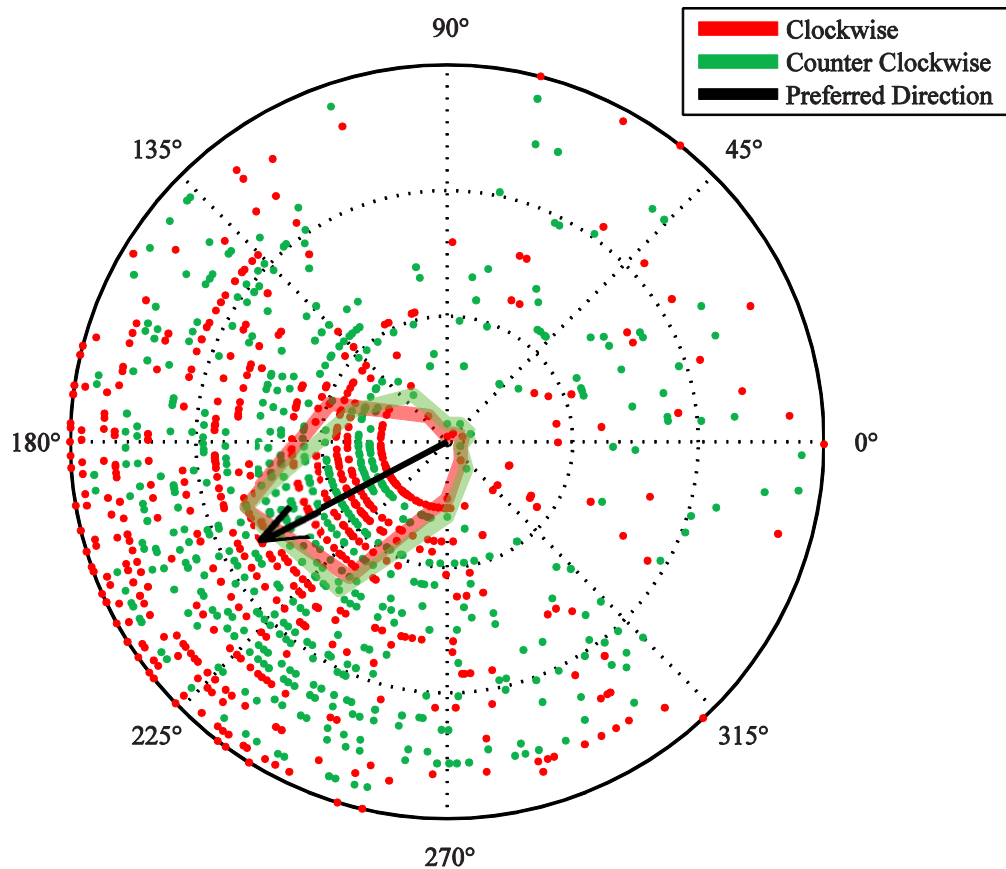
Figure 2: Motion tuning in area MT. A monkey fixated a central dot while a random dot pattern moved clockwise or counterclockwise on a circular trajectory (see (Schoppmann and Hoffmann, 1976)). When the random dot pattern was moving to the bottom left, the cell fired many action potentials. There were almost no spikes while the stimuli moved to the top or right.

fields, which exist in most areas of the posterior parietal cortex (e.g. 7a: (Andersen et al., 1985), MT: (Bremmer et al., 1997)). Gain fields modulate the visual response of a neuron to a stimulus depending on the position of the eye (for more details see section "Gain Fields" page 18).

Functional Architecture

Dubner and Zeki (1971) suggested that neighboring cells in MT are tuned for both similar locations (retinotopy) and similar motion directions. Advancing an electrode laterally through MT, they found that the RFs of neighboring neurons overlap for the most part, while the center of the RF slowly shifts along with the depth of electrode penetration. Retinotopy is the property that adjacent neurons in an area have adjacent receptive fields (RF) on the retina. This should not be confused with the reference frame of a neuron (discussed in detail in "Reference Frames" page 16).

Albright (1984) confirmed the retinotopic organization of neurons and established the ice
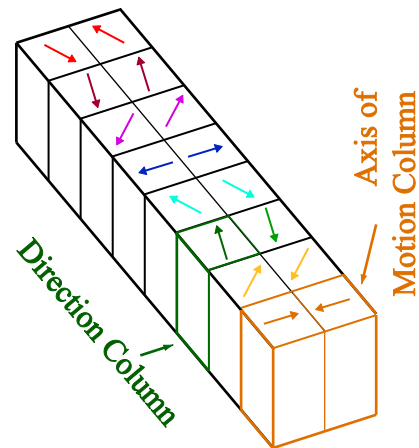
Figure 3: Ice Cube Model for MT. The preferred motion axis/orientation changes while moving along the long axis of the cluster. Each axis of motion column has two direction columns tuned for opposite preferred directions. Cells in the middle are often tuned for both motion directions along the axis of motion (Albright 1984).

cube model, first introduced for the columnar organization of V1 (Hubel et al., 1977), for area MT (see Figure 3). Neighboring cells are organized in cortical columns "ice cubes" and are tuned for the same axis of motion, but the sign of the direction may differ along an edge. DeAngelis and Newsome (1999) found zones with strong disparity tuning distributed in area MT. Within a zone the preferred disparity varies smoothly, similar to the direction columns. The functional organization is crucial, if we analyze not only well

isolated single cells, but multi unit activity (MUA) and the local field potentials (LFP). A typical MUA signal might reflect the activity of e.g. a dozen neurons. If these neurons have random direction selectivity, then the MUA signal is not, or only weakly, direction selective. But in areas such as MT, where neurons have similar direction selectivity, the MUA signal is strongly tuned. Thus, we can treat it in the analysis similar to the spikes from a single cell. This should be true for the LFP as well, and the LFP in area MT is indeed direction selective (Liu and Newsome, 2006).

Anatomical connection to area MT

Area MT's main input is only five synapses away from the photoreceptors. Two synapses (both gap junctions) are in the retina (from photoreceptors via bipolar cells to RGCs). The RGCs that are part of the retina to MT pathway are typically of the magnocellular (M) type. These ganglion cells receive mostly rod input, have rapid and transient responses and are therefore ideal
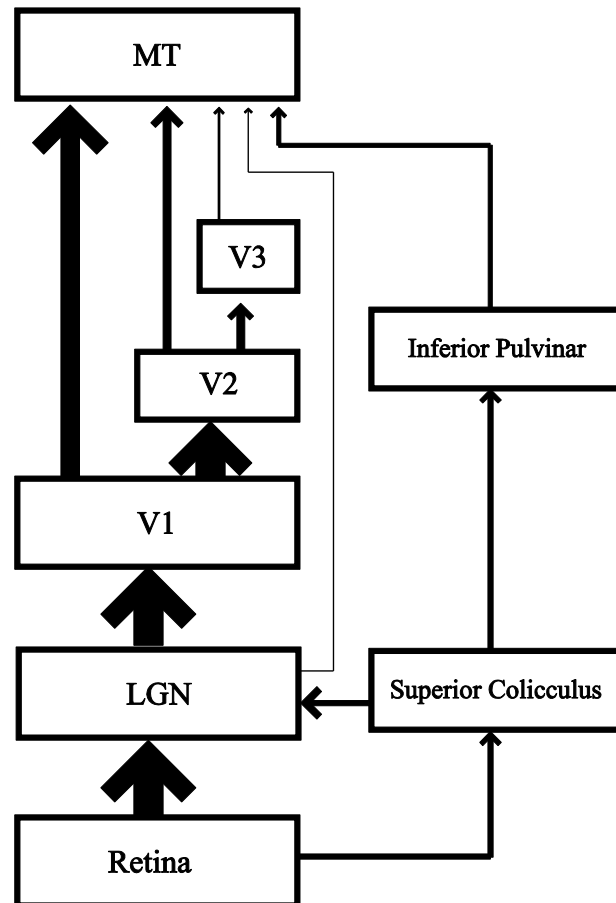
Figure 4: Detailed input map to area MT. (Adapted from Bradley and Born 2005).

for motion perception. The RGCs project directly to LGN neurons, which relay most of the signal to V1. Some LGN cells project directly to area MT (Stepniewska et al., 1999, Nassi et al., 2006). These neurons are relatively sparse and situated in the interlaminar layers of LGN. Their inputs do not necessarily come from the retina but most likely from the superior colliculus (SC) (Stepniewska et al., 1999). The majority of projections in the retina-MT pathway from LGN to V1 terminate in layer 4Cα. Specialized, mostly spiny stellate cells in layer 4B receive input from layer 4Cα and project to area MT via thick axons (3μm compared to the standard 1 μm)(Rockland, 1989, Shipp and Zeki, 1989b, a). Of projections from V1 to MT, 90% to 95% originate in layer 4B, with the rest originating primarily from large Meynert cells at the border of layers 5 and 6 (Tigges et al., 1981, Maunsell and van Essen, 1983a, Shipp and Zeki, 1989a).

There are also fewer but significant connections from neurons in the thick cytochrome oxidase strips of V2 (DeYoe and Van Essen, 1985). Other inputs come from V3, V3A, the ventral posterior area, and the posterior intraparietal area (Felleman and Van Essen, 1991). Based on the number of labeled neurons following injections of [3H] proline and horseradish peroxidase in MT, areas V1, V2, and V3 provide the predominant input to area MT (Maunsell and van Essen, 1983a) (see Figure 4 for an overview).

Area MT projects to structures that are strongly involved in the analysis of optic flow such as the middle superior temporal area (MST) and ventral intraparietal area (VIP), and areas involved in the generation of eye movements (e.g. the lateral intraparietal area (LIP), the frontal eye fields (FEF) and the SC). Areas MST and LIP were actually

discovered by labeling in area MT and searching for its output targets (Maunsell and van Essen, 1983a).

Functional connection to area MT

In this section we will focus on those parts of the functional connectivity that are important for direction selectivity in area MT. Ponce et al. (2008) showed that cooling V2/V3 reduces binocular tuning in area MT but not motion tuning. They hypothesized that the direct projections from V1 are most important for motion tuning. The projections from V1 are important for project 1 and we will discuss these inputs in detail.

Simple and Complex Cells

Hubel and Wiesel recorded in V1 and classified cells into two broad categories: simple and complex cells (Hubel and Wiesel, 1968). The standard model of simple and complex cells involves two stages.

Simple cells receive inputs from LGN neurons, illustrated in Figure 5A. Typically, these LGN neurons have center surround RFs. They either prefer a bright spot surrounded by darkness (on-center) or a dark spot surrounded by light (off-
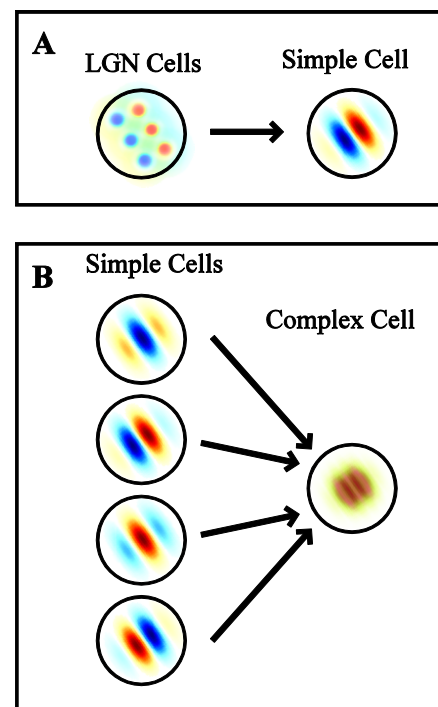
Figure 5: Simple and Complex Cells. Schema of the construction of simple cells (top) and complex cells (bottom), inspired by Hubel and Wiesel.

center). In the example in Figure 5A, a luminance edge (dark on the left, bright on the right, slightly tilted) would induce a high firing rate, because it fits the RFs of all the LGN cells well.

Neurons in V1 that respond to an edge independent of its location in the RF are complex cells (Hubel and Wiesel, 1962). They could combine the output of simple cells, which are all tuned to the same orientation but different positions of the edge within the RF (see Figure 5B). So wherever the edge is in the RF of the complex cell and whatever its polarity (is the left side of the edge dark or bright?); at least one of the simple cells will fire and stimulate the complex cell. A simple cell whose RF does not match the stimulus does not fire, and thus does not contribute to the complex cells firing rate, neither by excitation nor inhibition. That the cells contribute only if the stimulus positively correlates with the RF is often mathematically described as a half wave rectification.

In 1978, Movshon and colleagues tested the response of V1 neurons to black and white bars and moving gratings and quantified Hubel and Wiesel's findings (Movshon et al., 1978b, a). One group of neurons, the simple cells, respond to either a black or a white bar at a given location within the RF. If a grating moves through the RF, the firing rate is modulated depending on whether the grating matches the RF. Complex cells respond to both black and white bars in the same location, and fire constantly for a grating moving through the RF.

The Linear Nonlinear Model (LN) allows a simple mathematical description of simple and complex cells as defined by Movshon et al. in 1978 (Carandini, 2006). For a simple

cell, the stimulus is passed

through a linear filter (the RF of

the neuron) and an asymmetric

nonlinearity (usually a half wave

rectification, to take into account

that neurons cannot have

negative firing rates) to gain an

estimate of the expected firing

rate (Figure 6A). The model of a

complex cell consists of either

A Simple cell

Input Filters   Nonlinearity

Image →   →   → Response

B Complex cell

Image →   ↘ + → Response
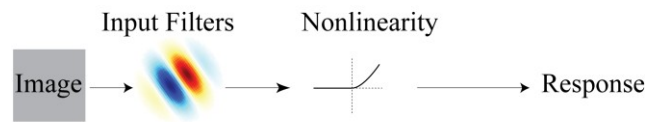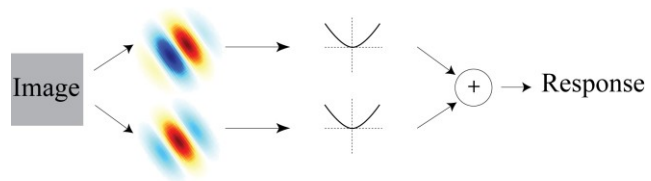
Figure 6: Linear Nonlinear Model for Simple and Complex Cells. The image is filtered through one (simple cell) or two (complex cell) input filters. The result is passed through the transfer function, or nonlinearity, to predict a firing rate.

two linear filters with symmetric nonlinearities (see Figure 6B) or four filters with

nonlinearities resembling half wave rectifications (Carandini, 2006), which is

mathematically identical.

Newsome and Movshon (1996) recorded from 12 V1 cells that were monosynaptically

connected to area MT, six from layer 4B and six from layer 6. They confirmed

antidromical activation with the collision test. They classified these neurons as special

complex cells, and concluded that all input to MT is of that kind. Special complex cells

respond to bars shorter than the length of the RF (Palmer and Rosenquist, 1974). They

tested the response of one neuron to the transition from dark to light and from light to

dark and did not find a difference, the cell was polarity insensitive. They concluded that

therefore all MT cells are also insensitive to the polarity of a stimulus. In summary, the

current view in the literature is that MT cells receive input from polarity insensitive

complex cells in V1 and therefore, MT cells

are polarity insensitive. Consistent with

this, our perception of motion does not

depend on the polarity of stimuli. Taken

together these findings have been

incorporated into the motion energy model

and current MT models.

Motion Energy Model

The motion energy model is an abstract

model that predicts responses to moving

Figure 7: Motion Energy Model. Stimuli are passed through a spatiotemporal filter, squared, and summed or subtracted, depending on the preferred direction of the initial spatio temporal filters (adapted from Adelson and Bergen, 1985).

stimuli (Adelson and Bergen, 1985). The models response is based on the spatial

temporal energy in the Fourier domain of stimuli. The first step of the model consists of

four linear filters, which are not only oriented in space but also in time. Each filter

detects an edge, which changes constantly over space and time (Figure 7). The time

component of the filter could be constructed via different temporal filters (proposed in

the original work by Adelson and Bergen), delay lines similar to those in the Reichardt

detector (Hassenstein and Reichardt, 1956), or - as our lab found recently - with

recurrent lateral connections between neurons (Joukes and Krekelberg, 2009). The

responses of the four linear filters are rectified through squaring, which makes the

responses polarity insensitive. The firing rate is the same whether the stimulus matches

the filter positively (e.g. a black-white edge) or negatively (e.g. a white-black edge).

After the squaring the responses for the motion in one direction are summed while the responses for motion in the opposite direction are subtracted to form the final response.

MT Model

Simoncelli and Heeger (1998) developed a model to explain MT responses. This model is based on the motion energy model, but unlike Adelson and Bergen, they explicitly mapped the model stages onto visual cortex based on physiological properties. The first stage consists of V1 simple cells, which have linear space-time filters as RFs. Each location in space is sampled by multiple simple cells which respond to an edge with different polarity within the RF. The response of the V1 cells is passed through a half wave rectifying nonlinearity and mapped onto complex cells, which project onto MT cells where, (after a few more stages intended to generate pattern motion sensitivity, which does not concern us here), the motion signal is read out. In this model all polarity sensitivity is lost after the first stage. In conclusion, both the physiology and the modeling literature assume that MT cells receive polarity insensitive input from complex cells. In contrast with this, we will show in the chapter "Polarity Sensitivity of MT Neurons (Project 1)" that the majority of MT neurons are, under certain conditions, polarity sensitive, and therefore behave like simple cells.

Spatial Stability

The density of photoreceptors varies considerably depending on the location on the retina. There is a low density at the periphery and a very high density at the center of

gaze, the fovea (the RGC density changes by a factor of 1000-4000 between peripheral and central retina in the macaque (Wassle et al., 1990)). The visual image at the fovea has the highest acuity. Someone with good vision (20/20) can distinguish letters, whose lines are 1 arc min visual angle apart, from 20 feet (ca. 6m). Peripheral vision is blurry; acuity 20° away from the fovea is so bad that it qualifies as legally blind. Therefore, in order to perceive the world in finer detail, it is necessary to move the eye.

During every day life, we are unaware of our eyes' movements, nor of the image moving across the retina. Herrmann von Helmholtz was one of the first to address perceptual stability (Helmholtz, 1856); he hypothesized that a mechanism exists that uses the effort of will, the motor signal, to generate stable percept. In the 1950's these ideas were formalized in two closely related theories: efference copy (von Holst and Mittelstaedt, 1950) and corollary discharge (Sperry, 1950). The efference copy theory states that every time a brain center sends a motor signal, it also sends an efference copy which suppresses the afferent signal resulting from the motor movement in the same center. Sperry postulates corollary discharge to be the neural basis of Helmhotz's effort of will, but does not propose a mechanism of its action. He labels it a central adjustor factor. Today we know that the center that sends the motor command, (e.g. Oculomotor Nuclei) and the center that receives the reafference (e.g. LGN), are not the same, thus the efference copy theory is incorrect in its details, but the principle still underlies most models of perceptual stability. We prefer to use the term corollary discharge, for the signal that coordinates processing between motor control and sensory areas because

the signal is not a true copy (for a review on corollary discharge, see Sommer and Wurtz (2008)).

Eye Movements

Our perception of visual space is stable during all of the typical six eye movements. Four of these keep the fovea on a target in the environment and two stabilize the eye during head movement. An active fixation system keeps the eyes on a stationary target. Saccades are performed to rapidly shift the fovea to a new target of interest. A moving target is kept on the fovea via smooth pursuit eye movements. Vergence movements function to position the image of an object at a different depth onto the foveae of both eyes, moving the eyes in opposite directions. During head movements, vestibulo-ocular movements maintain an image stationary on the retina; they are driven by the vestibular system. Optokinetic nystagmus (OKN) is driven purely by visual stimuli and stabilizes moving images on the retina (Kandel et al., 1991). OKN is induced when the whole visual field moves in one direction. This occurs for example, while looking out of a moving train. During OKN, smooth phases in which the eye tracks the visual scenery/stimulus are interrupted by short, fast phases in the opposite direction (for an example see Figure 11 page 29).

Saccades compared to the fast phase of OKN

Throughout this thesis, we will assume that the effects during saccades and during the fast phase of OKN are similar. We justify this with the similarity of saccades and the fast phase during OKN. Saccade duration and peak velocity increase with saccade amplitude,

this relation has been termed main sequence. Fast phases follow often the same main sequence as that of visually guided saccades (Mackensen and Schumacher). Misperception of briefly flashed targets around the fast phase is remarkably similar to that of saccades (Kaminiarz et al.).

Reference Frames

Retinal ganglion cells only code information about the physical position of an image on the retina. But when we reach for an object, we need the position of the object in space, not on the retina. The information coming from the eye about stimulus position has to be transformed from an eye-centered reference frame to a hand-centered reference frame to allow for an accurate reach. LGN neurons and V1 neurons receive input from the same location in the eye. Therefore, their reference frame is still eye-centered. If the eyes move and the visual image on the retina changes, so will the response of cells that code in an eye-centered reference frame. In (1997), Duhamel and colleagues found cells in area VIP, whose RFs are located at a location in space independent of eye position (Figure 8). The monkeys in these experiments had their heads fixed, so one can conclude that these RFs
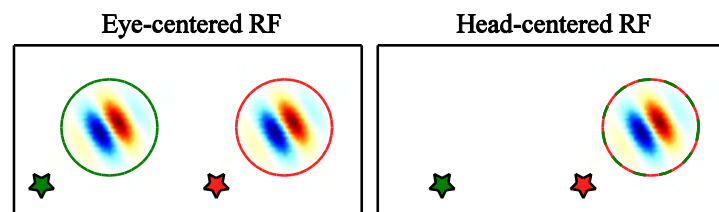
Figure 8: Reference Frames. Shown are the receptive fields (RFs) of two model neurons for two different eye positions (stars). The neuron on the left codes information in an eye-centered reference frame. The neurons RF on the right does not change with the eye, it codes in a head-centered reference frame (adapted from (Duhamel et al., 1997)).

were at least head-centered.

Other reference frames exists, such as the above mentioned hand- or body-centered coordinate system, useful for reaching. The ears are fixed to the head, and therefore all early auditory structures code information about the location of auditory stimuli in a head-centered reference frame. World-centered reference frames are independent of the body's position and depend on the position of objects in the world.

We use the suffix "—centered" to specify a reference frame for an RF; an eye-centered RF moves with the eye, while a head-centered RF moves with the head. These concepts are quite different (and in fact independent) of retinotopy which is traditionally used to describe the functional architecture of an area. As described above (see section "Functional Architecture" page 6) area MT is retinotopic; neighboring cells have neighboring RFs. In the literature, researchers often use retinotopic and spatiotopic when in fact they mean eye- and head-centered reference frames.

Early recordings in area MT were performed during general anesthesia; other studies were recorded during central fixation. Most researchers assumed an eye-centered reference frame. Recently, however, some evidence suggested differently. Ong and Bisley (2009) found evidence in a psychophysical study and d'Avasso et al. (2007) utilizing fMRI that area MT codes at least some information in an head-centered reference frame. Gardner at al. (2009) attempted to reproduce the fMRI result from d'Avasso et al., but could only find a significant eye-centered reference frame. Given this controversy, and the important implications for our understanding of perceptual

stability, we decided to investigate this issue in macaque MT. In "RF Positions during Slow Eye Movements (Project 2)" page 52ff we show that single neurons as well as the LFP activity in area MT code in an eye-centered reference frame.

Gain Fields

Even though their visual RFs are yoked to the retina, neurons can nevertheless code the current eye position. For example, the firing rates could always be higher while the eyes are directed to the top left compared to the bottom right. Such gain fields—visual responses that depend on eye position—exist throughout the posterior parietal cortex in monkeys: V3A, V6 (Galetti and Battaglini 1989), LIP, 7A (Andersen 1985), MT and MST (Bremmer 1997), and V1 (Trotter and Celebrini, 1999). On a population level, these gain fields provide enough information to make a transformation from an eye- to a head-centered reference frame. The hidden layer neurons of networks, which learned to represent head-centered space, were shown to have similar properties as the neurons in 7a with gain fields (Andersen and Zipser, 1988; Zipser and Andersen, 1988; Pouget at al 1993).

In V1, Durand and colleagues (2010) found gain fields of a different nature. Their analysis revealed that peripheral V1 neurons increase their firing rate when their RF is straight ahead (relative to the body midline). fMRI data showed maximal bold activity in V1 when eye and head were aligned (Andersson et al., 2007). These gain fields could enhance processing for objects right in front of us and therefore with a higher salience.

Gain fields also exist during slow eye movements. Monkeys performed smooth pursuit eye movements from different starting points while the responses from MT or MST neurons were recorded. The smooth pursuit eye movements were always in the preferred pursuit direction of the neuron under investigation. Similar to gain fields during fixation, the firing rates were modulated depending on the starting point of the smooth pursuit eye movements and therefore on the position of the eye (Bremmer et al., 1997). The direction of the gradient of the gain field during fixation is not correlated with the preferred motion direction of neurons in MT, nor is the direction of the gradient of pursuit gain fields correlated with the preferred pursuit direction (Bremmer et al., 1997). The population in area MT/MST does not show a bias for any slope. Given that gain fields are thought to be an important component of perceptual stability, we investigated their properties in area MT. The chapter "Gain Fields in Spikes and LFPs (Project 3)" shows that MT spikes as well as the local field potentials carry information on the position of the eye, even when the eye is smoothly changing position.

Mislocalization around Eye Movements and RF Shifts

During every day life, our visual world is stable. Thus we are able to "block" the signals coming from the retina induced by our self motion, as described by the efference copy and corollary discharge theories. But in the laboratory, we can find small cracks in this perceptual stability. If we understand these cracks, this could lead us to a better understanding of the underlying neural processes of perceptual stability.

Honda asked subjects to report the location of small targets. While subjects reported locations accurately during fixation, they made consistent misjudgments around the time of the saccade (Honda, 1989). The mislocalization of targets in the direction of the saccade started about 100ms before the saccades and reached its maximum just at saccade onset. Targets presented at the offset of the saccade are perceived in the direction opposite to the saccade. Briefly flashed targets are mislocalized
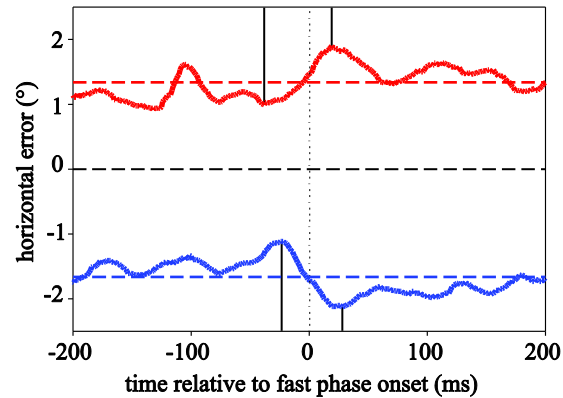
Figure 9: Mislocalization during OKN. The horizontal axis represents time relative to the fast phase onset; the vertical axes describe localization error of a briefly presented target. It shows mislocalization during OKN. Red represents rightward background motion and blue leftward background motion. The target is constantly perceived to be shifted in the direction of the smooth phase. On top there is a modulation around the fast phase, which looks similar to the one during saccades (courtesy of Andre Kaminiarz).

during smooth pursuit eye movements in the direction of the pursuit (van Beers et al., 2001). During OKN, targets are generally perceived shifted in the direction of the slow phase (Kaminiarz et al., 2007). But during the fast phase the perceived location is modulated, as if the modulation of error observed by Honda for saccades is overlaid onto the general mislocalization during the slow phase (Figure 9).

Fifty milliseconds before a saccade the visual image is still stable on the retina. But, if neurons that usually code for locations on the retina become responsive to new locations just before saccades, localization errors may occur. A study by Duhamel and

colleagues (1992) showed that a new zone of retinal sensitivity occurs right before a saccade in a subset of LIP neurons. The RF shifts in the direction of the eye movement and is thought to anticipate the future location of the RF (for review: see (Ross et al., 2001)).

Remapping or updating of the RF location has been shown in LIP, SC, FEF, V4, and V3a (Duhamel et al., 1992, Tolias et al., 2001, Nakamura and Colby, 2002) as well as in human parietal cortex (Merriam et al., 2003). On a population level, Krekelberg and colleagues (2003) showed that MT cells' location coding is disturbed up to 100ms before the start of an saccade. The temporal dynamics and also the magnitude of the disturbance are similar to those described in the psychophysical mislocalization experiments above and were therefore thought to be linked. In chapter "RF Positions during Slow Eye Movements (Project 2)", we investigate whether the RFs of MT neurons shift during the slow phase of OKN.

Saccadic Suppression

The human eye reaches speeds up to 1000 deg/s during a saccade. The visual image rushes across the retina, and despite the capability of the eye to detect the motion, no motion is perceived. This psychophysical phenomenon is referred to as saccadic suppression (for reviews, see (Ross et al., 2001, Wurtz, 2008)).

One theory states that the stimulus itself is filtered out at the level of the retina (Castet et al., 2001). The visual field does not move very often with speeds of 1000 deg/s (or 10 m/s only 57cm away from your eyes). Thus such stimuli could be detected and ignored.

That theory was rejected by an experiment in which a mirror simulated an eye movement and thus allowed the image to sweep across the retina the same way it does during a real eye movement (Diamond et al., 2000). In that experiment, a target had to be detected during a real or simulated saccade. During the actual saccade, the detection threshold is reduced, while for the simulated movement, the threshold remains constant.

Another way to achieve the suppression of motion percept would be to generate a "central anesthesia" during the saccades (Holt, 1903), using the efference copy signal (Zuber and Stark, 1966). In 1994, Burr and colleagues showed that stimuli of higher spatial frequency or isoluminant contrast (differing only in color) were not suppressed (Burr et al., 1994). They concluded, without physiological evidence, that only the magnocellular pathway is affected by saccadic suppression, probably at the early stage of the lateral geniculate nucleus (LGN). On the contrary, Watson and Krekelberg (2009) showed that stimuli omitted prior to saccades still induce a visual illusion after the saccade, indicating that stimuli get processed but do not reach awareness at a later stage of processing.

An equivalent noise investigation revealed that pre-saccadic suppression can be best explained, if we assume a mechanism that reduces the stimulus-independent response gain (Watson and Krekelberg, 2009). The response gain could be actively decreased by suppressing the complete input around the time of saccades or—not distinguishable in

the equivalent noise framework—by activity increase independent of stimuli (noise induction).

Wurtz argues that saccadic suppression is caused by backwards visual masking by the stable image at the offset of the saccade (Campbell and Wurtz, 1978). Saccadic suppression is followed by a detection threshold and reaction time decrease (Johns et al., 2009), so called post saccadic enhancement.

Electrophysiological Correlates of Saccadic Suppression

Firing rate modulations occur around the time of saccades in very early stages of visual processing, i.e. LGN (Ramcharan et al., 2001, Reppas et al., 2002), V1 (Wurtz, 1969, Leopold and Logothetis, 1998, Hass and Horwitz, 2011), V2, V4 (Leopold and Logothetis, 1998), and MT (Thiele et al., 2002, Price et al., 2005, Bremmer et al., 2009). Most often the firing rates decreases around the onset of the saccade and/or increases after the onset. While changes in spiking activity are consistently found around the time of saccades, the reported modulations vary greatly depending on visual area and recording and stimulus presentation method. Wurtz showed that the response of V1 neurons to rapidly moving stimuli and the pattern induced by a saccade look similar (Wurtz, 1969). He claimed that the modulation due to the saccade can be explained by the properties of the retinal slip and an involvement of an extraretinal efference copy is unlikely. More recent studies of LGN neurons in monkeys mainly found increases in activity during and after saccades (Lee and Malpeli, 1998, Ramcharan et al., 2001, Reppas et al., 2002). Notably, both Ramcharan and Lee found a presaccadic reduction that can only be

explained with an extraretinal signal suppressing the firing rate of neurons prior to the saccade execution. Bremmer and colleagues (2009) showed such presaccadic reduction in firing rate to flashed bars on the cell population level in areas MST, LIP and VIP.

Thiele and colleagues (2002) recorded from MT and MST neurons while monkeys either performed saccades with a stable low-contrast stimulus in the background or fixated a dot while the same stimulus swept across the visual field with the speed profile of a saccade. Nine out of 51 MT neurons showed a significant reduction in firing rate; their firing rates were reduced during the saccade compared to the firing rates recorded while the stimulus moved across the retina passively, even though the stimulus on the retina was identical. A bigger subset reversed its preferred direction, e.g. a neuron was tuned for the stimulus moving to the left during fixation as well as saccades performed to the left, even though in the latter the stimulus moves to the right. Price and colleagues (2005) performed a similar study, only the stimulus presentation and contrast differed. They found no reversal in any neurons, the vast majority of neurons responded to the preferred direction of retinal motion, independent whether the motion was induced by a saccade or by the stimulus projector. Thiele's study and Price's study, despite their similar designs, essentially show opposite effects.

Area MT neurons respond stronger and faster to stimuli presented right after the saccade (Ibbotson et al., 2007). The time to peak response for a flashed bar is reduced by 8ms (Bremmer et al., 2009), supplemental information). This matches the psychophysical effects of post saccadic enhancement mentioned above.

In conclusion, the literature is inconclusive when it comes to modulations around saccades in visual cortices and especially area MT. In "Modulations during Fast Eye Movements (Project 4)", we will test whether the firing rate in MT neurons is modulated around the time of fast phases, the equivalent of saccades during OKN. We found that single neurons show a variety of responses, which can at least partially be explained by the retinal motion signals induced by the saccade, although we cannot exclude some contribution of an extraretinal signal.

Chapter 2 General Material and Recording Methods

Subjects

The electrophysiological experiments involved two adult male rhesus monkeys (*Macaca mulatta*). Experimental and surgical protocols were approved for monkey S by The Salk Institute Animal Care and Use Committee and for monkey N by the Rutgers University Institutional Animal Care and Use Committee. Protocols were in agreement with the National Institute of Health's guidelines for the humane care and use of laboratory animals.

Animal Preparation

The surgical procedures that where performed on monkey S followed the standard surgery protocols established under Thomas Albright at the Salk Institute and have been described in detail elsewhere (Dobkins and Albright, 1994). In short, a head post and a recording cylinder were affixed to the skull using CILUX screws and dental acrylic (monkey S). Recording chambers were placed vertically above the anatomical location of area MT (typically 4mm posterior to the interaural plane and 17mm lateral to the midsagittal plane). This allowed access via a dorso-ventral electrode trajectory. All surgical procedures were conducted under sterile conditions, using isoflurane anesthesia. Monkey N's surgeries followed a similar protocol. We will describe the procedure in detail, because significant parts were performed by Till Hartmann. An intramuscular (or IM) injection of Ketamine initially anesthetized the monkey. The monkey was intubated for airway management and to maintain general anesthesia with

isoflurane gas. We administered antibiotics, fluids, and—at the end of the surgery—

analgesics via an intravenous (or IV) catheter. During the surgeries, we monitored the

ECG, breathing, pulse rate, pulse oximetry, and body temperature. A heat blanket kept

the monkey warm. The clean shaven head was placed in a stereotactic apparatus to

hold it in place and to serve as a coordinate frame. After disinfecting the top of the head

we injected the local anesthetic lidocaine into the skin at the planned incision sites. The

incisions were made to allow access to the skull where needed. In case of a chamber

placement surgery, a craniotomy was performed at -4mm posterior and -19mm

anterior. A plastic chamber was placed on top of the craniotomy and fixed to the skull

with titanium screws. During a head post placement surgery, a titanium post was affixed

to the skull with titanium screws. At the end, the skin was sutured or stapled around the

implants to cover the bone. The monkey received buprenorphine at the end of surgery

and for at least 3 days after.

Recording

We recorded extracellular activity in area MT of the macaque brain while presenting a

random noise stimulus. Below, we describe the methods used to acquire data. The data

analysis is described in the methods section of each individual project.

Electrophysiology

During a recording session we penetrated the dura mater with a guide tube to allow

access to the brain. An electric microdrive then lowered glass or parylene-C coated

tungsten electrodes (0.7-3MΩ; FHC, Bowdoin, ME or Alpha Omega Engineering,

Nazareth, Israel) into area MT through the guide tube. Single cells were isolated while they were visually stimulated using a circular motion stimulus (Schoppmann and Hoffmann, 1976, Krekelberg, 2008). The circular motion stimulus was used to determine the preferred direction of the isolated neuron (for an example, see Figure 2). After that, we confirmed that the size of the RF was matching those expected from area MT. We
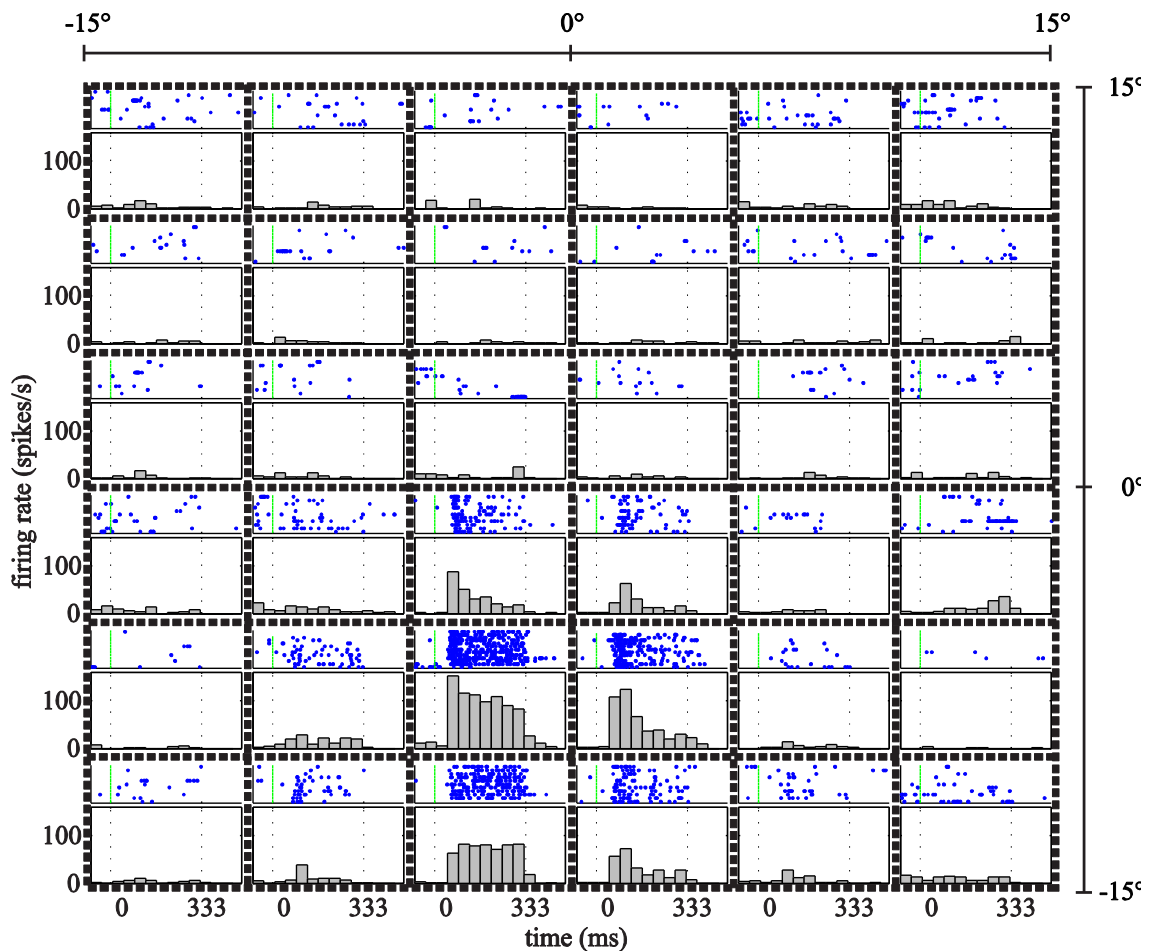
Figure 10: Example RF Map. The grid constructed by the dashed lines indicates the position of 36 random dot patterns moving in the preferred direction of the neuron under investigation. The blue dots in the upper part of each square represent single spikes dependent on time. Each row shows the spikes of a single trial. The lower part in each square shows the peristimulus time histogram. This neuron spiked with over 100 spikes/s when the random dot pattern was presented just left and 7.5° below the fovea

therefore presented small patches of random dots moving in the preferred direction for short periods of time (for one example with raw data, see Figure 10).

We recorded the spiking activity either continuously at 25 kHz using Alpha Lab (Alpha Omega Engineering, Nazareth, Israel, monkey N) or in 800µs windows triggered by threshold crossings with a Plexon system (Plexon, Dallas, Texas, monkey S). After detecting action potentials, we first used an automated superparamagnetic clustering algorithm (Quiroga et al., 2004) to coarsely assign spike wave-forms to single units, and then fine-tuned clustering by hand. The Alpha Omega and the Plexon systems sampled the LFP data continuously at 782 Hz and 1000 Hz, respectively. We filtered all LFP data with a band pass filter (low: 1Hz, high: 120Hz).

Eye position

We measured the eye position signal with infrared eye trackers (ISCAN®, Woburn, MA, 120Hz or EyeLink2000, SR Research, Ottawa, Canada, up to 2000Hz). We identified the fast phases of OKN offline by first detecting speeds of the eye that crossed a threshold set to 2 to 3 standard deviations (depending on the noise) above
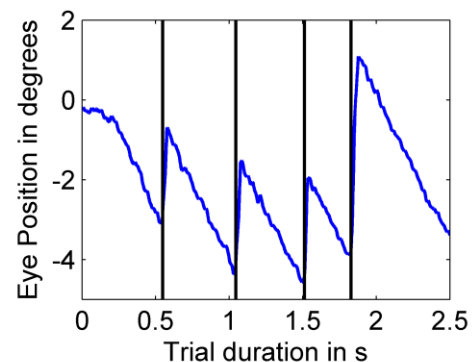
Figure 11: Optokinetic Eye Movements. A random dot pattern started to move to the left at 10 °/s at 0s. After approximately 200ms the eye moves with a similar speed to the left as well. These slow phases are interspersed with saccade-like fast phases in the opposite direction.

the mean speed. To estimate fast phase onset we then searched for the first time point before this threshold crossing where the speed was higher than the mean speed. The data recorded with the ISCAN eye tracker (monkey S) was noisy, therefore, we confirmed the time points of fast phase onset by fitting lines to both the fast phase and slow phase. The intersection of the two lines represents the true start of the saccade. We confirmed accurate detection of the fast phase by visually inspecting a subset of trials. For each slow phase, we determined the linear fit that best described eye position as a function of time. The slope of this line is the gain of the slow phase of OKN. A gain of one indicates that the eye follows the random dot pattern without lag.

Visual Stimuli

Stimuli were generated using the in-house software Neurostim, displayed on a 20" CRT monitor (Sony GDM-520) 57cm in front of the eyes (40° x 30°). All stimuli, except the red fixation point, were presented in equal energy white (x=0.33, y=0.33, CIE color space) with intensities ranging from 0.15 to 85 cd/m².

Random Noise Stimulus

The visual stimulus for the RF mapping
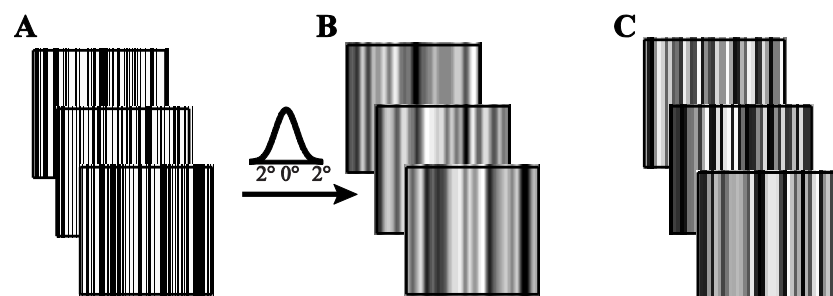
Figure 12: The visual stimulus. The monitor frames filling the entire screen. A: The raw stimulus composed of binary noise for monkey S. B: Stimulus A convolved with a Gaussian function. This is the actual stimulus presented to monkey S. C: The uniform noise presented to monkey N.

was a grating composed of randomly positioned, flickering bars. The bars were always oriented vertically on the screen and not adapted to the preferred orientation of neurons. In the case of monkey S, bars were 0.5° wide and either black or white (Figure 12 A). Each frame was spatially low pass filtered by means of a Gaussian function (average full width at half maximum was 1.0°, Figure 12B). Thus, the resulting luminance distribution was approximately Gaussian for monkey S. For monkey N, the bars were randomly positioned with the luminance for each bar chosen from a uniform distribution (Figure 12C). Each bar's luminance value was independent of all other bars. A new bar-pattern appeared on the screen with a temporal frequency of 60Hz (monkey S) or 50Hz (monkey N).

Procedure

A trial started with the presentation of a central red fixation target. Once the monkey fixated, the random noise stimulus appeared on the screen for 2.5 to 3s. The fixation target stayed on for this period (fixation condition) or disappeared. In the latter conditions, a black random dot pattern (dot diameter: 0.3°; dot density: $0.43 \text{dots}/(°)^2$) was superimposed on the noise pattern. The random dot pattern induced OKN by moving to the left or the right at 10°/s (leftward and rightward OKN conditions, respectively). All three conditions were randomly interleaved and occurred equally often. The animals received a drop of juice at the end of the trial for maintaining fixation in a 4° x 3° window (fixation condition) or for looking at the screen (36° x 28° window, OKN conditions) for the duration of the trial.

Chapter 3 Polarity Sensitivity of MT Neurons (Project 1)

Introduction

The perception of motion is crucial for survival, and a great deal of research has contributed to its understanding. In 1985, Adelson and Bergen published the motion energy model. In this model, the response of quadrature pairs of linear filters oriented in space and time are squared and summed, the result is a motion energy measure (see introduction section "Motion Energy Model" page 12 (Adelson and Bergen, 1985)). This model's response does not differ for a black or a white bar moving in the same direction: it is polarity insensitive. The model's prediction corresponds to our percept. We see a bar move, if it changes position consistently, irrespective of the bar's luminance.

The Motion Energy model has often been mapped onto the physiology of the visual cortex. Simple cells are seen as linear filters, while typical complex cells respond independent of the location and polarity of the stimulus presented within the RF (Movshon et al., 1978b, a, Carandini, 2006). V1 neurons monosynaptically connected to area MT, were classified as special complex cells (Movshon and Newsome, 1996). These results suggest that MT neurons are of the complex type.

The well known MT model from Simoncelli and Heeger (1998) is a good example for the general assumption that MT cells behave like complex cells. The model is an adaptation of the motion energy model. In the first stage, simple cells sample the stimulus with

multiple orientations and polarities. There output is half wave rectified and processed in complex cells, which provide the model input to area MT cells. The model is polarity insensitive due to the very early rectification between the simple and complex cell stages. Therefore, the model predicts area MT neurons to behave like complex cells and ignore the polarity of a stimulus. In other words, the response to briefly presented black or white bars should be identical.

We tested the model's prediction, i.e. that MT neurons are polarity insensitive. We presented randomly positioned flickering bars while we recorded responses from MT neurons. We performed reverse correlation and estimated the input filter (or RF) with spike triggered average (STA) and spike triggered covariance (STC), for use in the retina see (Chander and Chichilnisky, 2001), V1 see (Horwitz et al., 2005, Rust et al., 2005). A strong STA indicates strong polarity sensitivity and simple cell like behavior. If we can only find significant STC filters but no STA filter, the cell is polarity insensitive and complex-like (Rust et al., 2005). We compute the strength of the input filters with an information theoretic approach (Pillow and Simoncelli, 2006).

The first stage of the LN model is the linear input filter, the second the nonlinearity, which maps how well the stimulus matched the filter onto an expected firing rate (see introduction Figure 6 page 11). A symmetric nonlinearity indicates that both extremes of the filter contribute equally to the firing (complex-like) while an asymmetric nonlinearity indicates a strong preference for the sign of the stimulus (simple-like).

We found that the nonlinearities of the most informative filters were mostly asymmetric, which means that the vast majority of MT neurons' responses depended on the polarity of the stimulus. In other words, the behavior of MT neurons was more similar to that of simple cells than that of complex cells. Therefore, the current models of motion detection have to be altered significantly to take these new findings into account.

Materials and Methods

The monkeys viewed three randomly interleaved conditions, two OKN and one fixation condition. Here we only analyze the fixation condition. The task of the animals consisted of fixating a small red dot in the center of the monitor while we presented dynamic noise (see "Visual Stimuli" page 30). The animals received a drop of fruit juice for maintaining fixation in a 4° x 3° window.

Data analysis

Our data analysis is based on previously reported methods (Chichilnisky, 2001, Horwitz et al., 2005, Pillow and Simoncelli, 2006). Briefly, we reproduce the stimulus intensities for each pixel and time frame offline. In the case where we presented a smoothed stimulus (monkey S), we used the pre-smoothing stimulus, black or white bars, for the analysis, which is mathematically equivalent to whitening the smoothed stimulus we presented on the screen. The whitening is necessary because the STC requires that there is no covariation among luminance values in the stimulus itself. For the figures we low pass filtered the space-time filters from monkey S to present the filter the same way

as the stimuli were shown on the computer screen. We centered the luminance distribution on zero and normalized it with the standard deviation of the luminance values (z-score). Thus the mean of all luminance values is zero; the standard deviation is one. The data set with all luminance values presented over the course of the experiment is called the raw stimulus ensemble. For every single spike, we stored the 140ms preceding it in the spike triggered stimulus ensemble matrix.

The average of the raw stimulus ensemble is zero (with small deviations due to sampling); the covariance of the raw stimulus is the identity matrix (after whitening). The average of the spike triggered stimulus ensemble is the STA; the covariance of the spike triggered stimulus ensemble is the STC. Typically, spatiotemporal filters are extracted from the STC matrix with principal component analysis. We use information theoretic STA and STC analysis (iSTAC), an approach that finds the filters in both STA and STC at the same time (Pillow and Simoncelli, 2006).

Region of Interest Estimation

We defined a space-time region of interest (ROI) for each cell to reduce the number of dimensions (number of spatiotemporal pixels) used in the iSTAC analysis. This region of interest covers the complete RF and was calculated as follows. First, we calculated the significance of space-time filters for the following: the STA, the variance for the spike triggered stimulus ensemble, the average of the absolute spike triggered stimulus ensemble, and the first two and last two eigenvectors of a principal component analysis of the STC. For these seven filter types, we calculated random space-time filters—filters

based on zero correlation between stimulus and spikes—by creating a raw stimulus with different random luminance values and the corresponding spike triggered stimulus 256 times. For each of the seven filter types, we applied a threshold to the space-time maps at a significance level of 0.001 and counted the maximum number of neighboring, significant pixels. We define the ROI as a rectangle around all the pixels, which belong to a cluster bigger than 0.95 percent of the biggest random clusters of the 256 repetitions. Therefore, the ROI is defined as the region in space-time preceding spikes, where we found significant responses in at least one of the seven filters. Figure 13 shows the STAs of six neurons in their ROIs. We define the latency of a neuron as the time the firing of a cell was influenced by the stimulus, hence being in the ROI. A cell with an ROI that extends from -40 to -80ms in time has a latency of 40ms with the response extending to 80ms after the stimulus.

iSTAC

To estimate the information conveyed about the firing by the STA and STC, we apply the iSTAC method (Pillow and Simoncelli, 2006). For both STA and STC we only analyzed space-time pixels included in the ROI. In brief, the iSTAC analysis finds the filters that extend over the most informative subspace of the space spanned by the STA and STC. It minimizes the Kullback-Leibler (KL) divergence, an information theoretic measure of the difference between two distributions (Cover and Thomas, 1991). In the case of iSTAC, the raw and the spike triggered distributions are approximated with multi dimensional Gaussians. The iSTAC filters are sorted by the amount of information they contain, with

the biggest KL divergence corresponding to the first filter. The advantage of this method is that we perform optimization only on the STA and STC, not on the entire stimulus and spike train, which is computationally much more expensive. It also provides space-time filters similar to the traditional STA/STC analysis, hence simplifying interpretation.

We assessed the significance of an iSTAC filter with a nonparametric randomization test. To estimate the distribution of KL divergences under the null hypothesis of no correlation between stimuli and spikes, we created new raw stimulus ensembles with different values but identical statistics to the raw stimulus ensemble shown on the screen. We calculated the iSTAC filter and the corresponding KL divergences of the null stimuli. An iSTAC filter is significant, if its KL divergence exceeds 95% of the null KL divergences.

In the LN model framework the output of a linear filter is passed through a nonlinearity to estimate the firing rate of the neuron (Schwartz et al., 2006). We therefore project both the raw stimulus and the spike triggered stimulus into the dimension spanned by the iSTAC filters to estimate the probabilities of the raw stimulus and the stimulus in case of spike occurrences. We can divide the histogram of the spike triggered stimuli by the histogram of the raw ensemble and obtain the nonlinearity. We did this individually for each filter, because of the exponential growth of data needed to estimate the combined nonlinearities of several filters. The nonlinearity of the STA filter is asymmetric or flat (if the STA is 0). The nonlinearities of the STC filters are symmetric, STC filters cannot differentiate the polarity of the stimulus.

The iSTAC filters are independent of this classification, but often closely resemble either the STA or an STC filters. For comparison between cells, we normalize the nonlinearities of the iSTAC filters (see Figure 16A and B, page 44). To label the nonlinearities belonging to the iSTAC filters either symmetric or asymmetric, we fit a square polynomial to the nonlinearities of the five significant, most informative iSTAC filters of each cell. Non significant filters were excluded. We clustered the iSTAC filters into 3 groups based on the linear and a quadratic component of the fits (k-means clustering). The first group of nonlinearities had a strong linear component but a quadratic component around 0. This is typical for simple cells. The second and third groups had a linear component around zero and either a positive or negative quadratic component. The group with the positive quadratic component can be seen as belonging to complex excitatory filters, the group with the negative quadratic component belongs to complex inhibitory filters (Rust et al., 2005, Carandini, 2006).

For more detailed description and discussion of the iSTAC method, please refer to (Pillow and Simoncelli, 2006).

Simple/Complex Ratio Estimation

The KL divergence provides the information the iSTAC filters convey about the stimulus. We calculated the information ratio of simple and complex filters for all cells with significant ROIs. This was accomplished by dividing the KL divergence of a cell's first significant asymmetric nonlinearity (belonging to a simple filter) by the KL divergence of its first significant symmetric nonlinearity (belonging to a complex filter). Typical simple

cells should have a simple/complex ratio far above one, while typical complex cells have a simple/complex ratio near zero.

Preferred direction

We mapped all RFs with vertical bars. MT neurons that prefer different orientations could be affected by the mismatch of orientations. For most cells, we know the preferred direction from testing it with a circular motion stimulus (Schoppmann and Hoffmann, 1976, Krekelberg, 2008) prior to recording the responses to the dynamic noise. For some cells, where we could not record the responses to the circular motion, e.g. the cell was not well isolated at the start of the recording session; we used the preferred direction of neighboring cells. Neighboring cells in MT have similar properties (see Figure 3 page 6), thus we were able to infer the preferred directions of a cell from its neighbors. We defined the preferred direction as the absolute value of the cosine of the preferred angle. A preferred direction of one means the neuron was tuned for horizontal motion (perfect match with our stimulus orientation). Neurons with a preferred direction of zero were tuned for vertical motion, which did not fit the orientation of the stimulus presented.

Motion energy

In the motion energy model, the linear filters are slanted in space-time. If the filters with simple nonlinearities were less slanted than the filters with complex nonlinearities, then the contribution to motion detection would be weaker from simple filters. The simple

filters would be pure flicker detectors and not involved in motion detection. To test this, we transformed the filters into the Fourier domain and squared them, which resulted in a matrix where each entry corresponds to the motion energy for a spatial and temporal frequency. We subtracted the sum of motion energy corresponding to leftward motion from the sum of motion energy corresponding to rightward motion. Then, the absolute difference value indicated the strength of motion tuning. We divided the difference by the size of the ROI to make its value comparable between cells.

Results

We recorded the action potentials of 57 neurons in area MT of two awake behaving monkeys while presenting randomly positioned, flickering bars on a CRT computer
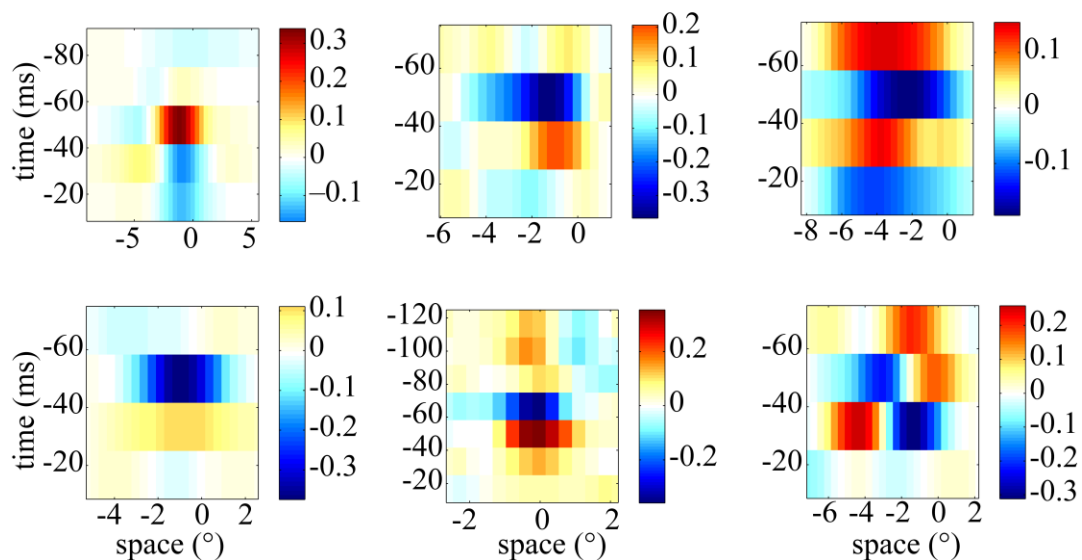
Figure 13: Example STAs. These are the filters of six MT neurons calculated with reverse correlation. The horizontal axis represents space, the vertical time before spikes. The figures only show the ROI, the area with significant responses (See Methods).

screen at 50 or 60 Hz. The bars were oriented vertically irrespective of the cells preferred direction. We recreated the stimulus offline and performed reverse correlation to estimate STA and STC (see Figure 13 for the STAs of six example neurons). The STA is composed of the average luminance values preceding the spikes; the STC is composed of the covariance of the stimulus preceding the spikes. STA and STC span a multidimensional subspace. We used iSTAC analysis (Pillow and Simoncelli, 2006) to find the most informative filters in this subspace.

Below, we first present the results of iSTAC analysis of two example neurons, one behaving like a simple cell (polarity insensitive) and one behaving like a complex cell (polarity sensitive). After that, we present the results of the MT neuron population.

iSTAC Examples

Both examples were recorded from monkey S. Figure 14 shows the space-time RF maps for one neuron, which behaved like a simple cell. The top left panel shows the first iSTAC filter, the most informative one. The STA of the same cell is in the top left subplot in Figure 13; they are almost identical. This is expected from simple cells in V1 (Rust et al., 2005, Carandini, 2006). Notice the similarity between the information conveyed in the STA (0.165 bit) and the first iSTAC component (0.172 bit) in the bottom right of Figure 14. We mapped the match between the stimulus and one of the iSTAC filters (the axis projection) onto a firing rate, which allows us to interpret the contribution of the individual iSTAC filters on the firing rate. This transfer function is called the nonlinearity. The blue line in the bottom left plot of Figure 14, the nonlinearity of the first iSTAC filter,
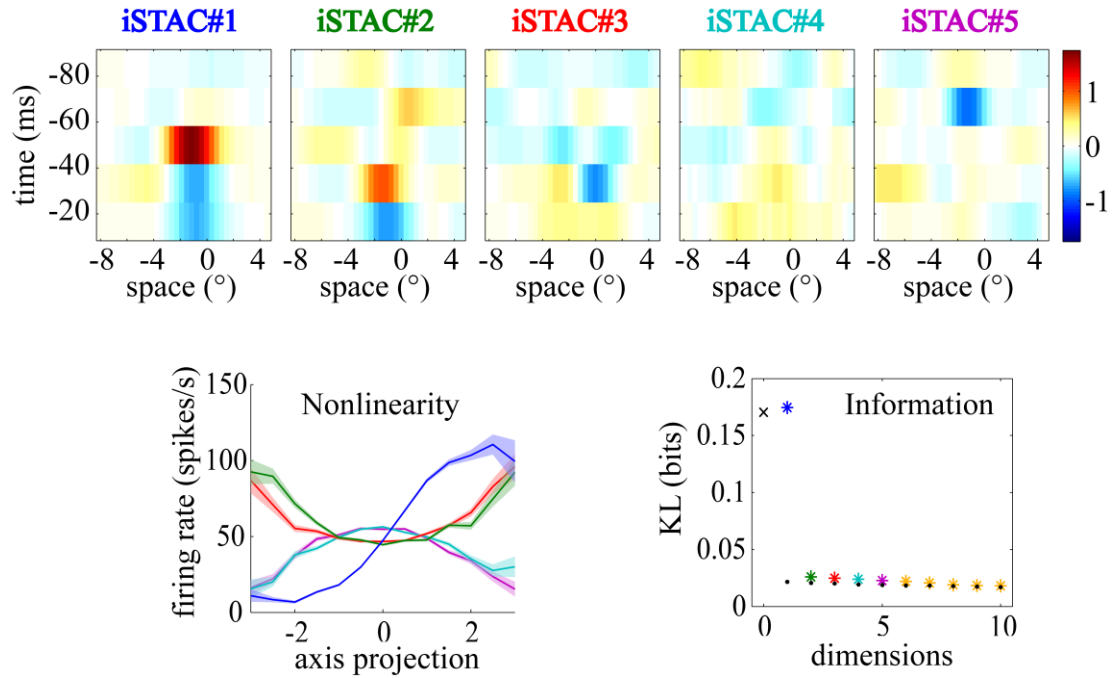
Figure 14: Example of Polarity Sensitive Neuron. The top shows the five most informative iSTAC filters (spatiotemporal RF filters) of the neuron zoomed into the ROI. The horizontal axes indicate space in degrees; the vertical axes represent time preceding the spikes in milliseconds. In the bottom left, the five independent nonlinearities for the first five iSTAC component are plotted in the following order: blue, green, red, cyan, and magenta. The shaded areas show the standard error. The plot on the bottom right shows the amount of information per iSTAC filter in bits for ten iSTAC filters. The black x located at 0 dimensions indicates the amount of information the STA by itself conveyed. The black error bars, visible as dots, show the information of filters estimated with random stimuli (see methods).

is clearly asymmetric. If the stimulus projected onto the first filter was zero—the stimulus is orthogonal—the response of the neuron was at the average level (55Hz). If the stimulus fit the iSTAC filter well, e.g. the axis projection is +2, the firing rate was high (up to 130Hz). If the axis projection was negative, the cell was firing much less (down to 15Hz).
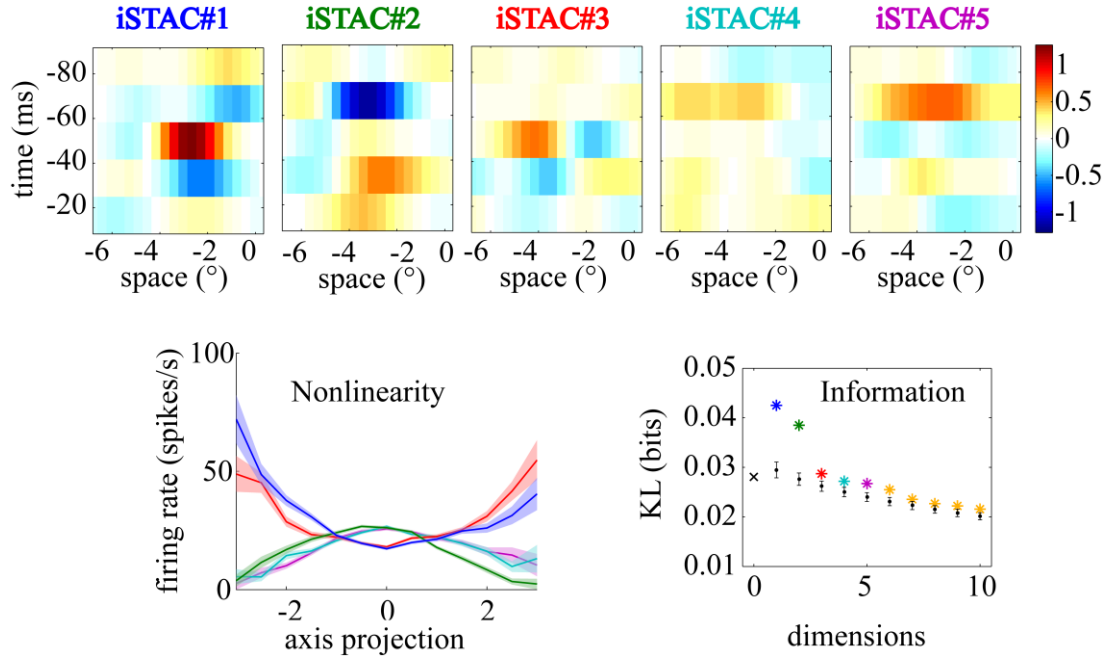
Figure 15: Example of a Polarity Insensitive Neuron. The plots are the same as in Figure 14. In brief, the top row shows the first five iSTAC filters. The bottom left shows the nonlinearities of the iSTAC filters, the bottom right shows the information conveyed by the iSTAC filters.

Figure 15 shows the same plots as Figure 14, but for a neuron that shows properties as expected of a complex cell. The information conveyed by the first two iSTAC components (0.042 and 0.038 bit) is higher than that of the STA (0.028 bit, indicated by the black x in the bottom right panel). The nonlinearities for the first five iSTAC filters are symmetric, indicating that the cell's response is independent of the polarity of the stimulus. If the firing rate is elevated for extreme axes projections, we say the filter is excitatory, if the firing rate is lowered for a good match of filter and stimulus, we call the filter inhibitory.

Nonlinearities:

The first iSTAC component has the most information about the stimulus. In Figure 16 A we show the normalized nonlinearities of all cells that had at least a first significant iSTAC component. The cells are sorted by the strength of the central component (axis projection zero) compared to the strength of the extreme components. Most cells had a strongly asymmetric nonlinearity, negative axis projections were low and positive projections are high (cells 2-50). To quantify we fit a quadratic polynomial to the nonlinearities.

Figure 16 C shows the linear components plotted against the
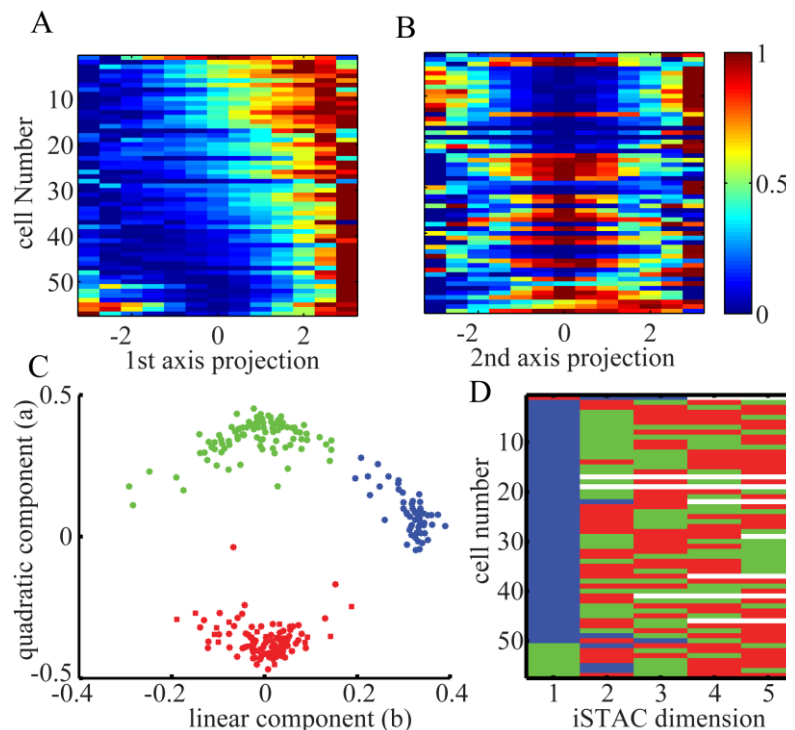
Figure 16: The Nonlinearities. A) The normalized nonlinearities for all cells with a significant iSTAC filter. They are sorted by the center value minus the mean of the most extreme values of the axis projection. B) The nonlinearities of the second iSTAC filters in the same order as A). C) The linear component is shown versus the quadratic component of quadratic fits of the normalized nonlinearities. K-means cluster analysis finds three clusters. D) examining the results form C) we assigned a color to the first five iSTAC components (blue: simple; green: excitatory; red: inhibitory) for all cells. Non significant iSTAC filters are replaced with a white patch.

quadratic components of all significant nonlinearities. Three clusters emerged, one with

a positive linear component (simple, marked blue) and two around a linear component

of zero, one with a positive quadratic component (excitatory, marked green) and one

with a negative quadratic component (inhibitory, marked red). In Figure 16 D we labeled

each iSTAC filter by one of these three categories. The first iSTAC component, which is

most informative, was most often asymmetric and hence simple cell like (blue).

Interestingly, even though there were a few complex-like cells with excitatory

nonlinearities (green), the first iSTAC component was almost never inhibitory (red).

Simple/Complex Ratio

In Figure 16, we show that the most informative filters of the majority of neurons had nonlinearities that were similar to nonlinearities which we expect from simple cells. In Figure 17 A, we quantify this by
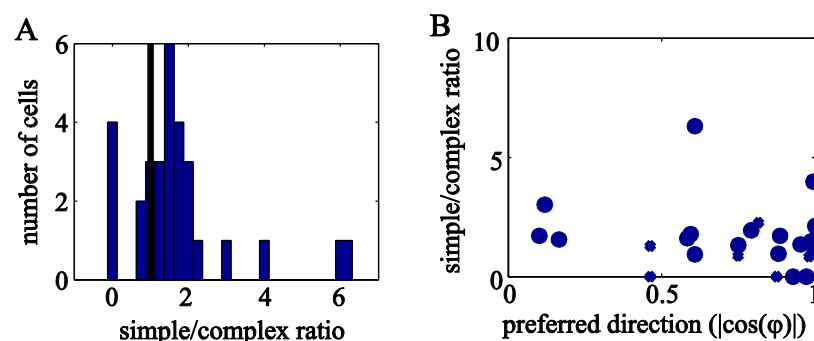
Figure 17: The Information Ratio for the Population. A) Histogram of the information ratio, calculated by dividing the information of the simple iSTAC component by the most informative excitatory or inhibitory dimension. B) The vertical indicates the information ratio (see A), the horizontal axis shows the preferred direction, which is the absolute value of the cosine of the preferred angle. If the cells like upward or downward motion, the preferred direction value is 0. Leftward and rightward motion result in a preferred direction value of one. Circled symbol indicate that the preferred direction is measured for the same cell, the preferred direction for other data points is derived from neighboring MT neurons.

presenting the simple/complex ratio, the ratio of the most informative asymmetric (thus simple-like) filter divided by the most informative excitatory or inhibitory (thus complex-like) filter. Cells with a simple/complex ratio higher than one were the cells labeled blue in the first column of Figure 17 D. The mean of the ratio was 2.2, indicating that for the complete population the simple filter carried more than twice the information compared to the strongest excitatory or inhibitory filter. Cells without any simple component have a simple/complex ratio of zero.

The stimulus on the screen always consisted of vertical bars. Therefore, random motion induced by the flickering could only move to the left or right. The preferred direction of MT neurons varies and hence, the prevalence of simple input could result from a mismatch of the preferred direction of neurons

and the motion induced by the stimulus. To investigate this we present the simple/complex ratio as a function of the preferred direction in Figure 17B. Clearly, the preferred direction did not affect the simple/complex ratio.

Motion Tuning of the iSTAC Filters

According to the motion energy model, all filters should be slanted in space-time. We define the motion tuning of a filter as the difference of filter power (motion energy) for leftward and
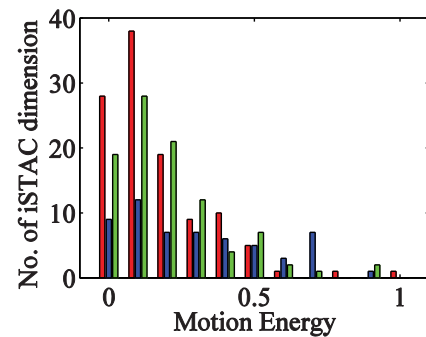
Figure 18: Motion Tuning of iSTAC Filters. The blue bars represent the number of simple-like iSTAC filters depending on their motion tuning, (see Methods). There are more complex-like iSTAC filters (red: inhibitory; green, excitatory), but their motion tuning is lower compared to the simple-like iSTAC filters.

rightward motion (see Methods). Figure 18 is a histogram, where all iSTAC filters shown in the bottom row of Figure 16 are represented with their corresponding motion tuning (same color code). The simple filters have on average more motion tuning than the complex excitatory (green) filters, thus are more direction selective. The complex inhibitory filters (red) are least tuned for direction.

Discussion

In project one of this thesis, we present an information theoretic motivated approach to determine the behavior of area MT neurons. We show, contrary to the current beliefs in the literature, that the majority of neurons in MT have spatiotemporal RFs (filters) that are sensitive to the polarity of the stimulus. Hence, a black bar and a white bar moving with the same speed in the same direction elicit different responses; the majority of MT neurons behave like simple cells. First, we will discuss the spatiotemporal filters we found in area MT. Second, we will discuss the implications of these findings for the presumed physiological and anatomical connections between V1 and MT. Third, we will discuss the implications for models of MT and motion processing.

Receptive fields in MT

For most neurons, we found a significant STA. This by itself is surprising, given the current understanding of area MT. Some of the STAs are space-time filters with a slant (e.g. the STA on the bottom right of Figure 13 page 40), as expected from direction selective cells. But others do not (e.g. bottom left of Figure 13). When we mapped the filters, we used vertical bars and therefore, any motion presented on the screen was

horizontal. iSTAC analysis of a neuron perfectly tuned to upward or downward motion would not reveal slanted space-time filters. We analyzed the preferred direction of each neuron and compared it to the simple/complex ratio, to rule out the possibility that the cells that were most simple are tuned to vertical motion. Figure 17 B shows that this was not the case; the simple/complex ratio was not correlated with the preferred direction. This shows that the simple-like filters contribute strongly to the motion tuning of MT neurons.

Different spatiotemporal filters than V1

Most of our spatiotemporal filters looked different from spatiotemporal filters reported previously in V1 measured with similar methods (Rust et al., 2005). Some methodological differences may have contributed to these differences. For instance, Rust et al. oriented the bars in the preferred direction of the neuron; we did not. Other differences, however, may be area specific. For instance, our MT neurons' latency and the extent of their temporal response were very short. The typical response lay between 40ms and 80ms (the range of ROIs). Neurons in area V1 usually integrate over time courses over 100ms when measured with reverse correlation (Horwitz et al., 2005, Rust et al., 2005). MT neurons sample from a sub-set of V1 cells, which receive fast input and respond fast. This makes these neurons well equipped to detect fast onsets or changes in the visual field.

Physiology

As described in the General Introduction, Hubel and Wiesel defined simple cells as cells with distinct antagonistic regions in their RFs and complex cells as cells that are not simple cells (Hubel and Wiesel, 1962). Later, it was shown that complex cells are mostly insensitive to the polarity of stimuli (Movshon et al., 1978b, a). Further, if mostly complex cells project to MT, as suggested (Movshon and Newsome, 1996), then MT cells would also be polarity insensitive. Our results clearly show that input to area MT cannot come solely from the typical complex cells as suggested in the literature.

In a study that identified V1 neurons that were monosynaptically connected to MT (Movshon and Newsome, 1996), all twelve V1 neurons were of the special complex type. Half of the neurons were found in layer 4 and half in layer 6, while the ratio expected from anatomical studies should be 10:1 (Maunsell and van Essen, 1983a). Movshon and Newsome did not measure polarity sensitivity directly but for one cell, which was polarity insensitive. We also recorded from some polarity sensitive neurons. And most neurons have some polarity insensitive filters, which likely arises from complex cell input. Thus their data do not directly conflict with ours. But, the interpretation (by Newsome and Movshon as well as others later) has been that only polarity insensitive special complex cells project to area MT. Contrary to this, we show that strong polarity sensitive input arrives in area MT.

Some complex cells in V1 lose some of their polarity insensitivity when tested with lower spatial frequencies (Movshon 1978b); they could be classified as simple cells

under these conditions. The highest frequency our random noise stimulus could have was around 0.5Hz and is therefore on the low end of the range tested by Movshon et al.. If the input to area MT arises in complex cells that show polarity sensitivity at low frequencies, then iSTAC filters should be polarity sensitive for low frequencies, which we tested, and polarity insensitive for high spatial frequencies. Further studies are needed to test this issue by testing MT cells with high spatial frequency noise.

Pillow and Simoncelli (2006) presented results of iSTAC analysis for one complex cell in V1, which had mostly symmetric nonlinearities. In future work, one could classify a population of direction selective V1 neurons and calculate their simple/complex ratio. We hypothesize that this population would have a continuum of ratios similar to our findings in MT. Comparing the iSTAC classification to traditional classification methods, i.e. moving light over a screen in a few directions, would allow us to test both the strength of the iSTAC classification and confirm how accurate traditional methods are. If most complex cells have a simple/complex ratio around one, i.e. simple and first complex input are equally strong, then our finding that MT cells have low ratio values would not be a surprise. But this would alter our understanding of complex cells. Complex cells could have some part of the RF that is polarity insensitive, but the rest could well be polarity sensitive.

Linearity

Often it is assumed that cells that have a linear response cannot be motion sensitive. And indeed, a truly linear cell cannot respond to e.g. leftward motion only, it would

always respond opposite to motion to the right (Poggio and Reichardt, 1973). But simple cells are not truly linear; we model them with a linear filter followed by a static nonlinearity. The nonlinearity abolishes the negative response to the motion to the right in our above example, and therefore the simple cells can be motion sensitive.

Models

Our findings do not imply that the population response of area MT is polarity sensitive. For population polarity insensitivity we simply have to assume that for each cell that we recorded, there is another cell with a simple filter with the opposite polarity but the same asymmetric nonlinearity. The responses of the two cells would then on average be polarity insensitive. This could be one explanation why motion perception is polarity insensitive even though our data show that individual MT cells are polarity sensitive.

The MT model from Simoncelli and Heeger, which maps the architecture of the motion energy model onto the physiology, tries to predict the responses of single neurons. One of the first stages of the model is half wave rectification of the output of simple cells, every step after that contains only signals that are polarity insensitive. This model is inconsistent with our physiological results. A new model of MT should take our findings into account. An easy solution could be to flatten the hierarchy. That is to include simple cell projections to area MT.

Chapter 4 RF Positions during Slow Eye Movements (Project 2)

Introduction

Humans perform approximately 100,000 eye movements per day, and with each eye movement, the physical image of the outside world lands on a different location on the retina. In early vision, RFs are eye-centered; if the eye moves 10° to the left so does the RF. This implies that the neural representation of the world in early visual cortex changes with every eye movement. Despite these changes in incoming information, however, the visually perceived world is relatively stable.

One way to create this perceptual stability is to construct spatial RFs that are independent of eye position. There is evidence for such head-centered RFs in the parietal cortex of the macaque (Duhamel et al., 1997, Galletti et al., 1999), for review: (Snyder, 2000). These RFs, however, are typically large (often covering more than a quarter of the visual field), and they represent only a small subset of the features known to be represented in earlier visual areas. It is difficult to see how these parietal neurons could underlie perceptual stability of elementary visual features at a fine spatial scale, hence a search for head-centered mechanisms in earlier visual areas is warranted.

The existence of head-centered mechanisms for the analysis and integration of motion signals has recently been a topic of debate. Some human behavioral studies have argued that motion is integrated by head-centered detectors (Melcher and Morrone, 2003, Ong et al., 2009), while others have shown that these phenomena can be understood using

only eye-centered motion detectors (Morris et al., 2009). Functional imaging of the main motion processing area in the human brain has also led to conflicting results, with one study showing head-centered (d'Avossa et al., 2007), and another only eye-centered responses (Gardner et al., 2008). Our study tests whether RFs in area MT are eye- or head-centered.

An alternative mechanism for the integration of spatial information across eye movements is to transfer information from neurons that respond to a given location in space before an eye movement to the neurons that respond to that same location after the eye movement. For a brief period of time, such neurons do not code in eye-centered coordinates. This mechanism—called remapping—was first observed in LIP (Duhamel et al., 1992), but others have reported similar temporary changes in the neural response profile around saccades in various regions of the brain, including the FEF (Umeno and Goldberg, 1997), SC (Walker et al., 1995), and in area V3 (Nakamura and Colby, 2002). Some of the functional reasons to integrate information across eye movements are the same whether the eye movements are fast or slow. Moreover, perceptual effects such as mislocalization of briefly flashed stimuli, occur not only during fast, but also during slow eye movements (Kaminiarz et al., 2007) and are often presumed to be related to remapping. For these reasons, we investigated whether a form of remapping could also be found during slow eye movements.

One previous study has shown indirectly that neurons in area MT likely encode spatial information in an eye-centered frame of reference (Krekelberg et al., 2003), but there

has been little quantitative research that directly addresses this question. Given the controversy in the literature, we considered it important to map MT RFs quantitatively and investigate their properties during eye movements. We determined the RFs of cells in area MT during fixation and OKN—slow pursuit phases interspersed with fast saccade-like movements in the opposite direction. To strengthen the link with functional imaging studies we not only determined the RFs based on extracellular action potentials, but also the RFs based on LFPs. Our data clearly show that both RFs, spike-based and LFP-based, in area MT are firmly yoked to the eye during the slow phases of OKN.

Materials and Methods

Below we describe the data analysis specific to this chapter (see "General Material and Recording Methods" pages 26ff for methods common to all chapters).

Data analysis

Estimation of the Linear RF

We determined the best linear approximation of the complex relationship between the neural response and the stimulus pattern. Formally, we expressed the stimulus pattern (Y) as a linear combination of the neural response (X) plus noise ε:

$$Y = X\beta + \varepsilon$$

In this form, the problem is equivalent to a General Linear Model (GLM), with Y being the regressand, X the design matrix, and β a matrix of regression coefficients. In our

case, these coefficients corresponded to the space-time RF map. Standard GLM methods not only provide the estimate of $\boldsymbol{\beta}$ that minimizes the error term, but also provide significance values for each of the coefficients based on F-tests.

Specifically, the regressand $\boldsymbol{Y}$ is an N x T matrix representing the stimulus. N is the number of pixels on the screen (1024). T is the number of stimulus frames (typically 25,000-75,000). We used the eye-position, as measured by the eye tracker, to align the monitor pixel at the fovea with the center of the matrix. After this alignment the value $\boldsymbol{Y}$(512,100), for instance, is the luminance of the pixel that was directly at the fovea in the 100th stimulus frame. In other words, the first dimension of the $\boldsymbol{Y}$ matrix represents stimulus location (in monitor pixels) in eye-centered coordinates. Stimulus locations beyond the edge of the screen were assigned a value of zero.

The design matrix $\boldsymbol{X}$ is a T x M matrix representing the neural data; each column is a regressor. The first regressor represents the neural data at zero delay compared to the stimulus. Each entry in this vector contains either the number of spikes per stimulus frame (to determine the spike RF), or the LFP averaged over a stimulus time frame (LFP RF). In the OKN conditions, we excluded neural signals recorded from 75ms before to 150ms after the onset of the fast phase. The other columns of the design matrix also contain the neural data vector, but each is shifted by a temporal offset. For each regressor this offset is increased by the duration of one frame. For example, the 4th regressor contains the neural activity that occurred 3 frames, i.e. 50ms (monkey S) or

60ms (monkey N), after the stimulus frame appeared on the screen. The last regressor is filled with ones; it is the constant term of the linear model.

Solving the regression model results in a coefficient matrix $\boldsymbol{\beta}$ with N columns and M rows. The last row of the coefficient matrix, the intercept, contains the average of all stimulus frames for each pixel. For an infinite data set, this would be zero (corresponding to the mean of the stimulus values). This intercept is required for the statistical evaluation of the data using F-tests, and plays a role analogous to the whitening procedure sometimes used in spike-triggered averaging. The next row in $\boldsymbol{\beta}$ represents the coefficients that predict the stimulus frames for all 1024 pixels from neural data recorded at the same time. Each following row contains the coefficients that establish the linear relationship between the stimulus and the neural data with a bigger temporal offset. Thus, the coefficient matrix establishes the linear model that relates the space-time stimulus to the neural data; we interpret it as the space-time RF map.

For the spike RF—the neural data X contained spike counts per stimulus frame—a high value in the RF map (e.g. at 5° and -50ms) indicates that a bright bar 5° to the right of the fovea was typically followed by spikes 50ms later (for example see Figure 19). The interpretation of the LFP RF map is similar, but with one difference that arises from the fact that—unlike the spike count—the LFP can be negative. As a result, a high LFP RF value can be explained two ways. Either a bright bar was often followed by a high positive LFP, or a dark bar was often followed by a low negative LFP. We used the raw LFP signal and not the LFP power (squared LFP) because the RF maps obtained with the

raw LFP yielded higher significance. This implies that locations on the screen at which a bright or dark bar consistently changed the LFP power, but with a random phase each time were not included in our definition of the LFP RF.

The GLM analysis provides a significance value per space-time pixel in the RF map. As a consequence, a simple uncorrected threshold of $p<0.01$, would lead to RF maps with, on average, ca. 100 significant pixels even for neural data consisting entirely of noise ($0.01*8*1024$, where 8 is the number of time points, and 1024 the horizontal number of pixels in the monitor). We used a bootstrap permutation test to exclude such Type-I errors without applying an overly conservative Bonferroni correction. For each neuron and LFP site, we generated a random stimulus sequence, and then calculated the size of the largest cluster of contiguous space-time pixels in the map. This process was repeated 100 times to create a null distribution of space-time cluster sizes. We then compared the cluster size obtained with the actual stimulus to this distribution and discarded all clusters whose size was less than the 95th percentile of the null distribution. The remaining pixels are significant at the $p<0.05$ level, corrected for multiple comparisons. We excluded cells and LFP sites if none of the pixels of the fixation RF Map passed this threshold; this removed 1 LFP site from monkey N and 19 neurons and 6 LFP sites for monkey S from our analysis.

We defined the location of the RF as the spatial coordinate of the centroid of the significant pixels and the size of the RF as the spatial extent spanned by the significant pixels.

RF Reference Frames

To determine an RF's reference frame, we estimated the RFs at different eye positions. We split the recorded eye positions during OKN into three blocks with an equal number of time points; the third of the data where the eyes were directed most leftward, the third where the eyes were directed most rightward, and the third of the data in between. The mean of the eye positions in these three blocks could be different depending on the condition (leftward versus rightward OKN), or recording day.

We used the corresponding subsets of neural data to fill the design matrix only with the data recorded at these different eye positions. This resulted in seven independent RF maps (three for each OKN condition, one for fixation), and seven corresponding average eye positions.

To determine the relative location of the RFs without making assumptions about RF shape, we cross-correlated each of the six independent RF maps recorded during OKN with the RF map estimated using the fixation data (Duhamel et al., 1997). The spatial shift at which the cross-correlation peaked was considered the shift of the RF relative to the fixation condition. For each of the six RF maps recorded during OKN, we then calculated the RF location on the screen as the sum of the mean eye position, the location of the fixation RF, plus the shift of the RF determined by cross-correlation.

The head-centered RF hypothesis predicts that RF location is independent of eye position, while the eye-centered hypothesis predicts that RF location is linearly related

to eye position. To test these hypotheses, we assumed a linear relationship between RF location and mean eye position:

$$RF = m * eye + b,$$

We determined the parameters of this equation by robust linear regression with a bisquare weighting method. The slope m is a measure of the reference frame; we refer to it as the reference frame index (RFI). Eye-centered cells have an RFI of 1; head-centered cells have an RFI of 0. The constant term b is the position of the RF while looking straight ahead (when eye and screen coordinates are equal). We used the standard error of the regression (σ) as a measure of the goodness of fit.

RF Remapping

Receptive fields have been shown to shift their location around fast eye movements (Duhamel et al., 1992). To investigate whether RFs shift similarly during the slow phase of OKN, we fixed the slope m of the linear fit to the value obtained while determining the reference frame, but allowed the offset b to vary independently for the leftward and rightward slow phase. The offset b is the retinal location of the RF while the eye is looking straight ahead. If RFs shifted in the direction of the eye movement, one would expect b to be greater in the rightward than in the leftward OKN condition. We defined the remapping shift as half the difference between the offsets in the leftward and rightward OKN conditions. Statistical significance of the remapping shift was assessed at the population level by performing a sign test. While it would be possible to investigate a model in which both b and m could vary depending on the direction of the eye

movement, such a model is underconstrained given that we have only three data points (i.e. eye positions) per condition.

We used a Monte Carlo simulation to determine the minimal size of the remapping shift at which our statistical analysis would reject the null hypothesis that no shift occurred. We simulated data sets in which a simulated offset (ε) was assumed for both the leftward and rightward OKN conditions. This ε was drawn - separately for each recording - from a Gaussian distribution with a mean that was systematically varied from -2° to 2° and a standard deviation equal to the standard deviation of the estimated offset parameter b for that recording. We repeated this procedure 1000 times for each simulated data set. We defined the upper bound of the remapping shift as the smallest mean simulated offset for which the sign test rejected the null hypothesis at the 0.05 significance level in more than 80% of cases. In other words, this is the remapping shift at which both type-I (false positive) and type-II (false-negative) statistical errors were controlled at conventional levels (alpha=0.05, beta= 0.8).

Results

We present data from 76 single neurons and 53 LFP recording sites in area MT in two right hemispheres of two macaque monkeys (monkey N: neurons = 31, LFPs= 23, monkey S: neurons = 45, LFPs = 30). Each trial started with the monkey fixating a target in the center; this triggered the start of dynamic noise on the computer screen, which elicited neural responses that we used to estimate the RF. The monkeys either fixated

throughout the trial, or they performed OKN induced by a random dot pattern moving leftward or rightward.

The average (± standard deviation) fast phase frequencies were 2.5Hz ±0.2Hz (monkey S) and 3.4Hz ±0.2Hz (monkey N). In humans, such high beating frequencies are typically associated with stare nystagmus (Konen et al., 2005, Knapp et al., 2008). The mean and standard deviation of the gain of the slow phase was 0.82 ± 0.05 (monkey S) and 0.95 ± 0.05 (monkey N). A separate behavioral experiment in which OKN was induced in the presence or absence of the flickering bar stimulus showed that presence of the full-field flicker did not affect the slow-phase gain of the OKN significantly (p>0.15).

First, we present examples of RF maps based on spikes and LFPs recorded during steady fixation and show how these RF measures are related. We then turn to the main question: how eye position and eye movement affect RF locations.

Spike and LFP Receptive Field Estimates

We estimated the RFs with a General Linear Model (see Methods). Figure 19 shows two pairs of RF maps for single units and LFPs recorded simultaneously with the same electrode.
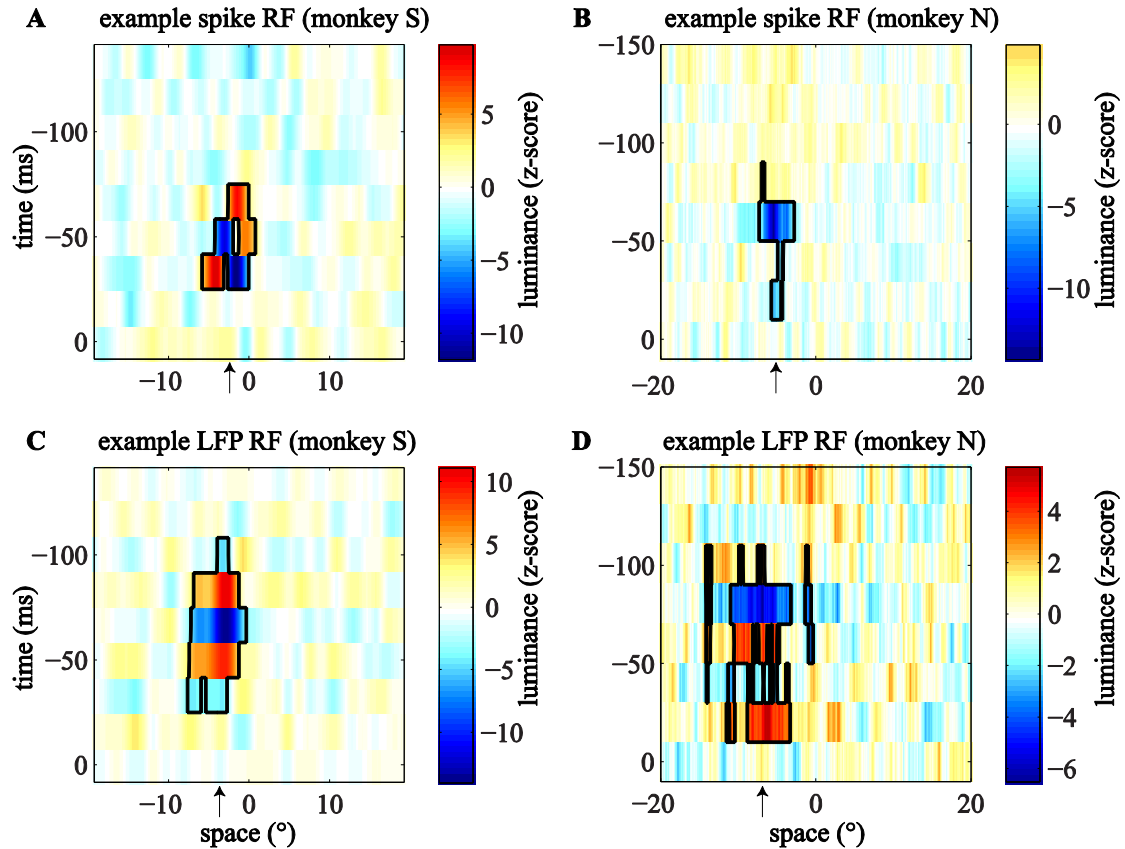
Figure 19: Example RF Maps. Each of the four images shows a spatiotemporal RF map. The axes are space (°), where 0 indicates the position of the fovea, and time (ms), where 0 is the time at which the neural data were recorded. The color represents luminance (Z scored) and indicates the strength and sign of the RF. The black borders show the clusters in the space-time RF map that were significant (bootstrap test; see Methods). A) The spike RF of a single cell recorded in monkey S. B) The spike RF of a single cell from monkey N. C) and D) The RF of the LFPs recorded at the same sites as the single cells in A and B, respectively. The black arrows indicate the estimated positions of the RFs. See main text for a full description.

In the spike RF maps, a bright red patch at a specific (x, t) location indicates that t ms before a high firing rate occurs, a higher than average luminance is typically seen at retinal position x. The interpretation of LFP RF is analogous, with the exception that unlike spike rates, LFPs can be positive or negative, hence a bright red patch can correspond to a higher than average luminance followed by a high positive LFP, or a

lower than average luminance followed by a very negative LFP. The color maps are centered on the same value, such that white represents the mean of the luminance distribution (i.e. no relation between neural activity and luminance), red represents luminance above the mean, and blue represents luminance below the mean.

To provide a scale that can be compared across recordings, we scaled the RF maps to the standard deviation of the luminance distribution outside the RF (z-score). At the same time, however, we wished to visualize RF structure independently of the degree of statistical confidence (which depends on the consistency of the neural response, as well as the somewhat arbitrary duration of the recording). To achieve this, we allowed the color scale (see Figure 19) to vary across RF maps. With this convention, numerical (z-score) values can be compared across RF maps to compare consistency of the RFs, but colors are defined per map only.

Note that the RF maps for monkey S (left side of Figure 19) appear smoother than those on the right (monkey N) because the stimulus presented to monkey S was spatially low pass filtered (see Methods).

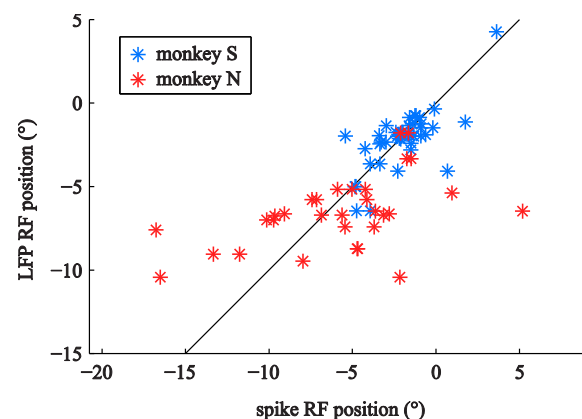We quantified the location of the RF as the centroid of all significant

Figure 20: RF Position Correlation. The LFP RF position (vertical axis) is shown as a function of the spike RF positions (horizontal axis). Gray elements represent RFs from monkey N, black elements from monkey S. For both monkeys, LFP and spike RF position were significantly correlated.

clusters in the RF map. In Figure 19, the spatial components of the centroids for the spike RF and the LFP RF were -2.34° and -3.69 (panel A and C) and -5.11° and -6.87° (panel B and D). The horizontal locations of the spike RF and LFP RF were highly correlated (see Figure 20). The Pearson correlation for monkey S was r = 0.70 (p < 10^{-7}) and r = 0.49 (p < 0.005) for monkey N. Similarly, we quantified RF size as the horizontal spatial extent of all significant clusters. For monkey S the average RF size ± standard deviation was 4.6° ± 2.6° for spike RFs and 5.9° ± 2.6° for LFP RFs, the mean RF sizes for monkey N were 4.7° ± 4.1° for spike RFs and 8.1° ± 7.4° for LFP RFs. The size of spike RFs and LFP RFs were not significantly correlated (p > 0.3) and LFP RFs were significantly larger than spike RFs (rank-sum test, p < 0.001). Please note that our one-dimensional stimulus pattern does not allow us to estimate vertical extent or retinal eccentricity of the RFs, thus they are not reported here.
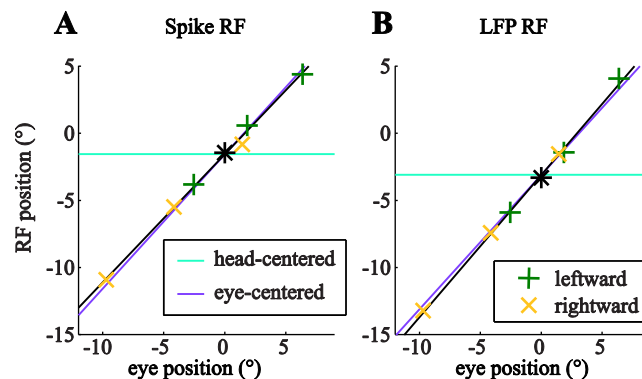
RF Reference Frames

Figure 21 shows the RF locations of one example neuron (panel A) and the simultaneously recorded LFP (panel B) for seven eye

Figure 21: RF Reference Frame Estimation. The 7 elements correspond to the 7 independent pairs of eye position and RF position in screen coordinates ((+: leftward slow phase; x: rightward slow phase; *: fixation). The purple lines show the prediction of a pure eye-centered RF (Reference Frame Index, RFI=1). The cyan lines show the prediction of a head-centered RF (RFI= 0). The black lines show the linear fit. A) RF location of a spike RF. B) RF location of the LFP RF from the same electrode (monkey N). These example recordings show receptive fields that clearly move with

positions (see Methods). The relationship between RF location and eye position was obviously well described by a line with a slope of 0.95 for the spike RF (panel A). We refer to this slope as the reference frame index (RFI, see Methods). The LFP RF had an RFI of 1.08. A perfectly eye-centered RF has an RFI of 1 (black dash-dotted line); a head-centered RF has an RFI of 0 (black dotted line).
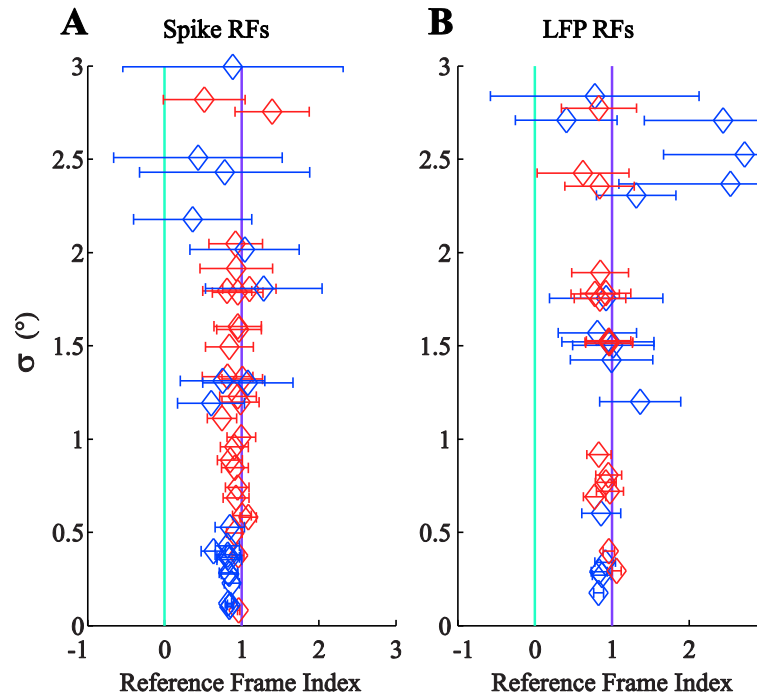
Figure 22: Population Overview of Reference Frames. A) Reference Frame Index (RFI) for all spike RFs (red, monkey N; blue, monkey S) with a goodness of fit (σ) better than 3° (for RFI and σ, see Methods). The horizontal bars on the data points show the confidence intervals for the estimates of the RFIs. B) RFIs for LFP RFs, same conventions as panel A. These data show that both spike and LFP RFs in MT moved with the eye.

Figure 22 shows the RFIs for the population. To give an indication of the noise in these RFI estimates, we plot σ as a function of the RFI (with confidence intervals). σ is the standard error of the regression, which is a measure of the goodness of fit. It is $0.38°$ for the cell in Figure 21A, and $0.29°$ for the LFP RF in Figure 21B. For both spike and LFP RFs the RFIs are near 1. The mean and standard deviation of all RFIs was 0.92 ± 0.50 for spike RFs and 0.97 ± 0.50 for LFP RFs. High RFIs (i.e. eye-centered reference frames)

were almost always found when we had enough data to get a reliable estimate of the RF

(small σ and small error bar). For instance, for σ < 3°, 79% of spike RFIs and 71% of LFP

RFIs lay between 0.8 and 1.2.

RF Remapping

Next, we investigated whether there were shifts in RF position that depended not on eye-position but on eye movement direction. For instance, one might expect RFs to run ahead of their retinal location during fixation; this would be analogous to the predictive remapping that is found before saccades in area LIP (Duhamel et al., 1992). We fit the RF positions during the

Figure 23: Assessment of RF Remapping during the Slow Phase of OKN. The 7 elements correspond to the 7 independent eye position/RF position pairs ((+: leftward slow phase; x: rightward slow phase; *: fixation). The lines in each plot correspond to two fits with the same slope to the rightward slow phase (yellow line) and the leftward slow phase (green line). The offsets of the fitted lines represent the retinal location of the RF when looking straight ahead. A) RF location based on spikes. B) RF location based on the LFP recorded from the same electrode (monkey N). The retinal locations of the RFs were not significantly different during leftward and rightward slow eye movements; there was no evidence for remapping in these example recordings.

two slow phases independently while keeping the slope of the lines fixed (see Methods).

The constant term in these linear fits corresponds to the retinal location of the RF when

the eye is pointing straight ahead. If RFs remapped their location during slow eye

movements, one would expect this retinal RF location to differ between rightward and leftward slow eye movements.

For the example shown in Figure 23A, the retinal location was -1.42° ± 0.67° during the leftward slow phase, while it was -1.80° ± 1.92° for the rightward slow phase (estimate ± 95% confidence interval). The two positions were not significantly different. Figure 23B shows the same analysis for the simultaneously recorded LFP RFs; again, the eye movement direction did not significantly affect the RF location (-3.13° ± 1.01 leftward slow phase, -3.01° ± 0.31 rightward slow phase). Figure 23 shows data from the same recording site as in Figure 20.

To provide a population overview, Figure 24 plots the retinal RF location while looking straight ahead during rightward OKN as a
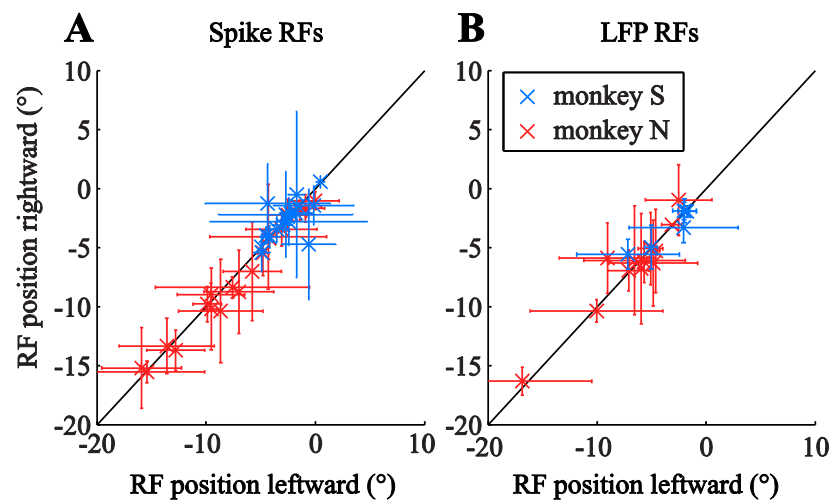
Figure 24: Population Overview of the (Absence of) Remapping. Error bars represent confidence intervals. Gray elements represent monkey N, black elements monkey S. A) The retinal RF position during rightward eye movements (vertical axis) compared to RF position during leftward eye movements (horizontal axis) for spike RFs. B) LFP RFs in the same format as panel A. For clarity, we excluded data where the confidence intervals of the RF position estimates were bigger than 10°. These data show that the RF positions did not depend on the direction of the slow eye movement. Hence, MT RFs are not remapped during the following phase of OKN.

function of the retinal RF location while looking straight ahead during leftward OKN. For this overview, we excluded RFs whose location could only be determined with great uncertainty (error bars larger than 10°). The average retinal RF location was shifted 0.04° (spike RFs; Figure 24A) and 0.38° (LFP RFs; Figure 24B) in the direction opposite to the slow phase. None of the distributions of differences showed a significant shift (all sign tests $p > 0.1$). Hence our data do not support the hypothesis that RFs shift during OKN slow phase. We also used Monte Carlo simulations to estimate an upper bound to the remapping shift (see Methods) and found that our methods would have been sensitive enough to detect remapping shifts as small as 0.14° for the spike RFs and 1.00° for the LFP RFs.

Discussion

We mapped receptive fields in macaque MT using well-isolated single units, as well as aggregate neural activity reflected in the local field potentials. During slow eye movements induced by a whole-field moving pattern these RFs moved with the eye. We found no evidence for either head-centered RFs, or for eye-movement direction dependent remapping of RFs.

We first discuss our mapping method, its advantages and limitations, and then the implications of our findings for theories of perceptual stability.

Mapping Method

Random noise RF mapping has been used extensively (e.g. on retinal ganglion cells (Chichilnisky, 2001) or V1 neurons (Horwitz et al., 2005, Rust et al., 2005)), and the data

are usually analyzed with spike-triggered averaging (STA). For an infinite spike dataset, GLM based analysis and STA result in the same linear kernel estimates. For finite datasets, however, STA requires whitening of the stimulus sample distribution, which the GLM method does implicitly. Moreover, while significance testing in STA is usually done with bootstrap methods, the GLM analysis allows the application of standard F-tests. Finally, the main advantage of the GLM approach arises in the context of the analysis of LFPs where unique trigger events (the equivalent of spikes in spike triggered averaging) cannot easily be defined. The GLM based analysis determines the best linear model that relates (any) neural activity to the visual stimulus.

Our method was able to quantify either a spike or an LFP RF at 92% of recording sites. Of course, the method fails in the absence of a response to flickering bars. This, however, is quite rare in MT (Krekelberg and Albright, 2005). Mapping could also fail during the OKN conditions because (retinal) motion of the dot pattern could suppress the response. Because, however, the retinal motion is rapidly (200-300ms) cancelled by the nystagmus whose gain was near 1, only a slow (< 2°/s for monkey S, < 0.5°/s for monkey N) moving retinal motion pattern remains. Given that most MT neurons prefer higher speeds (Rodman and Albright, 1987), this retinal slip is expected to have only a minimal influence on the neural response. Additionally, mapping could fail if the eye-movement strongly suppressed the neural response (Chukoskie and Movshon, 2009); this implies that a negative result (absence of a significant RF) should be interpreted with caution.

Given that we were interested in the relationship between RF location and horizontal eye movements, we used a one-dimensional stimulus and only mapped the horizontal position and extent of the RF. While there is no principled reason against using a 2D checkerboard to map 2D RFs, we found in practice that the dimensionality of a 2D full-field stimulus was too high to allow RF estimation within reasonable experimental time. Such a 2D method may still be successful on a coarser spatial scale.

Spike and LFP RFs

We found that the location of spike and LFP RFs were highly correlated. This is presumably a consequence of the retinotopic organization of MT; nearby neurons have similar retinal RF locations, hence the aggregate neural activity of these neurons reflected in the LFP should have a similar RF too.

Our results, however, also showed that the size of the LFP RF was a much more variable quantity (no correlation with the spike RF and a larger standard deviation in monkey N but not in monkey S). In part this may be due to the fact that the RFs of monkey N were closer to the boundary of the monitor, which may have affected our ability to map their full extent (see Figure 20). In addition, however, these differences may be attributed to a number of neural and experimental factors that are known to influence the range of spatial integration in the LFP. For instance, while an action potential—once it is detected—is independent of the impedance of the recording electrode, low impedance electrodes accumulate more lower frequency LFPs, and these are expected to integrate electrical activity over a larger radius (Bedard et al., 2004). This problem is exacerbated

by the dependence of the spatial spread of the LFP on the cortical layer (Murthy and Fetz, 1996). Hence, properties of neural populations based on LFP recordings can be obscured by the unknown range of spatial integration. This uncertainty, however, did not impact our particular question, because even the larger LFP RFs in monkey N were eye- and not head-centered (Figure 22).

Mixed Reference Frames

Previous work has shown that mixed reference frames - RFs that partially move with the eye - are prevalent in the VIP (Duhamel et al., 1997, Avillac et al., 2005, Schlack et al., 2005). Moreover, theoretical studies have shown that mixed reference frames are useful as part of a neural network for the optimal combination of multiple sources of sensory information (Deneve et al., 2001).

In our analysis, an RFI that is neither 0 (head-centered) nor 1 (eye-centered) corresponds to a mixed reference frame. The mean RFI for spike RFs (0.95) was not significantly different from 1, but the 0.81 mean RFI for LFP RFs was. Moreover, some individual RFIs were significantly below 1 (see confidence intervals in Figure 5A and B). Taken at face value, this implies that MT coded in a mixed reference frame, albeit it one that was strongly biased towards eye-centered. We note, however, that these apparent mixed reference frames could be artifactual. For instance, a bias in the position signal of the video eye tracker could lead to RFIs less than 1. Such a bias was indeed observed in the data obtained with the lower resolution video tracker used in monkey S. The oblique angle of the camera led to a presumably artifactual change in pupil size with eye

position, which caused a minor (~10%) overestimation of eye position. This is consistent

with an underestimation of the RFI. Similarly, the inability to map responses beyond the

physical boundaries of the screen introduces a bias towards central screen positions,

which our analysis would interpret as an RF that does not quite follow the eye. This

effect increases for peripheral RFs, and thus mainly affects the RFIs for the more

eccentric RFs recorded in monkey N (see Figure 20).

Perceptual Stability

There is a clear discrepancy between our findings of eye-centered RFs in MT, with the

head-centered RFs in human MT reported by d'Avossa et al (2007). Given the significant

functional and anatomical similarities between macaque MT and human MT (Orban et

al., 2004), this is not likely to be a species difference. Moreover, the large discrepancy is

also unlikely to be explained by methodological differences, especially because we not

only mapped the RFs of single units, but also those of the LFPs, which are known to be

more closely related to the BOLD signal (Logothetis et al., 2001, Viswanathan and

Freeman, 2007), but see (Nir et al., 2008)).

In recent work, (Burr and Morrone, 2011) have argued that head-centered

representations in MT arise only under conditions of spread-attention, and not while

the subject is performing a demanding task at fixation. This could explain the

discrepancy between d'Avossa et al (2007) and Gardner et al (2008). In our study, we

did not explicitly control the monkeys' allocation of attention, but the typically high fast-

phase frequency is consistent with stare nystagmus, which is a reflexive eye movement

that does not involve the tracking of an individual dot. Under these conditions, attention is likely spread across the screen, and unlikely to be highly focused at the fovea. Nevertheless, receptive fields moved with the eye. Moreover, the recent study by (Ong and Bisley, 2011) mimicked the fixation paradigm of d'Avossa et al (2007) and also reported eye-centered RFs in macaque MT. While we believe this suggests that spread attention may not be enough to explain head-centered representations in area MT, a study in which attention is carefully controlled is needed to fully address this possibility.

RF Remapping and Mislocalization

An inability to properly match the old image on the retina to the current one during or after an eye movement may explain the temporary cracks in perceptual stability that occur for briefly presented targets around the time of a saccade (Honda, 1989, Ross et al., 1997, Lappe et al., 2000). Many researchers have connected these localization errors to perisaccadic remapping in visual areas (for review, see (Wurtz, 2008)). Similar kinds of behavioral mislocalization, however, also occur during smooth eye movements (smooth pursuit (van Beers et al., 2001, Konigs and Bremmer, 2010), OKN (Kaminiarz et al., 2007)), and optokinetic afternystagmus (Kaminiarz et al., 2008)). This led us to investigate whether remapping also occurs during smooth eye movements. When the eyes move with 10°/s, then a neuron, which anticipates the stimulus location by 50ms, would shift its RF 0.5°. Our data, however, failed to find support for a shift of the RF location during the slow phase of the OKN. Moreover, our Monte Carlo simulations show that our methods were sensitive enough to detect shifts as small as 0.14°.

Of course, this could simply mean that the behavioral phenomenon of mislocalization, which is larger than 1° during the slow phase of OKN (Kaminiarz et al., 2007), is not based on neural activity in MT. However, this finding also led us to reconsider the hypothesized relationship between RF shifts and mislocalization. Let us assume that, just before a rightward saccade, a neuron that normally responds to foveal stimulation, responds to stimuli 10 degrees to the right of the fovea. If this neuron's message to the rest of the brain stays constant (i.e. assuming a labeled line code), then it signals the presence of a foveal stimulus when a flash is presented 10 degrees to the right of the fovea just before a rightward saccade. In other words, this predicts that mislocalization would be against the direction of the saccade, which is contrary to most of the behavioral evidence (Honda, 1989). This contradiction can be resolved by assuming a more complex code for retinal position (Krekelberg et al., 2003) that does not rely on labeled line codes, which may not be useful beyond the peripheral sensory system (Krekelberg et al., 2006). An alternative or possibly complementary source of the behavioral mislocalization is an error in eye position signals. In this view, perisaccadic stimuli are mislocalized not because the retinal position is incorrectly represented, but because the subject use incorrect information on the position of the eye (Honda, 1991, Dassonville et al., 1992). Recent evidence shows that perisaccadic errors in eye position signals in macaque MT, MST, VIP, and LIP are consistent with this hypothesis (Morris et al., under review). Whether similar errors in eye position signals could also explain mislocalization during smooth eye movements is a target for future studies.

Chapter 5 Gain Fields in Spikes and LFPs (Project 3)

Introduction

Gain fields provide enough information for the brain to calculate the current eye position (see the section on Gain Fields in the introduction page 18). Bremmer and colleagues fit planes (two dimensional first order polynomial fits) to the firing rate of MT neurons at nine different eye positions. The slope of these planes revealed strong modulation at a single neuron level. Similar to these eye position gain fields, they also reported pursuit gain fields. Specifically, the neurons in MT and MST exhibited pursuit-direction specific responses. Despite finding a significant slope when examining single neurons, no such modulation existed at the population level. The average plane of all gain fields they examined in area MT was flat. Therefore, they concluded that the slopes are evenly distributed across area MT (Bremmer et al., 1997)

All previous electrophysiological studies of gain fields have focused on the firing rate of neurons. Here, we investigate whether these gain fields also manifest themselves in other correlates of neural activity, i.e. the LFP and its derived measures. We chose to examine these measures because they look at neural activity that integrates over a broader area of cortex. If gain fields are organized in a systematic fashion across visual cortex, then we are more likely to find it searching with such methods.

Materials and Methods

Data analysis

All data used to estimate the gain fields were recorded while the monkeys performed OKN, which was induced by a random dot pattern moving either left or right with 10°/s. Behind the random dot pattern a random flickering pattern was presented (see section "Visual Stimuli" page 30). We excluded the data recorded in the first 500ms of each trial to remove any onset responses as well as the time around the fast phase— -50ms before onset to 100ms after offset—to reduce the influence of this saccade like movement to a minimum. The screen measured 20° x 15°, which we divided into 2° x 2° elements. We averaged the eye position signal for every 10ms and summed the spikes that happened within the same time period. We used this information to know how often the eye position was over an element and how many spikes happened at each. The firing rate per element was calculated by dividing the spike count per element by the time during which the eye was at that location. For each OKN direction, we estimated the firing rate for each neuron and fit a plane relating firing rate to eye position:

$$Z = a_x * x_{eye} + b_x * y_{eye} + c$$

x and y represent the horizontal and vertical eye position, respectively. The coefficients a_x and b_y are the slopes and determine the modulation of the firing rate with eye position. The constant term c reflects the average firing rate. To handle the variation in reliability of the firing rate across all eye positions, we first excluded the firing rates of

elements that had been visited ten times or less. Second, we assigned weights to the firing rate of each 2° x 2° element based on the square root of the count of eye positions at that element. The robust regressions resulted in planes with slopes a_x and b_y and the constant c and their confidence intervals. For the raw LFP gain fields we summed the raw voltage value and divided by the duration of fixation at each eye positions.

We also analyzed gain fields in the power spectra of the LFP. The Fourier transforms of 200ms LFP snippets were assigned to the eye position elements at the center of the snippet. The power of the LFP depends on the insulation of the electrode. In order to make the results comparable between recordings, we normalized the power of all frequencies by dividing them by the corresponding frequencies' power during fixation.

Results

During OKN, the eye position is not evenly distributed across the screen. In Figure 25 we present the eye position (binned to 2° x 2° elements) as they occurred during all experiments for the two monkeys. Most of the time, the eye position was close to the center.

We chose to present the
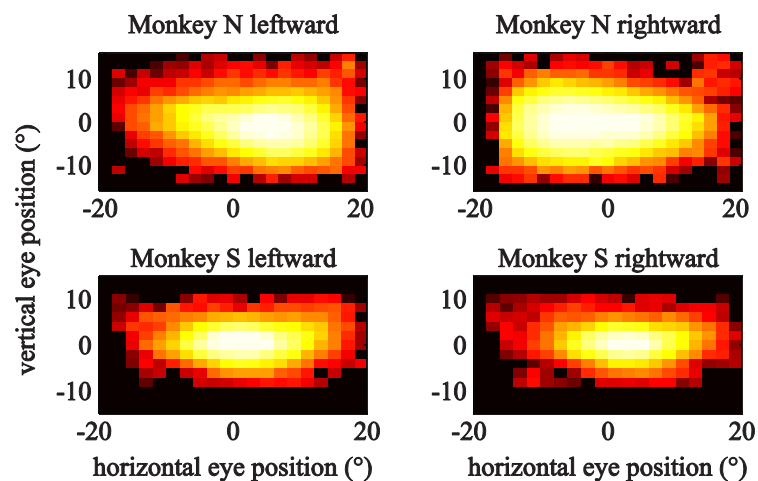
Figure 25: Eye Position for the Experiment. All four panels show the logarithm of the sum of all eye positions that happened during the experiments, sorted by monkey (top and bottom) and direction of the OKN.

logarithm of number of eye positions to see the distribution of eye position further

away from the center of the screen as well. Monkey N (top row) shows the typical

"Schlagfeld-Verlagerung" (Frenzel, 1928) during OKN, a bias of eye positions in the

opposite direction

of the slow phase

of OKN.

Gain Fields in the Firing Rate

Gain Fields exist in

area MT for

fixation and

during smooth

pursuit eye

movements

(Bremmer et al.,

1997), but have

not been shown to

exist during OKN.
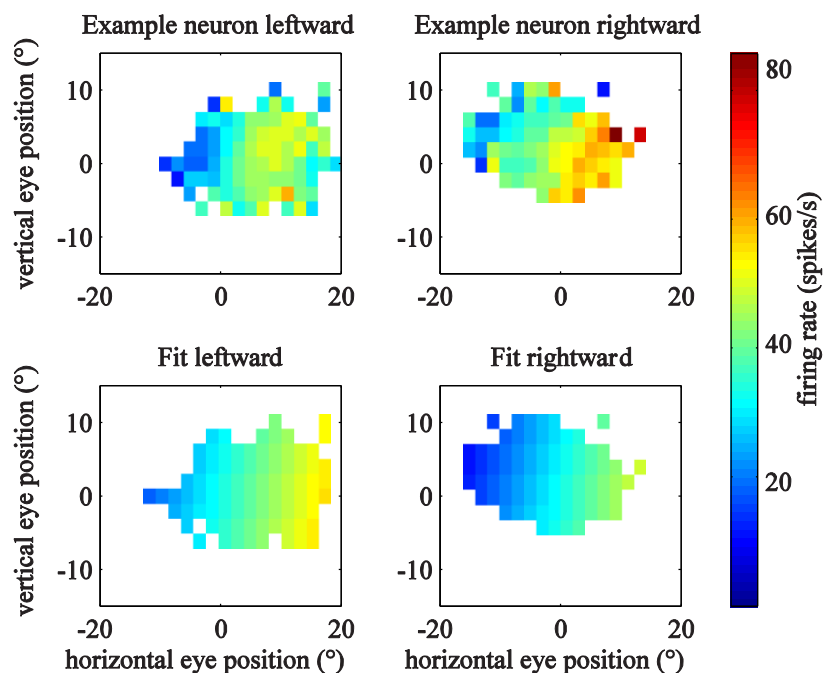
Figure 26: Gain Field Example for a Neuron. All four images show the firing rate coded in color depending on the horizontal (horizontal axes) and vertical (vertical axes) eye position. The top row shows the actual firing rate estimated for each 2° x 2° element, on the left while the slow phase of OKN moved to the left, on the right while the eye moved to the right. The bottom row shows the estimates of firing rate based on the fits. The dark blue area shows elements for which we had fewer than 10 repetitions.

The top panel in Figure 26 shows the average firing rate of a neuron depending on the

eye position. The firing rate was modulated in both OKN directions in such a way that at

eye positions to the right, the firing rate was approximately twice as high as positions to

the left. This neuron had a RF centered at 5° and not extending further than 7.5° to the

left of the fovea (measured with reverse correlation during the slow phase, see chapter

"RF Positions during Slow Eye Movements (Project 2)" page 52ff for details). For most

eye positions, the screen encompassed the entire RF. This excludes the possibility that

the apparent eye position modulation could have been due to the absence of visual

stimulation if an RF moved outside the physical boundary of the monitor. We fit a linear

plane to the two data sets in Figure 26 (leftward and rightward OKN). The fits resulted in

the following planes, which are shown in Figure 26's bottom panels:

$$Z_{leftward} = 1.15(\pm 0.28) * x_{eye} + -0.31(\pm 0.49) * y_{eye} + 31.9(\pm 2.5)$$

$$Z_{rightward} = 1.49(\pm 0.23) * x_{eye} + -0.67(\pm 0.44) * y_{eye} + 49.1(\pm 1.9)$$

The horizontal slope (a_x) of 1.15Hz/° represents an increase in firing rate by 1.15Hz

while moving 1° from right to left, the values in the parentheses indicate the confidence

interval. The slope during leftward OKN was lower than during rightward OKN, as was the firing rate. These data are consistent with the view that gain fields act as multiplicative gain.

Slopes of Spike Gain Fields
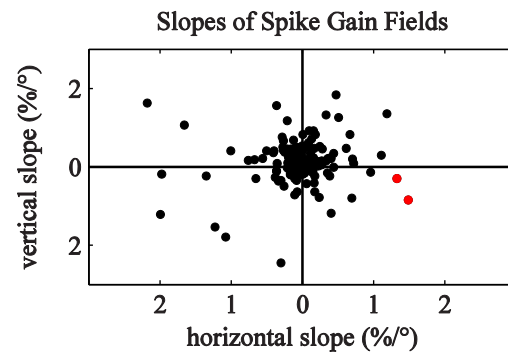
Figure 27 shows the slopes for gain fields of 77 neurons for both leftward and rightward OKN conditions. For all cells and directions, the average horizontal

Figure 27: Slopes of all Spike Gain Fields. The horizontal slope of the gain field fits (horizontal axis) is presented versus the vertical slopes (vertical axis) for all cells and leftward and rightward slow phase. The two red dots indicate the slopes of the example cell in Figure 26.

slope a_x was -0.034 (±0.040 SE), the average vertical slope b_y was 0.101 (±0.044 SE).

This average offset of the vertical slope was significantly different from zero (sign test,

p<0.005), suggesting that there is a small but significant upward bias in the vertical

slope.

LFP Gain Fields

We first fit planes to the average raw LFP, but found that none of the sites had

significant slopes. Next, we tested whether gain fields could be found in specific LFP
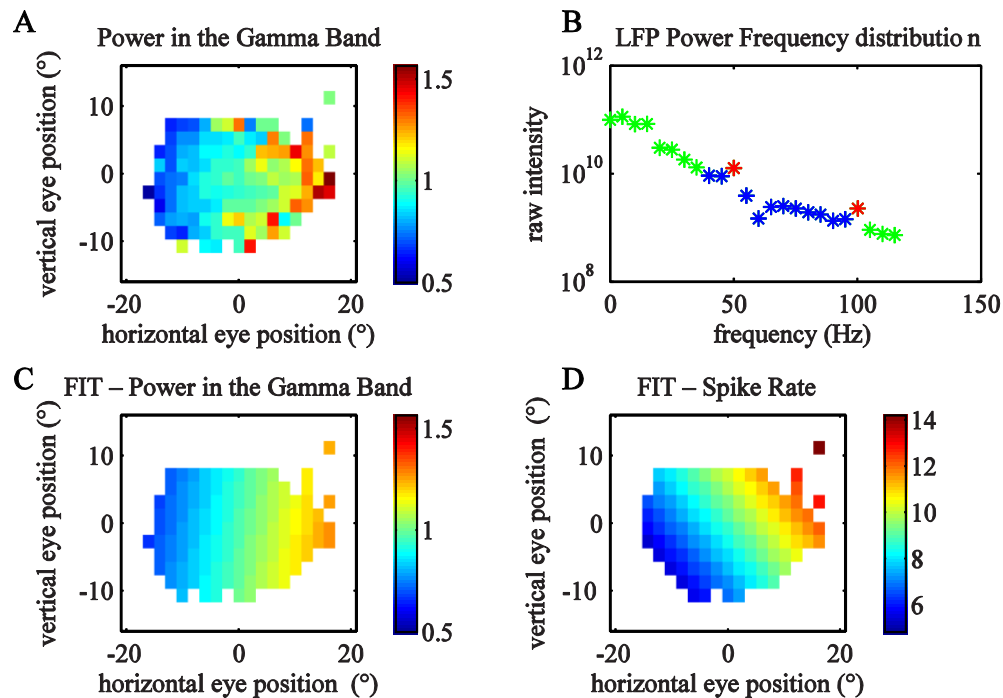
Figure 28: Example of a Gamma Band Gain Field. A) The power of the gamma band averaged in each 2°x2° element, normalized by the power during fixation. C shows the result of a linear surface fit to the data in A). In B) we demonstrate the absolute power over the frequencies from 0 to 120Hz. The blue frequencies fall within our definition of the gamma band. 50 and 100Hz are elevated due to the stimulus frequency of 50Hz; these frequencies were excluded from the gain field analysis D) shows the surface fit of a spike gain field recorded at the same time as the data in A. and B).

frequency bands. The gamma band, which we defined as the frequencies between 40 and 95Hz, showed clear gain fields. We excluded the stimulus frequency (50 or 60Hz). Figure 28A shows an example of such a gamma power gain field. The power while the eye is 15° to the left of the center of the screen was approximately 50% higher
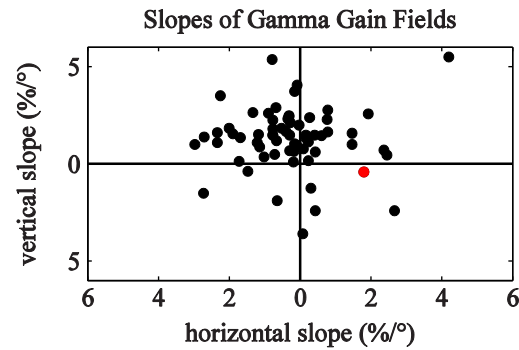
Figure 29: Slope Distribution for Gamma Band Gain Fields. Each dot represents the slopes fitted to the power of the gamma band at a recording site and slow phase direction. The red dot represents the fit from the example in Figure 28.

than during fixation. The power 15° to the right of the center was approximately 30% lower. The linear fit (see Figure 28C) produced a horizontal slope of 1.8 %/° (± 0.2) and a vertical slope of -0.31 %/° (± 0.35). The constant was 0.97% (± 1.5). Panel D shows the result for the gain field of a neuron recorded at the same time as the gamma power.

Figure 29 shows the gamma power gain fields of 33 recording sites independent for leftward and rightward OKN. Interestingly, 87% of the vertical slopes for gamma band gain fields were positive. This implies that there was more gamma power in the LFP when the eyes are looking up. 58% of slopes were both positive in the vertical direction and negative in the horizontal direction. The mean slopes were 0.98 %/° (±0.38) vertical and -0.18 %/° (±0.19) horizontal. The vertical bias to positive slopes was strongly significant (sign test, $p<10^{-8}$).

Discussion

We estimated gain fields of MT neurons during visual stimulation and the slow phase of OKN. First, we reproduced gain fields estimated with spikes, as has been done previously by Bremmer et al. (1997). In that study monkeys either fixated or engaged in smooth pursuit eye movements, whereas our monkeys performed OKN while a stimulus flickered on the screen. Due to our stimulus properties and the slow eye movements, it is hard to draw conclusions about the meaning of the horizontal slope. Bremmer at al. found neurons with gain fields during fixation or during pursuit. Let us assume that the eye position and the pursuit gain fields are independent. A horizontal slope reflects the eye position gain field, if the cell does not have a pursuit gain field. The horizontal slope reflects the pursuit gain field, if the cell does not have an eye position gain field. Most cells probably have both, and the interaction between the two kinds of gain fields is unknown. Therefore, we assume that the slope is the result of a mixture of both factors, with their weights depending on each cell individually.

Previously unknown, gain fields existed in the gamma band power of the LFP. Power in the gamma band was strongly modulated for different eye positions, up to 50% up or 30% down from the mean. Somewhat surprisingly, we found a strong upward bias in the gamma power gain fields (and a weak upward bias in the spiking gain fields). Previous work, looking at spiking activity did not find such a bias (Bremmer et al., 1997). We assume the reason that Bremmer and colleagues did not find a bias in MT/MST is an issue of statistical power. In an fMRI study DeSouza and colleagues (2000) kept the retinal stimulus identical while subjects fixated different locations. They found

consistent fMRI activity modulation in human parietal areas to depend solely on the eye position, thus gain fields. It was unclear how fMRI that looks at metabolic activity of millions of neurons, can find gain fields, when there are no biases in gain fields on a population level. By analyzing the LFPs, we gained direct insight into the average neural activity of a larger population of neurons, in which we found a bias. Our results can explain why fMRI is able to find gain fields in humans as well.

Most RFs of neurons and LFPs (see "RF Positions during Slow Eye Movements (Project 2)" pages 52ff) are positioned to the right of the fovea, which is to be expected, because we recorded in the left hemisphere. If the gain fields were a result of the RFs moving off the screen, because the eye moved too far to the left, then we would anticipate a strong positive bias in the horizontal slopes of the gain fields. However, this is not the case for neither spike nor gamma band gain fields. We do not know the exact vertical position of the RF, and we found a bias in the vertical slopes. If this bias resulted from the RF not being stimulated it should be equally strong for spike and gamma band gain fields. Since this is not true, we can exclude this as an explanation for the vertical bias.

We used, similarly to previous studies (Bremmer et al., 1997), a linear plane to estimate gain fields. Of course, gain fields do not necessarily have to be best fit by planes, e.g. a cell could fire strongest while the eye is directed to the center of the screen. Such a gain field, resembling a peak, should be fit with a second order polynomial. The use of such higher order fits would be further motivated by findings from Durand and colleagues (2010). Their analysis revealed that peripheral V1 neurons increase their firing rate

when their RF is straight ahead (relative to the body midline). They argued that stimuli in front of us should have a higher salience and consequently be encoded with higher firing rates. If MT gain fields behave similarly to V1 gain fields—most excitable while the RF is at the center—then we would expect the horizontal slopes to be biased to positive values. As previously stated, our data does not show this for spikes or gamma band gain fields. However, our horizontal slope estimates may be confounded by the slow phase of OKN and mask this bias found in V1 gain fields. We intend to address this in future work.

The origin of the gain fields is up to now unclear. The two candidates are either a corollary discharge signal or proprioceptive signals, which have been recently identified in somatosensory cortex (Wang et al.). Our study does not allow us to distinguish the two signals.

In conclusion, we confirmed the existence of eye position gain fields in area MT. Additionally, we found a small bias in slopes in the gain fields estimated with spikes and a strong bias with gain fields estimated with the power of gamma frequencies. These previous unknown gamma gain fields could explain the existence of gain fields found with fMRI. Furthermore, we hypothesize that synchrony place a vital role in the interpretation of gain fields.

Chapter 6 Modulations during Fast Eye Movements (Project 4)

Introduction

The detection of briefly flashed targets around fast eye movement is more difficult compared to fixation. Saccadic suppression has been reproduced many times and is introduced in detail in the general Introduction. A wide variety of changes in firing rates around the time of saccades have been reported in many cortical and subcortical structures. The link between saccadic suppression and the neural structure is complex and depends on factors such as brain area, stimulus properties, and background illumination. Here, we confirm that firing rate, when aligned to fast phases of OKN, is indeed strongly modulated. Additionally we analyzed the LFP, the power of the LFP, as well as the correlations between the stimulus and the spikes and the correlations between the stimulus and the LFP, all around the time of fast phases.

We show effects of the fast phase on firing rate that can be explained by the retinal image sweeping across the retina during the fast phase. Additionally, we propose layer specific integration of a post fast phase enhancement. The LFP is strongly modulated around the fast phase, which allows us to speculate about new mechanisms of saccadic suppression during saccades.

Materials and Methods

Data analysis

Most of our analyses performed around the time of fast eye movements were independent of the source of the neural signal. We describe these signals first, followed by the manner in which we aligned them to eye movements. The typical signal investigated during the time of saccades is firing rate of single neurons. We also included firing rates derived from MUA, which behave similarly, due to the functional architecture of area MT. The raw LFP is the continuous voltage change measured from the tip of the recording electrode. From the LFP we derived the spectral density. We accomplished this by transforming 200ms snippets of data every 10ms into the Fourier domain and stored the power of the frequencies between 0 and 115Hz in 5 Hz increments.

The last signals of interest were the correlations between the stimulus and neural signal. We modeled firing rate or LFP based on the stimulus utilizing the LN model (see "The Linear Nonlinear Model" page 10). The modeled firing rate or modeled LFP, which we call the projected stimuli, were correlated with the recorded firing rate and LFP around the time of fast phases. In detail, we recreated the random noise stimulus offline frame by frame. For every spike we recorded, we stored the luminance values preceding the spike for 0-120ms—the spike triggered stimuli. The average of this spike triggered stimulus ensemble is the STA. To weigh all stimuli by the LFP, we multiplied the LFP recorded during one stimulus frame by the luminance values presented on the screen

0ms to 120ms before we recorded the LFP value. This was repeated for each consecutive luminance frame. We define the average of all weighted stimuli as the LFP weighted stimulus average (LWA). To remove noise in the STA and the LWA we set any values less than 1.63 times the standard deviation of the STA or LWSA to zero. We chose 1.63 so that only the 10% most extreme values remain following this correction. The STA and LWSA resemble the linear stage of the LN model.

We project the complete stimulus into the dimension of the STA or LWA. The projected stimulus is therefore condensed to one value per frame; it is a measure how well the stimulus fits the RF of the cell or the RF of the LFP. The projected stimulus and spike train are naturally correlated. The projected stimulus is the output of the linear stage of the LN model. To increase the correlation even further, we estimated a transfer function, or nonlinearity, and transform the projected stimulus into a modeled firing rate. For some cells, there was not enough data to estimate the nonlinearity; in these cases we simply used the projected stimuli (for a detailed description of STA and nonlinearities, please see the data analysis sections of projects 1 pages 34ff). For the LFP, we did not calculate transfer functions.

In summary, we analyzed the spikes of neurons, the LFP, the spectral density, and the correlation between spikes and LFP and their projected stimuli around the time of an eye movement. We did not analyze signals recorded in the first 500ms of each trial to remove possible influences of stimulus onset.

For each fast phase we align the above mentioned signals to the onset. (For the reliable detection of the onset and the offset of the fast phase, see section "Eye position" page 29 in the General Material and Methods chapter.) Signals that were closer than 50ms to either the offset of the preceding fast phase or to the onset of the subsequent fast phase were excluded from analysis. All further analysis is performed on the data aligned to the onset. Excluding the correlation analyses, we averaged all data sets which provide us with the fast phase triggered average of the firing rate, LFP, and the spectral density. Occasionally, the fast phase was in the same direction of the slow phase, we did not include these fast phases in the fast phase triggered average. Spike rates vary from neuron to neuron and the size of the LFP depends on factors such as the impedance of an electrode. To permit comparisons between recordings despite these variances, we normalize both the fast phase triggered spike rates and LFP in the following way: we first calculate the mean of the fast phase triggered signal -500ms to -100ms before the onset of a fast phase and subtract it from the signal. After that, we divide it by the absolute value of the largest extreme in the signal. The spectral density depends on the size of the LFP as well. Therefore, we first calculate the spectral density during fixation and use the average values for each frequency to normalize the fast phase triggered spectral density. In the spectral density during fixation and OKN, the stimulus frequencies (50 or 60Hz) are increased. We define the gamma band as the frequencies between 40 and 95Hz, but remove power at the stimulus frequencies.

Firing rates and LFPs displayed a variety of modulations around the fast phase (see Results). We used principal component analysis to estimate shared components

between the modulations for either cells or LFP sites. For both, we searched whether k-means cluster could reliably identify two clusters in the space spanned by the first two principal components.

In the projected stimuli analysis, we measured the correlation between projected stimuli and neural signal as a function of the time relative to saccade onset. For example if the monkey performed 1000 fast phases to the left during rightward OKN, then we had 1000 projected stimuli lined up at the onset of the fast phases. We correlate these 1000 projected stimuli with the firing rate (or LFP) which is also aligned to the onset, resulting in a Pearson correlation value between -1 and 1. We estimate the correlation between projected stimulus and neural signal not only at the onset, but every 20ms for 500ms around onset time. To compare the strength of the correlations pre and post fast phase, we averaged the correlation values between -25 and 25ms (pre) as well as 175 and 225ms (post) relative to fast phase onset for each cell or LFP site. We tested for differences with a two tailed, paired T-test. The presented correlations are smoothed with a boxcar window (± 20ms wide).

Results

OKN consists of slow periods interspersed with fast phases. Figure 30 shows the distribution of the intervals between the onsets of fast phases (15recordings, monkey N; 31 recordings,

Figure 30: Inter Fast Phase Intervals. The two plots show the distributions of inter fast phase intervals for all recording sessions. Blue corresponds to the leftward OKN condition, red to rightward. The top plot shows saccades from monkey N, the bottom plot from monkey S.

monkey S). Monkey N made a fast eye movement on average every 236ms, monkey S every 311ms. The majority of saccades were in the direction opposite to the slow phase (69% monkey N, 81% monkey S)

LFP Modulation

The LFP was strongly modulated around the time of each onset. In fact, in some recordings it is possible to spot the onset of fast phases by looking at the raw LFP trace (not shown). In Figure 31 we present the fast phase triggered average of the LFP for 40 recording sites. With a few exceptions, the signal typically increased from -150ms before the onset. Approximately 30ms after onset, the average signal dropped, had two deep dips followed by two shallower peaks with a longer tail. Note that the signal increase
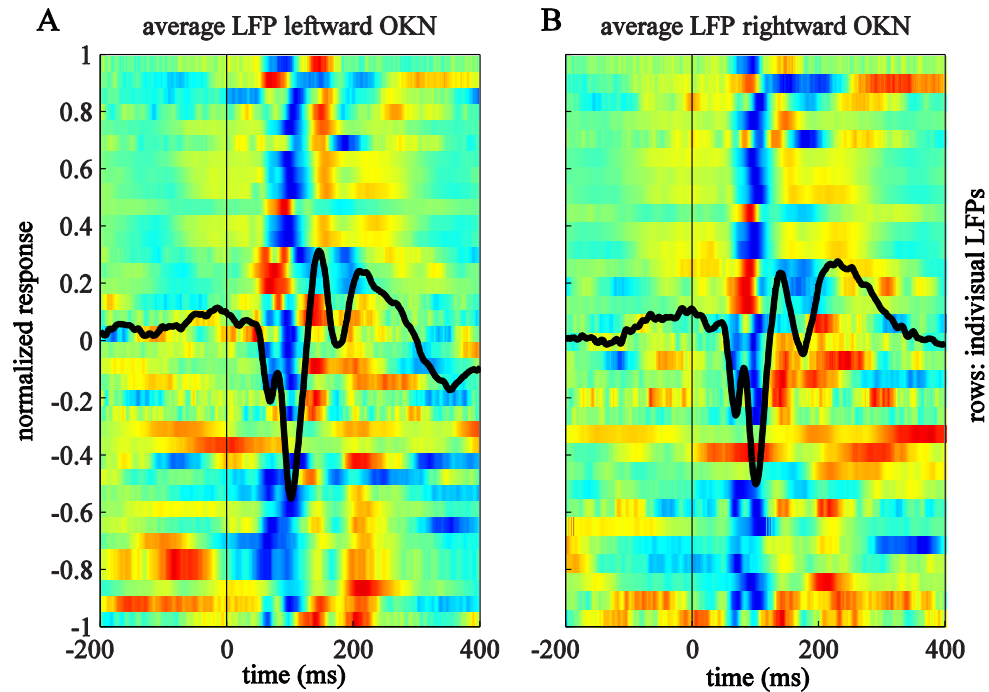
Figure 31: LFP Modulated by Fast Phase. The panel on the left represents data from fast phases to the right during leftward OKN, the panel on the right fast phases directed to the left during rightward OKN. Both panels indicate signal change over time. Each colored row represents the normalized LFP of a recording site. The black lines are the means across recording sites.

prior to the onset is not necessarily linked to the upcoming onset; it could also result from a fast phase that happened 200 to 350ms before the current fast phase.

The modulation described is the average modulation, but clearly some of the LFPs behaved differently. To find common sources of variation we performed principal component analysis on the combined (left and right) set of LFP changes (see Figure 32). Principal components one to three explain almost 70% of the variation seen in the different LFPs. The sign of a principal component is arbitrary, hence the upward

deflection in principal
components one and
three do not
necessarily imply that
the majority of sites
had upward
deflections.

In Figure 33A we
display how well the
LFP modulation of
each site fit the first
principal component
(horizontal axis)
compared to the third
principal component
(vertical axis). The
colors indicate the
result of clustering the
two components into
two groups. In the
right panel of Figure 33
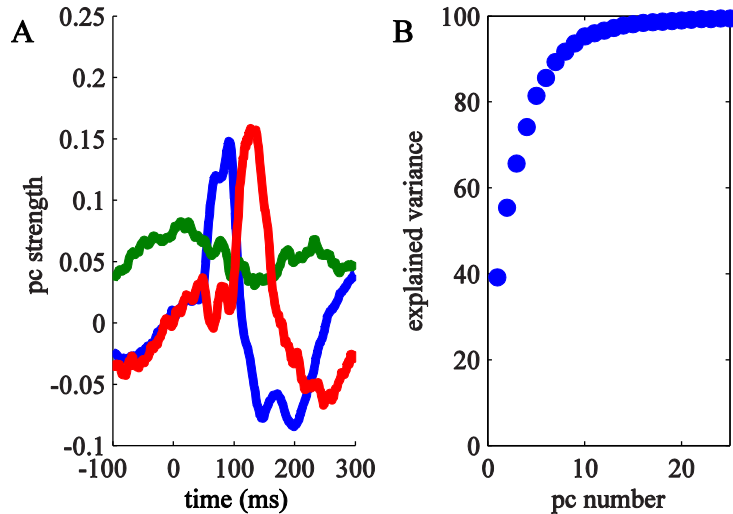
Figure 32: Principal Components of the LFP Modulations. The left panel shows the first three principal components of the LFP modulation (1st: blue, 2nd: green, 3rd: red). Together they almost explain 70% of the variance (right panel) in the modulations seen in Figure 31.
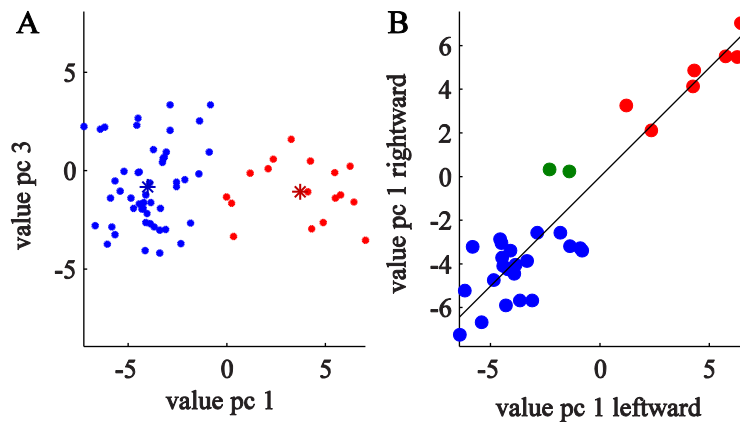
Figure 33: Principal Component Clusters. A) The projection of the LFP modulations onto principal component one (horizontal axis) is plotted against the projection onto principal component three. The clusters (red and blue) are assigned based on a cluster analysis. B) The projection onto principal component one of the modulations for fast phases to the right (horizontal axis) and to the left (vertical axis). The color represents which cluster the site belonged to. Green represents sites where left and right fast phase modulations did not belong to the same cluster.

Figure 34: LFP Modulations by Cluster. The figure has the same layout as Figure 31. The left panel shows all LFP modulations for the blue cluster (see Figure 33), the right for the red cluster. Color represents the normalized raw LFP signal; the black lines represent the mean over all sites in a panel.

we compare the value of the first principal component between fast phases to the left during rightward OKN and fast phases to the right during leftward OKN for the same recording site. The correlation between the conditions was very high (r = 0.93, p<10^{-13}). This implies that the LFP modulation at a recording site was independent of the fast phase direction.

In Figure 34 we divided the LFP modulations based on their cluster. The blue cluster in Figure 33 had a strong downward deflection after fast phase onset. The sites belonging to the red cluster did the opposite; their average LFP has a strong upward deflection after fast phase onset.

Firing Rate Modulation

Figure 35 illustrates the distribution of spikes around the time of fast phases in a raster plot (panel A and B). For both fast phase directions, there was a clear reduction in firing rate after fast phase onset. The right panel demonstrates this drop in activity by showing the average firing rate over time. An increase in neural activity is also visible about 100ms after fast phase onset. In Figure 36 we present the significant firing rate modulations around fast phase onsets for all cells. The firing rates changed markedly approximately 30ms until almost 200ms after onset. The population average modulations (black line) were relatively modest, which we attribute to the variety of the responses across the population. That is why we utilized principal component analysis to
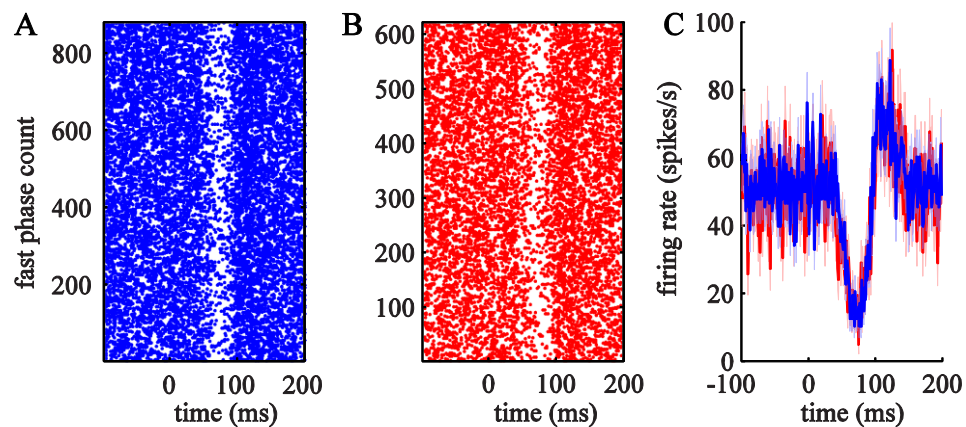
Figure 35: Spike Raster for an Example Neuron. In the two raster plots to the left and in the middle represent the change of spike density aligned to the fast phase. Every dot represents one recorded spike. The spikes are aligned to the onset of the fast phase (horizontal axis). Each row represents one fast phase. The right plot shows the average firing rate on a millisecond scale. Red stands for spikes recorded during the combination rightward slow phase - fast phase to the left; blue indicates a fast phase to the right during leftward OKN. The horizontal axes represent time to fast phase onset in all three plots.

find common sources in the firing rates' variations. Principal components one, two, four, and five describe modulations with one, two, three, and four extremes, respectively. The third principal component reflects a general increase in firing rate over time. Such an increase or decrease after the fast phase is expected if the cell's firing rate was modulated by a gain field (see chapter "Gain Fields in Spikes and LFPs (Project 3)" page 75ff).

Visual inspection of the relationships between the principal components revealed two clusters (see Figure 37). Running cluster analysis and searching for two cluster reliably
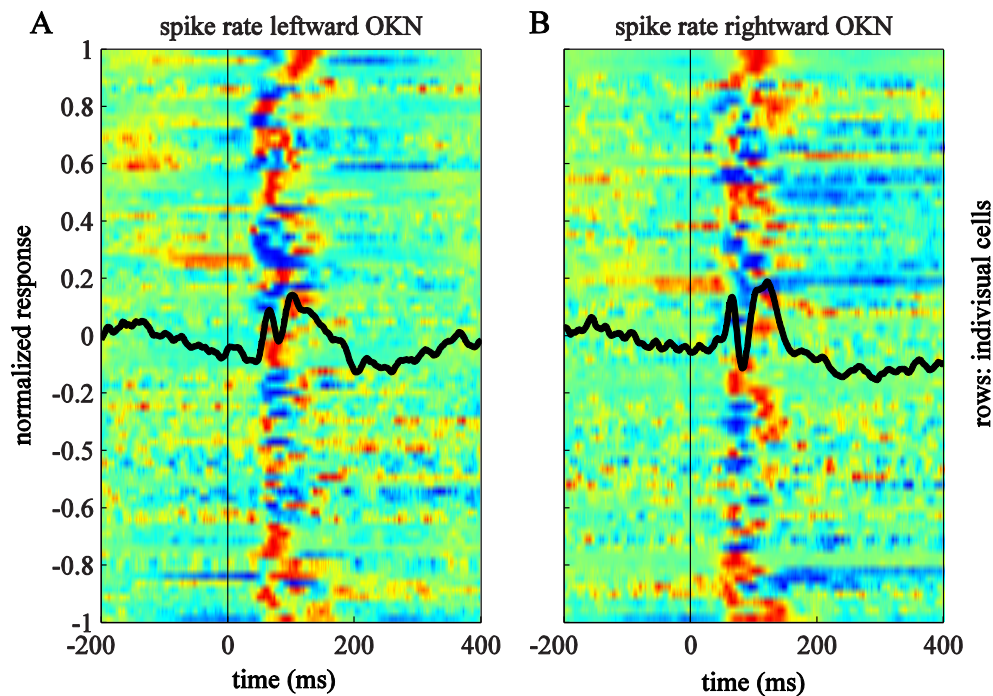
Figure 36: Firing Rate Modulations Alinged to the Onset of each Fast Phase. The Figure has the same graphical conventions as Figure 31. The left panel shows the modulation during leftward OKN and fast phases to the right, the right panel shows modulations around fast phases to the left during rightward OKN. Each row in the colored image represents one cell. The black line is the average of all responses.

returned the clusters illustrated in Figure 37A. The correlation between the different

fast phases was highly significant (r = 0.56, p<10^{-6}). This shows that a cell that fit

principal component one well during a fast phase to the left also fit that same principal

component during the fast phase to the right (Figure 37B). In other words, the fast

phase modulations were independent of the direction of the eye movement.

Figure 39 illustrates the difference between the two clusters. The typical response for a blue cluster cell was a reduction in firing rate and a slight increase approximately 120ms after fast phase onset. The cell presented in Figure 35 is a good example of a cell that belongs to this cluster. The red cluster showed a weak decrease before saccade onset, a strong increase after onset followed by a slow decrease back to the base line activity.
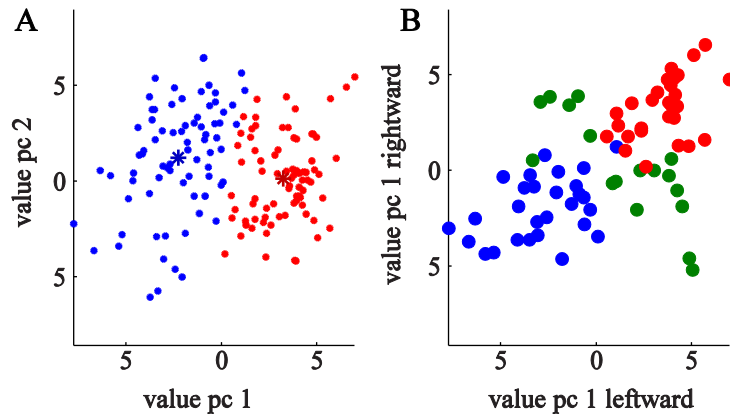
Figure 37: Principal Component Clustering. On the left we illustrate the dependency of the principle component one on the principle component two. The color indicates the result of a k-means cluster analysis. The stars represent the center of each cluster. On the right we compare the value of the first principle component during right (horizontal) and left (vertical) fast phases. The colors represent the cluster. Cells with modulations in different clusters for different eye movement directions are marked green.
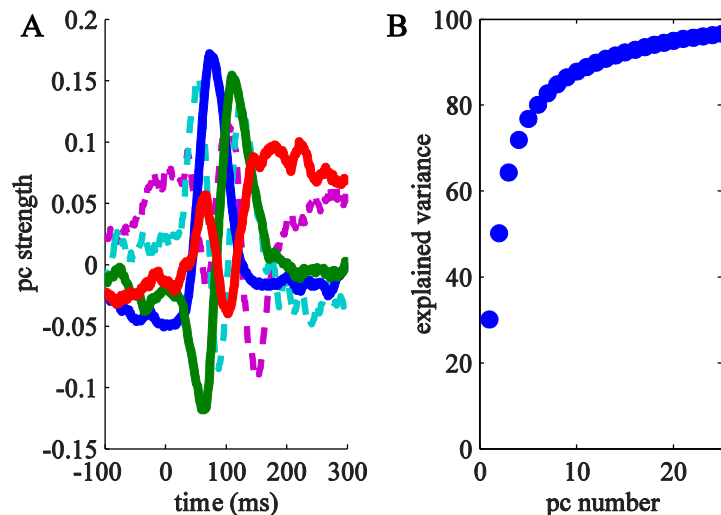
Figure 38: Principal Components of Firing Rate Modulation. The left panel shows the first five principal components; they explain almost 80% of the variation (1st: blue; 2nd: green, 3rd: red, 4th: cyan, and 5th: magenta. The right panel shows the cumulative amount of variance explained by the principle components.
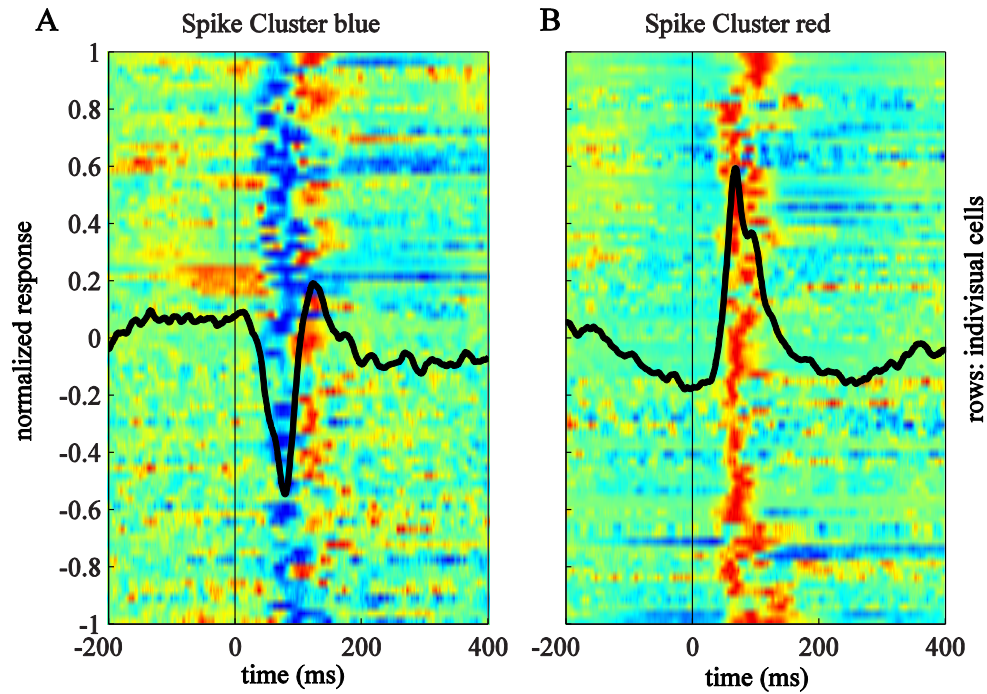
Figure 39: Firing Rate Modulations sorted by Cluster. The figure follows the same scheme as Figure 36. The colored rows indicate the modulation of single cells for fast phases to either the right or the left, the mean of al presented firing rates are the black lines. The left panel shows the firing rate modulations of the blue cluster, the right panel shows the red cluster.

So far, we clustered the LFP and the spike modulations into two groups each. In Figure 40 we show the average firing rates for both the clusters based on firing rates (same as Figure 39) as well as the average firing rate dependent on the LFP cluster recorded with the same electrode at the same time. Interestingly, the initial peak approximately 65 ms after fast phase onset (dotted black line) in the firing rates based on the LFP cluster was
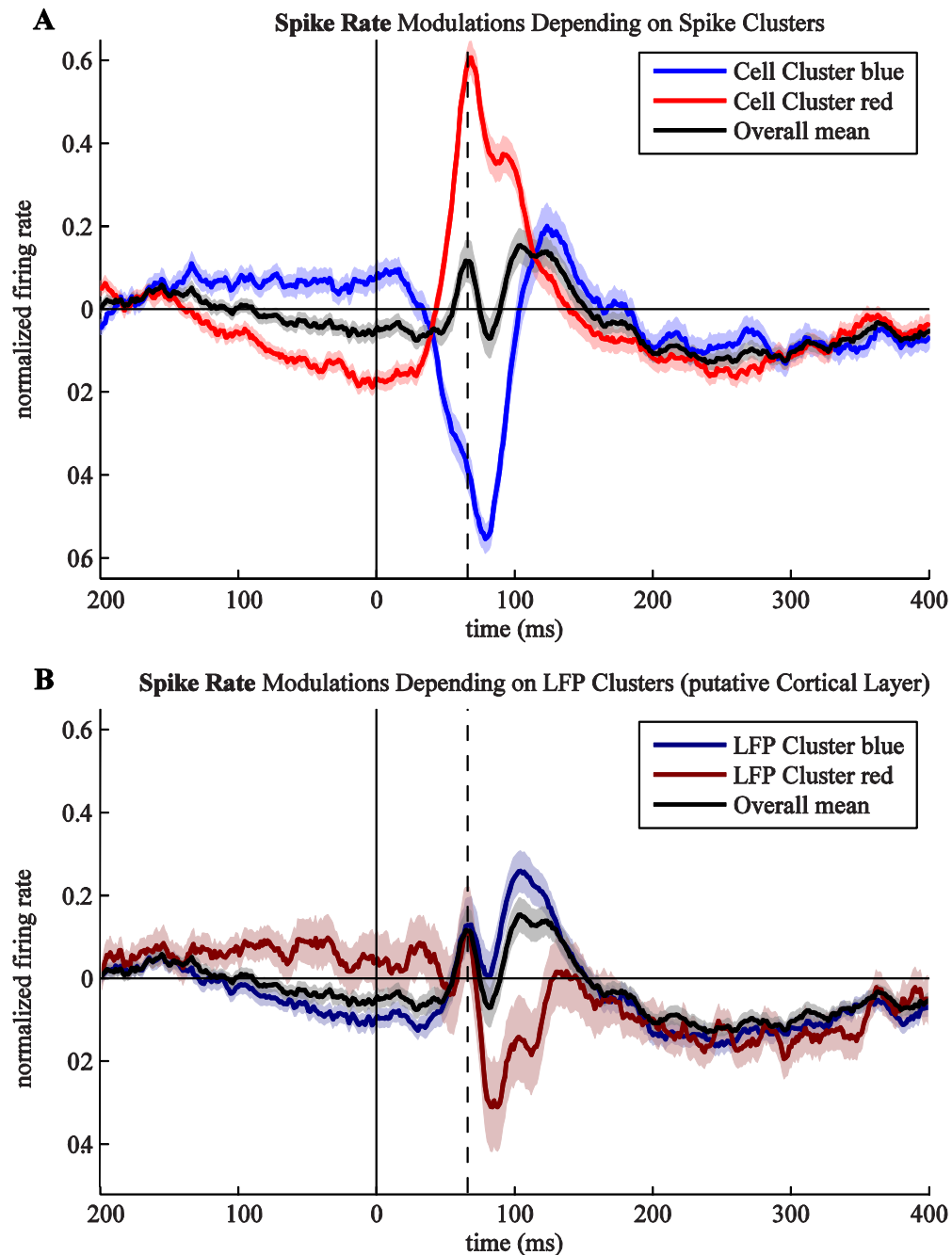
Figure 40: Average Firing Rate Modulations for Clusters. All curves represent firing rates. The blue and the red curves in A are the average firing rates from Figure 36 belonging to the red or the blue cluster, respectively. The dark red and dark blue averages in B show the firing rates grouped by the LFP cluster from the previous section and indicates a putative layer dependency. The black modulation represents the average of all firing rates. The shaded areas indicate the standard error of each average. The black dotted line indicates the maximum of the first peak of the overall average.

identical and matched the response of the overall average. However, there was a difference in the second part of the response. Cells that were recorded at a site that belonged to the blue cluster had firing rates above average after 100ms. The firing rates of cells recorded at a red site were below average for that time period.

Spectral Density Modulations

In the section "LFP Modulation" above we presented strong evidence for changes in the LFP around the time of the fast phase. Here we investigate in which frequency bands of the LFP these changes appear. Figure 41A shows the power of the LFP's frequencies at one recording site aligned to the onset of the fast phase. The power was normalized by the power of the LFP frequencies during the fixation condition. The frequency bands at 5 and 50Hz pop out; at these frequencies power was higher than the power of the other bands. The 5Hz
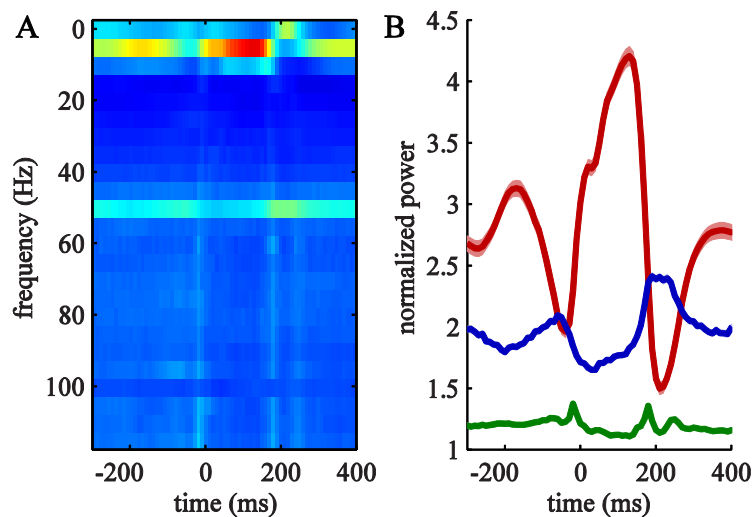
Figure 41: Spectral Density Modulation for one Example Site. The color in the left image shows the power of the LFP recorded in area MT aligned to the time of fast phase onset (horizontal axis). The frequencies run from 0 (DC component) to 115Hz (vertical axis). The power is normalized by the power during fixation. The right plot illustrates a subset of the data presented in the left panel, but focuses on theta (5Hz, red line), 50Hz (stimulus refresh rate, blue line), and gamma (40-95Hz, stimulus frequency excluded). The shaded area reflects the standard error.

frequency band is usually called theta. The stimulus frequency at this site was 50Hz. We therefore refer to this band as the stimulus band. The stimulus frequency power and the theta power are presented in Figure 41B (blue and red). The curves appear smooth because we estimate the power in a sliding window 200ms wide. The stimulus frequency power dropped at the beginning of the fast phase, rose afterwards, and dropped down again, probably because of the next fast phase. The theta frequency mirrored the signal change in the stimulus frequency band; its power was increased during the time of the fast phase. The green line reflects gamma power (40-95Hz, stimulus frequency excluded).

The LFP power for the population behaved similarly to the power of the example neuron (Figure 42). The stimulus frequency (50Hz for monkey N, 60Hz for monkey S; blue line) was decreased during the fast phase, while the theta band (red line) showed a strong enhancement.
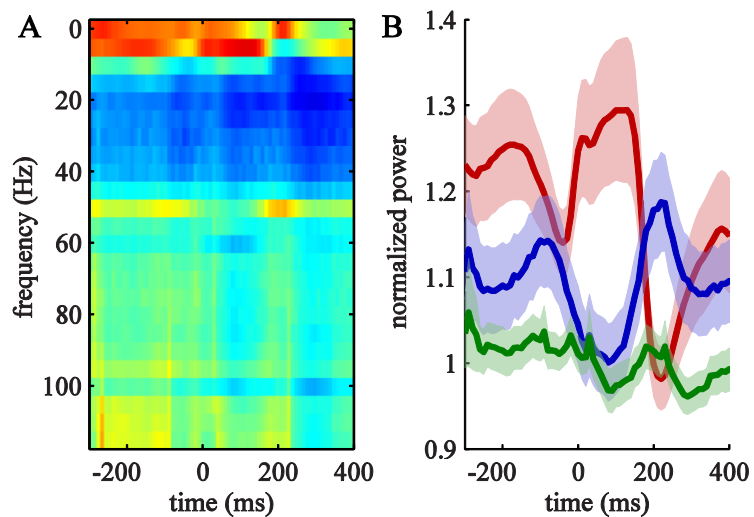
Figure 42: Spectral Density for all Sites. The figure follows the same conventions as Figure 41. The left panel presents the average power of the frequency bands for all recording sites depending on onset time. The left panel illustrates the power of the stimulus frequency (50 or 60Hz; blue), theta (5Hz, red), and gamma (40-95Hz, green).

Over all there was a trend for higher power before compared to after the fast phase (see decrease of the gamma power, green line).

Correlation changes between Stimulus and Neural Signal

In these experiments the eyes were continuously stimulated by the random flickering input. During the slow phase we can measure the RF with reverse correlation of both single cells and the LFP (see RF Positions during Slow Eye Movements (Project 2) pages 52ff). In this section we investigate how reliable the neuron responds to the stimulus around the fast phase. First, we note that it is not feasible to estimate the RF during the fast phase. It is too short to collect enough data for reverse correlation. However, we can analyze how well the RFs estimated during the slow phase or fixation correlate with the neural signals around the time of
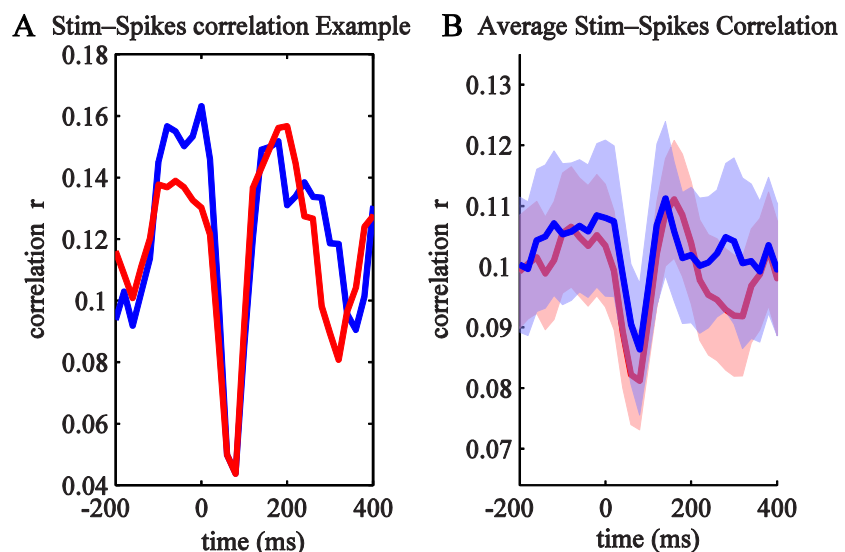
Figure 43: Projected Stimulus Correlation with Spiking. The projected stimulus (see methods) is correlated with the spike rate of a single neuron (left). The horizontal axis indicates time to fast phase onset, the vertical axis the pearson correlation. The right panel shows the average of the correlations of all single cells (shaded area: standard error). Red stands for rightward OKN (fast phase to the left); blue for leftward OKN (fast phase to the right).

the fast phase. We use this as a proxy to determine how much information the neural

activity carries about the stimulus. To do this, we projected the stimulus into the

dimension spanned by the filter estimated with reverse correlation and correlated it

with the neural signal in a sliding window around the fast phase.

Figure 43 displays these correlations for a single neuron (left) and the population (right). If we take the latency of the neural signal into account, then the correlations between projected
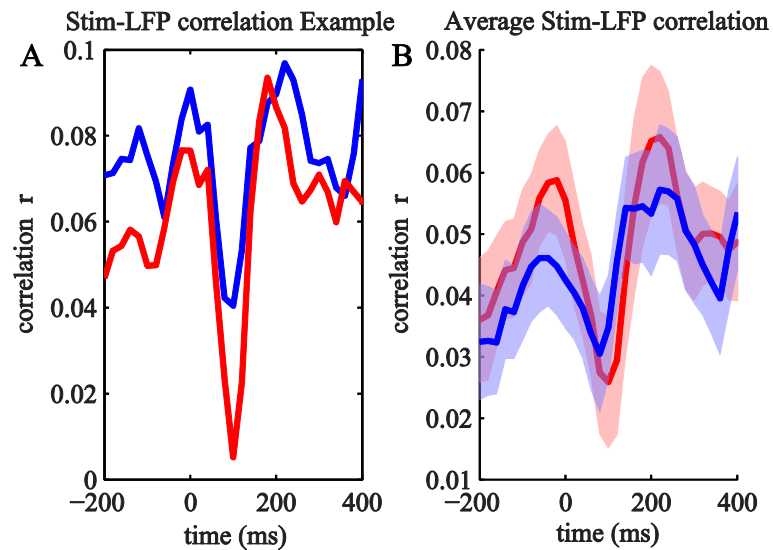
Figure 44: Correlation between the Projected Stimulus and LFP. The plots follow the same format as Figure 43

stimulus and spikes during the fast phase were significantly reduced. The correlation

was reduced long before and after the fast phase as well. The post fast phase

correlations are not significantly larger than the pre fast phase correlations (paired T-

test, p>0.05). In general, the correlation between projected stimulus and LFP followed a

similar trend (Figure 44). But the stimulus-LFP correlation displayed a significantly higher

correlation after compared to shortly before the fast phase (paired T-test, p<0.05). This

could not have been caused by differences in eye movements, the eye was moving with

approximately 10°/s during both periods.

Discussion

Saccadic Suppression is a psychophysical phenomenon found right before and during a saccade and fast eye movement (for recent reviews, see (Wurtz, 2008) or (Ibbotson and Krekelberg, 2011). In our study, we do not test the perception of the monkeys and can hence only correlate our findings with saccadic suppression as reported in other studies.

There is an ongoing debate in the literature about how visual stimuli are suppressed. There are strong arguments for a corollary discharge signal actively suppressing the percept of stimuli during saccades. Activity in a subpopulation of MT and MST neurons is suppressed (Thiele et al., 2002). Backward temporal masking has a strong contribution as well (Campbell and Wurtz, 1978), the visual stimulus at re-fixation overpowers the input during the saccade. Recently it has been proposed that backward masking is strengthened by an extraretinal signal enhancing the post saccadic response (Ibbotson and Cloherty, 2009).

The firing rate of LGN neurons is modulated prior to saccade in complete darkness (Lee and Malpeli, 1998, Ramcharan et al., 2001). Consistent changes in firing rate prior to the onset of saccades are a proof for an extraretinal signal. In our data, no effect started clearly earlier than 30ms after fast phase onset, thus the timing does not allow us to distinguish between retinal or extraretinal origin of the modulations.

The very strong modulations of the firing rate we found occurred during and after the fast phase. While there were upward or downward trends in the firing rate prior to fast phase onset, there was no strong modulation preceding the onset. This leaves room for

discussion whether the changes are due to changes on the retina or an extraretinal signal.

Two groups recorded from MT neurons while monkeys either performed saccades across a stationary stimulus or they fixated while the same contrast stimulus was moved across the screen with a speed profile identical to that of the saccades. Thiele et al. (2002) found a reversal in direction tuning in 40% of MT cells. That is, a cell that responded with an increase in firing rate to passive retinal motion to the right preferred retinal motion to the left, if this motion was induced by a saccade. Price et al. (2005) found no reversal of such kind at all. Interestingly, most neurons in our study respond with a firing increase or decrease independent of the direction of the eye movement. We presented the stimuli with relatively low refresh rates (50 and 60Hz) on a CRT screen. At 50Hz, aliasing causes gratings with a spatial frequency of e.g. 0.5cycle/° to look identical, if they move with 50°/s. During the fast phases, speeds are much higher, thus leftward and rightward fast phases induce a similar visual image on the retina. The same visual image causes the same spike rate; we therefore do not find differences in the firing rate induced by the leftward or rightward fast phases. Thiele and Price both used permanently illuminated screens, and hence did not suffer from aliasing. We cannot explain the differences in their two studies; further investigations will be needed to explain the two opposing results.

The firing rates of the two main groups of neurons—the clusters (blue: reduced firing rate; red: increased firing rate)—are similar during the slow phase. Hass and Horwitz

(2011) recorded neuronal activity in area V1 while presenting a flickering random noise pattern. They aligned the spikes to the onset of microsaccades and found a response reduction followed by a small enhancement, which resembles the responses we found in the MT cells belonging to the blue spike cluster. Therefore V1 cells would belong to the blue cluster. We know that one of the tuning properties not shared between MT and V1 neurons is the tuning for high speeds. V1 neurons prefer speeds up to 32°/s, while a lot of MT neurons prefer speeds up to 256°/s (Rodman and Albright, 1987).

We hypothesize that the two clusters in MT are tuned for low and high speeds. During the slow phase, the random dot pattern inducing the OKN is almost stationary on the retina, while the bars of the random noise stimulus flicker in the background. The speeds in the flickering stimulus vary, and both fast speed preferring and slow speed preferring neurons are stimulated. During the fast phase, there are no slow speeds on the screen. Every frame is smeared across the retina, and aliasing makes different fast phase directions indistinguishable. The blue cluster cells prefer slow speeds, and stop firing. The red cluster cells prefer high speeds and hence increase their firing rates.

There are other possibilities that can explain our results. In complete darkness, LGN neurons show a reduction of firing rate around the time of a saccade, which proves an active suppressive mechanism (Lee and Malpeli, 1998). The decrease in firing rate of one neuronal cluster could be explained by such suppression. Alternatively, the other cell cluster, which showed an increase in firing rate, could contribute to saccadic suppression by stimulus independent noise induction (Watson and Krekelberg, 2011).

The direction unspecific spikes found around the time of the fast phase could mask any stimulus specific signal. However, we do not believe that the increase in the one cluster is a mechanism to increase the stimulus independent noise. We base this assumption on previous results (Thiele et al., 2002, Price et al., 2005) which showed that MT cells do fire specific to the direction of the motion on the retina, when the screens are continuously lit.

Several studies investigating saccadic suppression found varying latency decreases for MT neurons responses after a saccade (Thiele et al., 2002, Price et al., 2005, Ibbotson et al., 2007, Ibbotson et al., 2008, Bremmer et al., 2009). In our experiment, we continuously stimulate and therefore cannot estimate typical stimulus onset response latency for MT neurons. We can define latency as the time between spikes and the frame shortest before that spike with a significant contribution to the RF. Typically that results in 30 to 40ms latencies, at the very short end of reported latencies. Price and colleagues report 67ms for a moving noise pattern during passive viewing and 30-37ms latency for stimuli motion induced by saccades. We think that our stimulus, which is continuously flickering, is already processed with a short latency. Latencies lower than 30ms seem physiologically improbable, and therefore the latency following the fast phase should not be shorter.

Both clusters showed an average increase about 100ms after the fast phase. Increases like this have been reported previously and associated with post saccadic enhancement (Reppas et al., 2002, Ibbotson et al., 2007, Ibbotson et al., 2008, Rajkai et al., 2008).

We presented the event related LFP for multiple recording sites in area MT. The signal at most recording sites shows a strong downward deflection, followed by a voltage increase above the mean. At some recording sites, this signal was reversed; a strong positive peak was followed by a negative LFP (red LFP cluster). Complete reversals in signal polarity at sites only 1 or 2mm apart must come from within the area, which proves the local nature of the LFP modulation. It has been reported that the polarity of the LFP reverses in cortex between layers 2/3 and 4 (Murthy and Fetz, 1996). We hypothesize that the recording sites belonging to red cluster were situated in layers 2/3, while the majority of recording sites (blue LFP cluster, downward deflection) were in layers 4-6. Given that more neurons are located in layers 4-6, such a bias in our selection of recording sites is not unexpected. We want to test this hypothesis by recording layer specific spikes and LFPs with a long shank electrode (see "Limitations and Future Direction" page 119).

The post fast phase firing rate increase can be seen in the example cell (Figure 35), the averages depending on fast phase direction (Figure 36), and in the split depending on spike clusters. Other groups reported post saccadic firing rate enhancements in area MT as well (Price et al., 2005, Ibbotson et al., 2007). Interestingly, when we separated the firing rate modulations based on the LFP cluster, we found a group of neurons that did not have a post fast phase increase in firing rate. These cells belonged to the red LFP cluster, therefore may have been recorded in layers 2/3. So far, there have been no reports on layer specific functional differences in area MT, and this could be a first insight into a local network involving layers in area MT. The upper layers are the layers

receiving feedback from higher visual areas (Maunsell and van Essen, 1983a). If the post fast phase enhancement is caused by a signal from a visual area involved in the generation of the eye movement, i.e. LIP, that signal would arrive in the upper layers. It will be exciting to see whether this hypothesis holds true when tested with a shank electrode (see "Limitations and Future Direction").

Assuming that we can truly identify the recording layer by the modulation of the LFP, it is worth looking at the gain fields described in chapter 5 and see whether we could identify differences there. We found that a dependents of slope for neither spikes nor the gamma band LFPs existed. Like most negative results, this should be seen cautiously. With less noise and less competing factors (such as pursuit direction, variability between monkeys) there might be an effect of layer that is currently not significant.

We saw that the fast phase triggered LFP was composed of a biphasic modulation that took roughly 150ms-200ms (5-7.5Hz). By itself, the analysis of the average LFP modulation did not tell us whether there also might have been high power in the theta (5Hz) frequency at other times, but with varying phase relative to the onset of the fast phase. The power analysis, however, showed that the power in the theta band was strongly enhanced during the fast phase, but low before and after it. Note that our analysis window for spectral analysis was 200ms wide, therefore an increase in power before the onset does not necessarily mean that the signal truly started before the onset. Hence we cannot conclude that these signals have an extraretinal origin. Moreover, in our recordings, another fast phase happened on average 200-300 ms

before and after each onset. We attribute the increases in the theta power long before and after the fast phase to the previous and next fast phase, respectively. A decrease in gamma power has been reported in V1 and V4 starting at the onset of microsaccades (Bosman et al., 2009). But they did not find an increase in the theta band, which might be MT or dorsal path specific.

The power at the stimulus frequency was significantly higher than the power for neighboring frequencies. If the increase had been an artifact of the voltage changes on the screen, then there should have been no power changes when the signal was aligned to the fast phase. Contrary to this, the stimulus frequency power showed a strong modulation, opposite to the modulation exhibited by the theta band. It appears that during the fast phase, while the visual image sweeps with high speeds across the retina, the synchronization between the stimulus and the LFP is broken. This could be caused by an extraretinal signal such as the previously discussed theta increase. Another explanation could be the changed temporal dynamics of the stimulus during the fast phase. During 1ms, the images moves 0.01° during the slow phase, but up to 0.5° at the peak of the fast phase. One pixel on the screen is 0.04° wide. On a CRT screen, the luminance peaks for a few milliseconds. Thus during the slow phase, the same pixel on the screen is eliciting responses from the same group of photoreceptors. During the fast phase, the luminance of one frame and one pixel is blurred across more than a degree.

The gamma power without the stimulus frequency is only weakly affected by the fast phase. We introduce a new neural mechanism based on synchronization in the General

Discussion, where we combine the results of this chapter and chapter 5 "Gain Fields in Spikes and LFPs (Project 3)" pages 75ff.

Correlation changes between Stimulus and Neural Signal

Typically, one would analyze the tuning curve of neurons right before or after an eye movement to find changes in visual processing. We chose the correlation of the projected stimulus and the spikes or LFP as a measure for tuning, which has its advantages and drawbacks. One advantage is the continuous measure. The projected stimulus tells us for every stimulus frame the expected firing rate or LFP strength (see Methods). Hence, this approach provides high temporal resolution. A disadvantage is that we cannot distinguish between several mechanisms that may reduce stimulus information in the response. For instance, a latency shift during the fast phase could induce a reduced correlation, but an active suppression of the neural response could too. For both spiking of cells and the LFP the correlation becomes smaller after the onset of the fast phase. A typical fast phase lasts approximately 30ms. A typical MT neuron integrates approximately from 40 to 80ms (see "Polarity Sensitivity of MT Neurons (Project 1)"). Hence, we expect that the retinal slip evoked by the saccade to affects the retinal stimulus from 40ms after onset to 80ms + 30ms = 110ms after onset. That is exactly the time window during which we see a reduced correlation between the projected stimulus and the neural activity. In other words, it seems likely that this reduced correlation is simply the consequence of retinal slip. After 110ms, however, the correlation is significantly higher than right before the fast phase. This effect is strongest

between the LFP and the projected stimulus. We interpret this increase of correlation as a sensitivity increase of MT neurons, probably via a gain increase. This is evidence of a saccade related extraretinal signal in MT.

Chapter 7 General Discussion

In the general discussion, we lay out the implications of our findings reported in projects two thru four, the three projects concerning spatial stability. The conclusion of the results in "Polarity Sensitivity of MT Neurons (Project 1)" was previously talked about in detail in the discussion of project one.

Frequency

In the late 1980's Engel and Singer as well as Eckhorn et al. proposed a solution to the binding problem: different neurons coding different features of the same object are synchronized (Eckhorn et al., 1988, Gray et al., 1989). This idea of synchronization has been debated ever since. In support of this hypothesis, Kreiter and Singer (1996) showed that neighboring MT neurons fire in synchrony if they respond to the same stimulus, but not if responding to different stimuli. Additionally Wilke et al. (2006) showed that spiking activity in V1 and V2 coded for the visual stimulus, and LFP power was reduced for stimuli that were the same on the retina but not perceived. Rajkal and colleagues (2008) also demonstrated an increase in synchronization in V1 after fixation onset in darkness. Similarly, Bosman et al. (2009) found gamma band power modulation, when the power was aligned to the onset of microsaccades in V1 and V4. Specifically, they reported a power decrease at the onset of a microsaccade in the 40-60Hz range, followed by an increase.

Here, we raise the possibility for an additional mechanism to be involved in saccadic suppression: de-synchronization. We will support this claim by showing that neither spike nor LFP are correlated with the flickering random noise stimulus during fast phases. This coincided with a strong decrease in the stimulus frequency power.

The LFP is strongly modulated by our flickering stimulus as evidenced by our ability to extract the RF for the LFP using the GLM (see "Polarity Sensitivity of MT Neurons (Project 1)"). To extract the RF, we averaged the LFP frame by frame—the stimulus frequency. Interestingly, when investigating the power of the frequencies between 5 and 115 Hz, the power of the stimulus frequency and its harmonics are higher than their neighbors—there is more power at these frequencies. We believe that the power of the stimulus frequency is a direct result of the stimulus flickering; activity in MT is synchronized by the input. As stated earlier, area MT neurons fire in synchrony when coding the same stimulus (Kreiter and Singer, 1996). If spikes coding properties of the same stimulus are synchronized, then destroying this synchrony would result in the spike not being interpreted as stimulus spikes. We would expect this to result in a loss of stimulus perception. In support of this, we find a strong reduction in power in the stimulus frequency band during the fast phase (see "Modulations during Fast Eye Movements (Project 4)"). The power in the theta band is our candidate for causing the reduction in the stimulus frequency power; its modulation profile is essentially mirrored to that of the stimulus frequency power. If a signal with a theta signature destroys the synchrony in the stimulus frequency, then spikes occurring during the fast phase might

not be attributed to any stimulus. Consequently, strong stimuli still causing spikes might not induce perception.

In areas V1 and V2, identical retinal stimuli typically cause similar firing rates, independent of context (Wilke et al., 2006). During the presentation of similar but not visible stimuli, the LFP power revealed sustained and consistent changes based on perceptual visibility. These results suggest that synchrony may be necessary for perception. Watson and Krekelberg (2009) demonstrated the persistence of an illusion across saccades, even though the inducer of the illusion was not always perceived. They concluded that early visual cortices must code the non-perceived stimulus; otherwise subjects could not report an illusion. This effect can be explained, if the illusion inducing stimulus was associated with less synchrony, but cells still code it, and therefore still induced the illusion.

Spike rates also change—unrelated to the stimulus—based on eye position (see "Gain Fields in Spikes and LFPs (Project 3)"). The example neuron we present in Figure 26 changes its firing rate by more than 1 spike per second per degree. Over 40°, that is a change in firing rate of at least 40spikes/s. To impress the magnitude of this variance it should be noted that the average firing rate for this neuron was approximately 40spikes/s as well. Typically, we see an area MT neuron as an indicator for motion direction or speed of stimuli. How can a neuron that receives input from our example neuron differentiate between spikes received because the eye is directed to the left and the stimulus is moving at a non-preferred speed versus the eye is directed to the right

and a stimulus is moving at the preferred speed? Synchronization of all eye position spikes is a possible solution to this problem. Spikes that are synchronized to the rest of the eye position spikes inform about the eye position (or pursuit direction), while spikes synchronized with the stimulus inform about stimulus properties. The strong gamma band gain fields we found are in support of this hypothesis.

We also find power modulations in the gamma band without the stimulus frequency, but not during the fast phase. The gamma power modulations we found are dependent on eye position (see "Gain Fields in Spikes and LFPs (Project 3)"). Morris and colleagues (under review) analyzed the temporal profile of gain field changes around saccades and found a sluggish change, which they used to explain perisaccadic mislocalization (see below). We found no strong dynamic changes around the fast phase in the gamma power. We view this as an indication of support of gain fields' slow change.

In conclusion, we predict that synchronization has a strong influence on saccadic suppression and position estimation via gain fields. Spikes caused by visual stimuli are de-synchronized during saccades thru a signal in the theta band. The de-synchronization works with other suppression mechanisms such as that resulting from corollary discharge signal and backward masking. The theta signal could allow an increase of stimulus spike coherence following a saccade and enhance visual perception. During fixation or pursuit, gain fields allow estimation of current eye position. Neural activity involved in gain fields is synchronized, allowing its identification as non-stimulus related activity. Previously, Kreiter and Singer (1996) hypothesized that synchrony in area MT

permits the distinction between one or two objects. We speculate that synchrony may play a more general role in the cortex. That is, cell assemblies spiking together code the same, whether it be a moving stimulus or a gain field.

The idea of synchrony has been proposed many times, but questions still remain. For example, Thiele and Stoner (2003) showed moving plaid patterns composed of gratings produce more synchrony when perceived as two surfaces rather than one. Meanwhile, the binding by synchrony hypothesis predicts the opposite. There are also unique problems with our stimulus. Our stimulus conditions are well defined for frequency synchronization, as the stimulus itself is oscillating. However, in everyday life, we do not look at CRT screens refreshing at a frequency in the gamma band range but instead view scenes with constant illumination. It is unclear how theta de-synchronization signal may determine which spikes to de-correlate.

Perisaccadic Mislocalisation and Gain Fields

Mislocalization around eye movements is a reliable finding, particularly the shift of perceived location in the direction of an eye movement at the start of the movement. The RF location shifts in the direction of the eye movement outside of MT as well. Both effects share similar properties in magnitude and timing, thus they have been linked. However, there are problems with this connection. First, in "RF Positions during Slow Eye Movements (Project 2)" we show that the RF does not shift during the slow phase of OKN, despite psychophysical results demonstrating a clear shift (Kaminiarz et al., 2007). Second, another to us more convincing explanation has been proposed.

It has been suggested by Dassonville et al. (1992) that saccadic mislocalization results from a dampened representation of eye position. Morris et al. identified such a signal as being the previously known gain fields (under review). They analyzed activity of neurons in MT, MST, LIP, and VIP during fixation at different locations. First, they confirmed the existence of gain fields in all areas. They then created a model extracting the position coded for by the gain fields of the all neurons. Upon a saccade, the gain fields start to encode the future eye position up to 100ms before onset; 150ms after the saccade the gain field is completely coding for the new position. In accordance with these previous results we find gain fields in both spikes and LFP power. Whereas the spike rates change strongly around the time of fast phases, the gamma power does not. Typically fast phases were 4 °, quite small when compared to the gain field size (our analysis resolution was 2° x 2°). It is possible gamma gain fields could provide a more stable code of eye position due to the direct influence of the visual stimulus being weaker at these frequencies. It would be interesting to find a lag in the gamma gain fields which could explain mislocalization, resembling the way spike rates can (Morris et al., under review). The exact timing of power is difficult to estimate and thus, determining a lag is more problematic. A time lag in the gamma gain fields would allow the brain to code position information independent of stimulus strength and could explain the psychophysical phenomena, perisaccadic mislocalization, discussed in "RF Positions during Slow Eye Movements (Project 2)", independent of neurons firing rates and therefore stimulus conditions.

Limitations and Future Direction

In "Polarity Sensitivity of MT Neurons (Project 1)" we showed an unexplained polarity sensitivity of MT neurons using an information theoretic approach. This information theoretic approach is not necessarily the most straight forward approach; polarity sensitivity testing can be achieved with simpler methods. In V1, for example, polarity sensitivity has been tested quantitatively since the 70's (e.g. (Movshon et al., 1978b, a)). To verify our findings we should present the stimuli used in these V1 studies and confirm our results. We could present gratings in the RF moving with different speeds and different spatial frequencies to calculate the ratio of the response at the stimulus frequency divided by the average firing rate—f_1/f_0—as a measure of polarity sensitivity. Additionally, we could test the RF with single black or white bars to confirm that parts of the RF only respond to black or white bars. We would like to also record the response to random noise. This would help to understand differences in case the results of the traditional stimuli and the random noise stimuli are different.

Ultimately, we want to understand the neural correlates of perception. All experiments lack a behavioral component; the monkeys never report their percept. Both perisaccadic mislocalization and saccadic suppression are behavioral effects. From psychophysical studies we know that there is great inter and intra subject variability in effects. Ideally, we want to train monkeys to report the effects (saw stimulus or not, location of stimulus). We could then correlate a neural substrate candidate with the trial by trial perception. A true saccadic suppression signal should be high on trials the monkey did not see a target and low when the target was perceived.

The results of "Gain Fields in Spikes and LFPs (Project 3)" and "Modulations during Fast Eye Movements (Project 4)" were recorded during OKN. Human vision mostly consists of fixation periods interspersed with saccades. Therefore, it is desirable to repeat the experiments with fixation and saccades, rather than slow and fast phases. The gain field analysis would not suffer from the confounding fact that there are two gain fields, the eye position gain fields and those related to the direction of the slow phase (similar to the pursuit gain fields reported in MT). During OKN, the eye positions are unequally distributed across the screen, which makes statistical analysis more challenging. During fixation, we can choose a fixed number of positions on the screen with an equal amount of recording time. Changes in gain fields around the fast phase of OKN are very difficult to analyze, the eye rarely starts the fast phase from the same location. Planned saccades would allow multiple repetitions of the same eye movement, enhancing statistical strength of the data set.

In the future, we could test whether the strong LFP RFs found truly depend only on the stimulus frequency, as we hypothesize in the previous section. We could test this by filtering the stimulus frequency out and reanalyzing the LFP in the same manner as before. In a second experiment, we could replace the CRT screen with an LED panel that allows control of the luminance on a microsecond scale. With such a device, we would be able to ensure that the visual stimuli on the retina are identical regardless of the stage of the eye movement. Also, we could present stimuli at different temporal frequencies to confirm that the stimulus frequency oscillations really depend on the stimulus.

During the slow phase, the random dot pattern is approximately stationary on the retina. During the fast phase, the dots move to either the right or the left, depending on the fast phase direction. These dots, which might influence the firing of MT, could be omitted and excluded as a source for systematic noise. The estimation of projected stimulus to neural signal correlation would benefit from an RF estimate while the eye is not in motion.

Another control should be done without any or with minimal visual stimulation. Instead of a computer screen with fixation points and a flickering background, we could use low luminance photo diodes as fixation points in an otherwise completely dark room. Most of the signal change could possibly be attributed to an extraretinal signal. A problem with this control could be low firing rates and low gamma band power, because of a lack of excitation. Baseline firing rates are typically low, which makes it difficult to find a significant decrease.

The random noise stimulus is ideal for recording from multiple sites at the same time, which makes the methods very valuable while recording with a multi electrode array. Currently, array recordings in area MT are technically unfeasible; as an alternative we could record from areas such as V1 or V4 to understand their contribution to spatial stability. A shank electrode, a single electrode with multiple sites hundreds of micrometers apart, would be ideal to test the hypothesis that the LFP clusters depend on the layer. We are cooperating with NeuroNexus to test such an electrode in area MT. We hope to record the first layer-specific data in area MT at the end of 2011. Recording

the LFP at different MT layers would prove or reject our hypothesis put forward in "Modulations during Fast Eye Movements (Project 4)". Explicitly, whether the polarity of the LFP modulation around the time of the fast phase depends on the layer it is recorded in. This could strengthen our theory that area MT neurons in the upper layers receive a top-down signal that increases their firing rate and correlation with the stimulus after fast phase offset. MT neurons in layers 2/3 do not receive such an input and therefore do not show a post saccadic enhancement in firing rate.

Conclusions

In this document, we presented the results of four projects. In "Polarity Sensitivity of MT Neurons (Project 1)" we studied area MT during passive sensing. While the monkeys kept the visual image still on the retina, we analyzed the input—output (the visual image—spikes of MT neurons) relationship and revealed that area MT neurons, contrary to the beliefs in the literature, are sensitive to the polarity of stimuli.

In daily life monkeys and humans do not fixate red dots for extended periods of time. Rather, we actively sense our environment by moving our eyes to stimuli with high salience or to keep the image stable on the retina. One such eye movement is OKN. We studied its influence on the activity of MT neurons in projects 2-4. In "RF Positions during Slow Eye Movements (Project 2)", we showed that the RF of MT neurons as well as the RF of the LFP remain stable during the slow phase of OKN. At all times the RFs are yoked to the eye, neurons in area MT code in an eye-centered reference frame. However, this does not mean that neurons in area MT are clueless about the eyes

current position. In "Gain Fields in Spikes and LFPs (Project 3)" we prove the existence of gain fields—a gain modulation of firing rates depending on eye position—during OKN. Previously, gain fields have only been shown during fixation and pursuit. Interestingly, the power in the gamma band of the LFP also shows strong modulations that depend on eye position. Most of these gamma band gain fields have positive vertical slopes, suggesting a previously unknown bias in gain fields in area MT.

In "Modulations during Fast Eye Movements (Project 4)" we found heterogenic responses in neural activity to the fast phase of OKN. Approximately half the neurons responded with a decrease, the others with an increase of firing rate starting 30ms and peaking 70ms after fast phase onset. One possible explanation assumes that cells tuned for low speeds decrease the firing rate during the high retinal stimuli speeds during the fast phase. Cells that increase the firing rates are presumed to be tuned for high speeds. The LFP is also modulated around the time of the fast phase. We hypothesize that the sign of the deflection around the fast phase informs us about the layer we recorded. Firing rates that were recorded in the upper layers showed a post-fast phase enhancement, which was missing in firing rates recorded in layers 2/3. On this basis, we speculate that this enhancement may arise through feedback from higher visual areas.

In conclusion, our research provides new insights into mechanisms important for motion processing in area MT. Furthermore we present novel concepts pertaining to the understanding of spatial stability.

List of Abbreviations

FEF	Frontal Eye Fields
iSTAC	Information theoretic Spike Triggered Average and Covariance
KL	Kullback-Leibler (Divergence)
LFP	Local Field Potential
LGN	Lateral Geniculate Nucleus
LIP	Lateral Intrapariental (Area)
LN	Linear Nonlinear (Model)
LWA	LFP weighted stimulus average
MST	Middle Superior Temporal (Area)
MT	Middle Temporal (Area)
OKN	Optokinetic Nystagmus
RF	Receptive Field
RFI	Reference Frame Index
RGC	Retinal Ganglion Cells
ROI	Region of Interest
SC	Superior Colliculus
STA	Spike Triggered Average
STC	Spike Triggered Covariance
V1	Primary Visual Cortex
VIP	Ventral Intrapariental (Area)

References

Adelson EH, Bergen JR (1985) Spatiotemporal energy models for the perception of motion. Journal of the Optical Society of America   Part A, Optics and Image Science (Washington) 2:284-299.

Albright TD (1984) Direction and orientation selectivity of neurons in visual area MT of the macaque. J Neurophysiol 52:1106-1130.

Albright TD, Desimone R, Gross CG (1984) Columnar organization of directionally selective cells in visual area MT of the macaque. J Neurophysiol 51:16-31.

Allman JM, Kaas JH (1971) A representation of the visual field in the caudal third of the middle temporal gyrus of the owl monkey (Aotus Trivirgatus). Brain Res 31:85-105.

Andersen RA, Essick GK, Siegel RM (1985) Encoding of spatial location by posterior parietal neurons. Science 230:456-458.

Andersson F, Joliot M, Perchey G, Petit L (2007) Eye position-dependent activity in the primary visual area as revealed by fMRI. Hum Brain Mapp 28:673-680.

Avillac M, Deneve S, Olivier E, Pouget A, Duhamel JR (2005) Reference frames for representing visual and tactile locations in parietal cortex. Nat Neurosci.

Bedard C, Kroger H, Destexhe A (2004) Modeling extracellular field potentials and the frequency-filtering properties of extracellular space. Biophys J 86:1829-1842.

Born RT, Bradley DC (2005) Structure and function of visual area MT. Annu Rev Neurosci 28:157-189.

Bosman CA, Womelsdorf T, Desimone R, Fries P (2009) A microsaccadic rhythm modulates gamma-band synchronization and behavior. J Neurosci 29:9471-9480.

Bremmer F, Ilg UJ, Thiele A, Distler C, Hoffmann KP (1997) Eye position effects in monkey cortex. I. Visual and pursuit-related activity in extrastriate areas MT and MST. J Neurophysiol 77:944-961.

Bremmer F, Kubischik M, Hoffmann KP, Krekelberg B (2009) Neural Dynamics of Saccadic Suppression. J Neurosci 29:12374-12383.

Burr DC, Morrone MC (2011) Spatiotopic coding and remapping in humans. Philos Trans R Soc Lond B Biol Sci 366:504-515.

Burr DC, Morrone MC, Ross J (1994) Selective suppression of the magnocellular visual pathway during saccadic eye movements. Nature 371:511-513.

Campbell FW, Wurtz RH (1978) Saccadic omission: why we do not see a grey-out during a saccadic eye movement. Vision Res 18:1297-1303.

Carandini M (2006) What simple and complex cells compute. J Physiol 577:463-466.

Castet E, Jeanjean S, Masson GS (2001) 'Saccadic suppression'- no need for an active extra-retinal mechanism. Trends Neurosci 24:316-318.

Chander D, Chichilnisky EJ (2001) Adaptation to temporal contrast in primate and salamander retina. J Neurosci 21:9904-9916.

Chichilnisky EJ (2001) A simple white noise analysis of neuronal light responses. Network 12:199-213.

Chukoskie L, Movshon JA (2009) Modulation of visual signals in macaque MT and MST neurons during pursuit eye movement. J Neurophysiol 102:3225-3233.

Cover TM, Thomas JA (1991) Elements of Information Theory.

d'Avossa G, Tosetti M, Crespi S, Biagi L, Burr DC, Morrone MC (2007) Spatiotopic selectivity of BOLD responses to visual motion in human area MT. Nat Neurosci 10:249-255.

Dassonville P, Schlag J, Schlag-Rey M (1992) Oculomotor localization relies on a damped representation of saccadic eye displacement in human and nonhuman primates. Vis Neurosci 9:261-269.

DeAngelis GC, Newsome WT (1999) Organization of disparity-selective neurons in macaque area MT. J Neurosci 19:1398-1415.

Deneve S, Latham PE, Pouget A (2001) Efficient computation and cue integration with noisy population codes. Nat Neurosci 4:826-831.

DeSouza JF, Dukelow SP, Gati JS, Menon RS, Andersen RA, Vilis T (2000) Eye position signal modulates a human parietal pointing region during memory-guided movements. J Neurosci 20:5835-5840.

DeYoe EA, Van Essen DC (1985) Segregation of efferent connections and receptive field properties in visual area V2 of the macaque. Nature 317:58-61.

Diamond MR, Ross J, Morrone MC (2000) Extraretinal control of saccadic suppression. J Neurosci 20:3449-3455.

Dobkins KR, Albright TD (1994) What happens if it changes color when it moves?: the nature of chromatic input to macaque visual area MT. Journal of Neuroscience 14:4854-4870.

Dubner R, Zeki SM (1971) Response properties and receptive fields of cells in an anatomically defined region of the superior temporal sulcus in the monkey. Brain Res 35:528-532.

Duhamel JR, Bremmer F, Ben Hamed S, Graf W (1997) Spatial invariance of visual receptive fields in parietal cortex neurons. Nature 389:845-848.

Duhamel JR, Colby CL, Goldberg ME (1992) The updating of the representation of visual space in parietal cortex by intended eye movements. Science 255:90-92.

Durand JB, Trotter Y, Celebrini S (2010) Privileged processing of the straight-ahead direction in primate area V1. Neuron 66:126-137.

Eckhorn R, Bauer R, Jordan W, Brosch M, Kruse W, Munk M, Reitboeck HJ (1988) Coherent oscillations: a mechanism of feature linking in the visual cortex? Multiple electrode and correlation analyses in the cat. Biol Cybern 60:121-130.

Felleman DJ, Van Essen DC (1991) Distributed hierarchical processing in the primate cerebral cortex. Cerebral Cortex 1:1-47.

Galletti C, Fattori P, Gamberini M, Kutz DF (1999) The cortical visual area V6: brain location and visual topography. Eur J Neurosci 11:3922-3936.

Gardner JL, Merriam EP, Movshon JA, Heeger DJ (2008) Maps of Visual Space in Human Occipital Cortex Are Retinotopic, Not Spatiotopic. Journal of Neuroscience 28:3988-3999.

Gray CM, Koenig P, Engel AK, Singer W (1989) Oscillatory responses in cat visual cortex exhibit inter-columnar synchronization which reflects global stimulus properties. Nature 338:334-337.

Hass CA, Horwitz GD (2011) Effects of microsaccades on contrast detection and V1 responses in macaques. J Vis 11:1-17.

Hassenstein B, Reichardt W (1956) Systemtheoretische Analyse der Zeit-, Reihenfolgen und Vorzeichenauswertung bei der Bewegungsperzeption des Russelkaefers Chlorophanus. Zeitschrift für Naturforschung 11 B:513-524.

Helmholtz Hv (1856) Handbuch der Physiologischen Optik. Leipzig: Voss.

Holt EB (1903) Eye movements and central anaesthesia. Psychological Review 4:3-45.

Honda H (1989) Perceptual localization of visual stimuli flashed during saccades. Percept Psychophys 45:162-174.

Honda H (1991) The time courses of visual mislocalization and of extraretinal eye position signals at the time of vertical saccades. Vision Res 31:1915-1921.

Horwitz GD, Chichilnisky EJ, Albright TD (2005) Blue-yellow signals are enhanced by spatiotemporal luminance contrast in macaque V1. J Neurophysiol 93:2263-2278.

Hubel DH, Wiesel TN (1962) Receptive fields, binocular interaction and functional architecture in the cat's visual cortex. J Physiol 160:106-154.

Hubel DH, Wiesel TN (1968) Receptive fields and functional architecture of monkey striate cortex. J Physiol 195:215-243.

Hubel DH, Wiesel TN, Stryker MP (1977) Orientation columns in macaque monkey visual cortex demonstrated by the 2-deoxyglucose autoradiographic technique. Nature 269:328-330.

Ibbotson MR, Krekelberg B (2011) Visual perception and saccadic eye movements. Curr Opin Neurobiol.

Ibbotson MR, Cloherty SL (2009) Visual perception: saccadic omission--suppression or temporal masking? Current biology : CB 19:R493-496.

Ibbotson MR, Crowder NA, Cloherty SL, Price NS, Mustari MJ (2008) Saccadic modulation of neural responses: possible roles in saccadic suppression, enhancement, and time compression. The Journal of neuroscience : the official journal of the Society for Neuroscience 28:10952-10960.

Ibbotson MR, Price NS, Crowder NA, Ono S, Mustari MJ (2007) Enhanced Motion Sensitivity Follows Saccadic Supression in the Superior Temporal Sulcus of the Macaque Cortex. Cerebral Cortex 17:1129-1138.

Johns M, Crowley K, Chapman R, Tucker A, Hocking C (2009) The effect of blinks and saccadic eye movements on visual reaction times. Atten Percept Psychophys 71:783-788.

Joukes J, Krekelberg B (2009) A motion model based on a recurrent network. In: Computational and systems neuroscience 2009 Salt Lake City, UT, USA: Front. Syst. Neurosci. Conference Abstract.

Kaminiarz A, Krekelberg B, Bremmer F (2007) Localization of visual targets during optokinetic eye movements. Vision Research 47:869-878.

Kaminiarz A, Krekelberg B, Bremmer F (2008) Expansion of Visual Space During Optokinetic Afternystagmus (OKAN). Journal of Neurophysiology 99:2470-2478.

Kandel ER, Schwartz JH, Jessell TM (1991) Principles of Neural Science.

Knapp CM, Gottlob I, McLean RJ, Proudlock FA (2008) Horizontal and vertical look and stare optokinetic nystagmus symmetry in healthy adult volunteers. Invest Ophthalmol Vis Sci 49:581-588.

Konen CS, Kleiser R, Seitz RJ, Bremmer F (2005) An fMRI study of optokinetic nystagmus and smooth-pursuit eye movements in humans. Exp Brain Res 165:203-216.

Konigs K, Bremmer F (2010) Localization of visual and auditory stimuli during smooth pursuit eye movements. J Vis 10:8.

Kreiter AK, Singer W (1996) Stimulus-dependent synchronization of neuronal responses in the visual cortex of the awake macaque monkey. J Neurosci 16:2381-2396.

Krekelberg B (2008) Perception of Direction is not Compensated for Neural Latency. Behavioral and Brain Science 31:208-209.

Krekelberg B, Albright TD (2005) Motion mechanisms in macaque MT. Journal of Neurophysiology 93:2908-2921.

Krekelberg B, Kubischik M, Hoffmann KP, Bremmer F (2003) Neural correlates of visual localization and perisaccadic mislocalization. Neuron 37:537-545.

Krekelberg B, van Wezel RJ, Albright TD (2006) Interactions between speed and contrast tuning in the middle temporal area: implications for the neural code for speed. J Neurosci 26:8988-8998.

Lappe M, Awater H, Krekelberg B (2000) Postsaccadic visual references generate presaccadic compression of space. Nature 403:892-895.

Lee D, Malpeli JG (1998) Effects of saccades on the activity of neurons in the cat lateral geniculate nucleus. J Neurophysiol 79:922-936.

Leopold DA, Logothetis NK (1998) Microsaccades differentially modulate neural activity in the striate and extrastriate visual cortex. Exp Brain Res 123:341-345.

Liu J, Newsome WT (2006) Local field potential in cortical area MT: stimulus tuning and behavioral correlations. J Neurosci 26:7779-7790.

Logothetis NK, Pauls J, Augath M, Trinath T, Oeltermann A (2001) Neurophysiological investigation of the basis of the fMRI signal. Nature 412:150-157.

Mackensen G, Schumacher J (1960) [Rate of the rapid phase of optokinetic nystagmus]. Graefes Arch Clin Exp Ophthalmol 162:400-415.

Maunsell JH, Newsome WT (1987) Visual processing in monkey extrastriate cortex. Annu Rev Neurosci 10:363-401.

Maunsell JH, van Essen DC (1983a) The connections of the middle temporal visual area (MT) and their relationship to a cortical hierarchy in the macaque monkey. Journal of Neuroscience 3:2563-2586.

Maunsell JH, Van Essen DC (1983b) Functional properties of neurons in middle temporal visual area of the macaque monkey. I. Selectivity for stimulus direction, speed, and orientation. J Neurophysiol 49:1127-1147.

Maunsell JH, Van Essen DC (1983c) Functional properties of neurons in middle temporal visual area of the macaque monkey. II. Binocular interactions and sensitivity to binocular disparity. J Neurophysiol 49:1148-1167.

Melcher D, Morrone MC (2003) Spatiotopic temporal integration of visual motion across saccadic eye movements. Nat Neurosci 6:877-881.

Merriam EP, Genovese CR, Colby CL (2003) Spatial updating in human parietal cortex. Neuron 39:361-373.

Mishkin M, Ungerleider LG (1982) Contribution of striate inputs to the visuospatial functions of parieto- preoccipital cortex in monkeys. Behav Brain Res 6:57-77.

Morris AP, Kubischik M, Hoffmann KP, Krekelberg B, Bremmer F (2009) The spatiotemporal structure of eye position signals in macaque cortical neurons. Society for Neuroscience Abstracts.

Morris AP, Kubischik M, Hoffmann KP, Krekelberg B, Bremmer F (under review) Dynamics of eye-position signals in the dorsal visual system. Current Biology X:XXX.

Movshon JA, Newsome WT (1996) Visual response properties of striate cortical neurons projecting to area MT in macaque monkeys. J Neurosci 16:7733-7741.

Movshon JA, Thompson ID, Tolhurst DJ (1978a) Receptive field organization of complex cells in the cat's striate cortex. J Physiol 283:79-99.

Movshon JA, Thompson ID, Tolhurst DJ (1978b) Spatial summation in the receptive fields of simple cells in the cat's striate cortex. J Physiol 283:53-77.

Murthy VN, Fetz EE (1996) Oscillatory activity in sensorimotor cortex of awake monkeys: synchronization of local field potentials and relation to behavior. J Neurophysiol 76:3949-3967.

Nakamura K, Colby CL (2002) Updating of the visual representation in monkey striate and extrastriate cortex during saccades. Proc Natl Acad Sci U S A 99:4026-4031.

Nassi J, Lyon D, Callaway E (2006) The Parvocellular LGN Provides a Robust Disynaptic Input to the Visual Motion Area MT. Neuron 50:319-327.

Nir Y, Dinstein I, Malach R, Heeger DJ (2008) BOLD and spiking activity. Nature Neuroscience 11:523-524; author reply 524.

Ong WS, Bisley J (2011) A lack of anticipatory remapping of retinotopic receptive fields in the middle temporal area. J Neurosci 31:10432-10436.

Ong WS, Hooshvar N, Zhang M, Bisley JW (2009) Psychophysical evidence for spatiotopic processing in area MT in a short-term memory for motion task. J Neurophysiol 102:2435-2440.

Orban GA, Van Essen D, Vanduffel W (2004) Comparative mapping of higher visual areas in monkeys and humans. Trends Cogn Sci 8:315-324.

Palmer LA, Rosenquist AC (1974) Visual receptive fields of single striate cortical units projecting to the superior colliculus in the cat. Brain Res 67:27-42.

Pillow JW, Simoncelli EP (2006) Dimensionality reduction in neural models: An information-theoretic generalization of spike-triggered average and covariance analysis. Journal of Vision 6:9-9.

Poggio T, Reichardt W (1973) Considerations on models of movement detection. Kybernetik 13:223-227.

Ponce CR, Lomber SG, Born RT (2008) Integrating motion and depth via parallel pathways. Nat Neurosci 11:216-223.

Price NS, Ibbotson MR, Ono S, Mustari MJ (2005) Rapid Processing of Retinal Slip During Saccades in Macaque Area MT. Journal of Neurophysiology 94:235-246.

Quiroga RQ, Nadasdy Z, Ben-Shaul Y (2004) Unsupervised spike detection and sorting with wavelets and superparamagnetic clustering. Neural Computation 16:1661-1687.

Rajkai C, Lakatos P, Chen CM, Pincze Z, Karmos G, Schroeder CE (2008) Transient cortical excitation at the onset of visual fixation. Cereb Cortex 18:200-209.

Ramcharan EJ, Gnadt JW, Sherman SM (2001) The effects of saccadic eye movements on the activity of geniculate relay neurons in the monkey. Vis Neurosci 18:253-258.

Reppas JB, Usrey WM, Reid RC (2002) Saccadic eye movements modulate visual responses in the lateral geniculate nucleus. Neuron 35:961-974.

Rockland KS (1989) Bistratified distribution of terminal arbors of individual axons projecting from area V1 to middle temporal area (MT) in the macaque monkey. Vis Neurosci 3:155-170.

Rodman HR, Albright TD (1987) Coding of visual stimulus velocity in area MT of the macaque. Vision Res 27:2035-2048.

Ross J, Morrone MC, Burr DC (1997) Compression of visual space before saccades. Nature 386:598-601.

Ross J, Morrone MC, Goldberg ME, Burr DC (2001) Changes in visual perception at the time of saccades. Trends Neurosci 24:113-121.

Rust NC, Schwartz O, Movshon JA, Simoncelli EP (2005) Spatiotemporal Elements of Macaque V1 Receptive Fields. Neuron 46:945-956.

Schlack A, Sterbing-D'Angelo SJ, Hartung K, Hoffmann KP, Bremmer F (2005) Multisensory space representations in the macaque ventral intraparietal area. Journal of Neuroscience 25:4616-4625.

Schoppmann A, Hoffmann KP (1976) Continuous mapping of direction selectivity in the cat's visual cortex. Neuroscience Letters 2:177-181.

Schroeder CE, Wilson DA, Radman T, Scharfman H, Lakatos P (2010) Dynamics of Active Sensing and perceptual selection. Curr Opin Neurobiol 20:172-176.

Schwartz O, Pillow JW, Rust NC, Simoncelli EP (2006) Spike-triggered neural characterization. Journal of Vision 6:13-13.

Shipp S, Zeki S (1989a) The Organization of Connections between Areas V5 and V1 in Macaque Monkey Visual Cortex. Eur J Neurosci 1:309-332.

Shipp S, Zeki S (1989b) The Organization of Connections between Areas V5 and V2 in Macaque Monkey Visual Cortex. Eur J Neurosci 1:333-354.

Simoncelli EP, Heeger DJ (1998) A model of neuronal responses in visual area MT. Vision Res 38:743-761.

Snyder LH (2000) Coordinate transformations for eye and arm movements in the brain. Curr Opin Neurobiol 10:747-754.

Sommer MA, Wurtz RH (2008) Visual perception and corollary discharge. Perception 37:408-418.

Sperry RW (1950) Neural basis of the spontaneous optokinetic response produced by visual inversion. J Comp Physiol Psychol 43:482-489.

Stepniewska I, Qi HX, Kaas JH (1999) Do superior colliculus projection zones in the inferior pulvinar project to MT in primates? Eur J Neurosci 11:469-480.

Thiele A, Henning P, Kubischik M, Hoffmann KP (2002) Neural Mechanisms of Saccadic Suppression. Science 295:2460-2462.

Thiele A, Stoner G (2003) Neuronal synchrony does not correlate with motion coherence in cortical area MT. Nature 421:366-370.

Tigges J, Tigges M, Anschel S, Cross NA, Letbetter WD, McBride RL (1981) Areal and laminar distribution of neurons interconnecting the central visual cortical areas 17, 18 19 and MT in squirrel monkey (Saimiri). J Comp Neurol 202:539-560.

Tolias AS, Moore T, Smirnakis SM, Tehovnik EJ, Siapas AG, Schiller PH (2001) Eye movements modulate visual receptive fields of V4 neurons. Neuron 29:757-767.

Umeno MM, Goldberg ME (1997) Spatial processing in the monkey frontal eye field. I. Predictive visual responses. J Neurophysiol 78:1373-1383.

van Beers RJ, Wolpert DM, Haggard P (2001) Sensorimotor integration compensates for visual localization errors during smooth pursuit eye movements. J Neurophysiol 85:1914-1922.

Viswanathan A, Freeman RD (2007) Neurometabolic coupling in cerebral cortex reflects synaptic more than spiking activity. Nature Neuroscience 10:1308-1312.

von Holst E, Mittelstaedt H (1950) Das Reafferenzprinzip (Wechselwirkung zwischen Zentralnervensystem und Peripherie). Naturwissenschaften 37:464-476.

Walker MF, Fitzgibbon EJ, Goldberg ME (1995) Neurons in the monkey superior colliculus predict the visual result of impending saccadic eye movements. J Neurophysiol 73:1988-2003.

Wang X, Zhang M, Cohen IS, Goldberg ME (2007) The proprioceptive representation of eye position in monkey primary somatosensory cortex. Nat Neurosci 10:640-646.

Wassle H, Grunert U, Rohrenbeck J, Boycott BB (1990) Retinal ganglion cell density and cortical magnification factor in the primate. Vision Res 30:1897-1911.

Watson TL, Krekelberg B (2011) An equivalent noise investigation of saccadic suppression. J Neurosci 31:6535-6541.

Watson TL, Krekelberg B (2009) The relationship between saccadic suppression and perceptual stability. Curr Biol 19:1040-1043.

Wilke M, Logothetis NK, Leopold DA (2006) Local field potential reflects perceptual suppression in monkey visual cortex. Proc Natl Acad Sci U S A 103:17507-17512.

Wurtz RH (1969) Comparison of effects of eye movements and stimulus movements on striate cortex neurons of the monkey. J Neurophysiol 32:987-994.

Wurtz RH (2008) Neuronal mechanisms of visual stability. Vision Research 48:2070-2089.

Zuber BL, Stark L (1966) Saccadic suppression: elevation of visual threshold associated with saccadic eye movements. Exp Neurol 16:65-79.

Curriculum Vitae of Till S. Hartmann

1980	Born on October 14th in Marburg, Germany

1991-2000   Attended and graduated from Gymnasium Philippinum (High School) Marburg, Germany

2001-2006   Undergraduate and graduate studies in physics, Philipps University Marburg, Germany Finished with a Diploma in physics (equivalent to M.Sc. in physics).

2004-2005   Diploma thesis research in the Vision Center Laboratory at The Salk Institute for Biological Studies, La Jolla, CA under Bart Krekelberg and Thomas D. Albright.

2006-2011   Graduate Fellowship at the Center for Molecular and Behavioral Neuroscience under Bart Krekelberg.

2011   PhD Thesis "White Noise Analysis of visual selectivity in area MT during Fixation and Eye Movements"

Publications:

Receptive Field Positions in Area MT during Slow Eye Movements; Till S. Hartmann, Frank Bremmer, Thomas D. Albright, and Bart Krekelberg; Journal of Neuroscience 31(29): 10437-10444 20 July 2011

Conference Abstracts:

Predictive Neural Signals Related to Eye Movements in Visual Cortex; Bart Krekelberg, Jacob Duijnhouwer, Till S. Hartmann; European Conference on Eye Movements 2011
Simple cells provide strong input to MT neurons; Till S. Hartmann, Bart Krekelberg; Cosyne Meeting 2011
Perisaccadic Response Properties of MT Neurons; Till S. Hartmann, Frank Bremmer, Bart Krekelberg; Vision Sciences Society Annual Meeting, 2010
Changes of visual response properties in area MT due to eye movements; Till S. Hartmann, Thomas D. Albright, Frank Bremmer, Bart Krekelberg; Cosyne 2009 Program
Receptive Field Shifts in Area MT during Smooth and Rapid Eye Movements; Till S. Hartmann, Frank Bremmer, Thomas D. Albright, Bart Krekelberg; Vision Sciences Society Annual Meeting, 2006
Spatiotemporal Receptive Fields of MT Cells during Smooth Eye Movements Till S. Hartmann, Bart Krekelberg, Frank Bremmer, Thomas D. Albright; Society for Neuroscience, 2005